Numerical Modeling of Soil Gas Mobility in Shallow Unsaturated Zones

by

Jiaqi Weng

A thesis

presented to the University of Waterloo

in fulfillment of the

thesis requirement for the degree of

Master of Science

in

Earth Sciences (Hydrogeology)

Waterloo, Ontario, Canada, 2021

Author's Declaration

I hereby declare that I am the sole author of this thesis. This is a true copy of the thesis, including any required final revisions, as accepted by my examiners.

I understand that my thesis may be made electronically available to the public.

Abstract

In 2016, greenhouse gases (GHG) released from agricultural soils were estimated to be between 19 and 24 megatonnes of carbon dioxide equivalent with an increasing temporal trend. The processes controlling soil gas mobility in the vadose zone are poorly understood and significantly influence GHG emissions during a seasonal cycle. In this research, conceptual models of the fate of GHG in the vadose zone are presented and investigated through numerical modeling tools. By employing HydroGeoSphere (HGS), the soil gas emissions are estimated by tracking transient variations in soil water storage, assuming that soil pores are occupied either by gas or by water. It is also assumed that the compression, dissolution, and reactions within the water and gas phases are negligible. Therefore, variations in soil water saturation can be converted to variations in soil gas saturation and subsequently, GHG emissions. Field data collected at one of Agriculture Canada's WEBS research stations near Ottawa, Ontario were used to inform the numerical experiments. One- and three-dimensional simulation domains were used to investigate the influence of soil type, weather, macropore fraction, tile depth and number, ground surface relief, soil heterogeneity, and storm intensity on the mobility and emission behavior of soil GHG. Conceptual storm simulations of 10 days and 21 days and a longer-term climatic simulation utilizing field precipitation and evapotranspiration data were used to investigate the transient nature of soil GHG mobility. The results suggest that permeable soils and soils with low water saturation under dry weather conditions tend to have the highest potential for GHG emission. Macropores may significantly facilitate soil degassing by enhancing the drainage capacity and lowering the initial water saturation of soils. However, the variation of macropore fraction seem to have negligible influence on soil gas emission. Reductions in tile spacing and depth promote soil drainage and consequently act to reduce soil degassing processes. Ground surface topography may promote the soil degassing by generating surface water ponding, which enables soils to absorb more water. Heterogeneously layered soils tend to

have less water storage increase and soil gas emission than homogeneous soils during storms, because water may pond on the interface between soil layers with different hydraulic properties resulting in higher overall soil water content. Soil GHG emission tends to increase with increasing storm intensity. In addition, evapotranspiration appears to increase the soil gas emission. However, the strength of these effects is strongly influenced by the drainage capacity and water saturation conditions of soils.

Acknowledgements

I would like to express my gratitude to my supervisor, David L. Rudolph, and my committee members Steven Frey and David Blowes. They helped me to solve problems I came across in modeling and analyzing and provided valuable suggestions on my thesis, from which I benefited greatly. I really appreciated their patience and care on me during the Covid-19 period. With their help and encourage, I am able to complete my graduate program.

I want to thank Iwona Widurska for her careful work in the WEBS field site. She provided valuable field data and helped me on the construction of models. I also want to thank all members from Agricultural Greenhouse Gases Program. They gave great suggestions on my work and helped me to improve my models.

I want to thank my family and my friends who accompanied me and encouraged me. They helped me to fight the stress and loneliness during such a special period. The love and kindness they gave me is my treasure.

Table of Contents

List of Figures

List of Tables

Chapter 1

Introduction

In 2016, the amount of greenhouse gases (GHG) released by agricultural producers was estimated to be approximately 60 megatonnes of carbon dioxide equivalent (Mt CO_2 eq), which represented 8.5% of the total GHG emission in Canada (Environment and Climate Change Canada (ECCC, 2018). The percentage of GHG emission attributed to the agriculture sector increased from 7.9% to 8.5% from 2011 to 2016 and has been predicated to be continually increasing. Agricultural soil is an important agricultural source of GHG, with an increasing contribution from 19 Mt CO_2 eq in 2005 to 24 Mt CO_2 eq in 2016. Hence, the management of GHG related to agricultural operations needs to be carefully considered in the long-term.

Soil gas emissions are considered to be one of the most significant sources of agricultural GHG emissions. GHG can be produced through microbial metabolism and chemical reactions in soil. Vermoesen, Ramon and Cleemput (1991) suggested that soil gases contain higher concentrations of GHG than fresh atmospheric air. The soils can act as both sinks and sources of GHG. The mobility of the soil gases is primarily controlled by variations in soil gas pressure. When the soil gas pressure is higher than the barometric pressure, the soil gases tend to be released to the atmosphere, potentially increasing atmospheric GHG levels. When the soil gas pressure is lower than the barometric pressure, the fresh air enters the soil and the GHG level in the atmosphere remains unchanged. Hence, the transient gas exchange between the soils and the atmosphere may lead to the elevation of atmospheric GHG concentration.

In soils, gases move mainly through hydrodynamic dispersion and advection within the gas-filled pores (Scanlon, Nicot, and Massmann, 2002). The hydrodynamic dispersion refers to the combination of mechanical dispersion and molecular diffusion. The mechanical

dispersion is influenced by variations in the velocity of gas flow and is usually considered as a negligible process in soils. The molecular diffusion involves the random movement of gas molecules from areas of highly concentration to areas of lower concentrated. Advection is the movement of the gases driven by the pressure gradient resulting from the external factors like seasonal or climate changes that influence barometric and in-situ gas pressures.

Previous studies have generally focused on the diffusion of soil gases under static and equilibrium hydraulic conditions. Few studies have considered soil gas advection. However, advection may result in a significant increase in soil GHG mobility in a short time span. For example, infiltrating rainwater will occupy some of the pore spaces that were initially gas-filled, during the precipitation event, displacing the soil gas. Hence, the soil gas pressure increases and a gaseous gradient is formed at the interface between the soils and the atmosphere. Thus, the GHG-rich gases are pushed out from the soils through advection, potentially contributing to an increase in atmospheric GHG levels When the rainwater drains deeper into the soil profile, the shallower water filled pore spaces will empty again and an opposite gaseous gradient is formed. Hence, fresh atmospheric air may re-enter the soil. Because the gas advection process is potentially able to introduce significant amounts of GHG to the atmosphere during short time intervals, it is significant to investigate this transport process to improve the understanding of GHG mobility.

Six primary influence factors are considered for soil gas advection. The first factors is the soil system components, including the soil matrix (pm), macropores (dual), and agricultural tiles (tile). The macropores refer to soil cavities that have diameters larger than 75 μm, which are preferred pathways for water during infiltration (Soil Science Society of America, 2020). The agricultural tiles refer to drainage systems installed in the shallow subsurface to remove excessive water in support of crop growth The introduction of macropores or tiles to soil systems may vary the hydraulic properties and further influence soil degassing. The second factor is the soil matrix characteristics. Three conceptual agricultural soil types with different hydraulic properties are assessed including the sandy

loam, silty loam, and clay loam. The third factor is the macropore characteristics, investigated as macropore volumetric fraction to in this research. The macropore volumetric fraction is the portion that the macropores occupied by the total porosity (Aquanty, 2015), which may relate with the efficiency of macropore transportation. The fourth factor is the agricultural tile characteristics. The tiles may connect with natural macropores and influence the drainage capacity. It might be significant to investigate the influence of the tile depth or tile number on soil degassing. The fifth factor is the soil profile characteristics, including the ground surface topography and soil heterogeneity. The surficial topography and heterogeneity of the soil layers may influence surface water ponding and soil water distribution in the subsurface, which may further influence the soil degassing. The sixth and final primary factor relates to variations in climatic drivers including precipitation and evapotranspiration. Both the intensity and frequency of precipitation events are considered. Evapotranspiration acts as a water sink in soils, which may diminish the water influx during an infiltration event and reduce the water storage variation and soil gas displacement. However, the evapotranspiration can also reduce water stored in soil pores between rainfall events, which would enable the soil to accept more water during precipitation. Hence, the evapotranspiration can either increase or decrease the soil gas emission.

The main objective of this research work is to quantitatively assess the influence of the primary factors described above, on the mobility of soil gases and GHG. The assessment is based on a series of numerical simulation experiments utilizing observational data collected at the Agriculture and Agri-Food Canada's (AAFC) Watershed Evaluation of Beneficial Management Practices (WEBs) field site near Ottawa, Ontario. The numerical experiments are based on 1-dimensional (1D) and three-dimensional (3D) domains considering conceptual and field-based scenarios designed to investigate the influence of various combinations of the primary controlling factors on the movement of soil gas in variably saturated conditions.

It is difficult to simulate gas movement in soil directly. However, multiple approaches

have been developed to simulate the movement of water in soil. In the current research, gas transport in soil is considered to be the inverse of the soil water transport. It is assumed that the soil pores are filled with either gas or water. The compressibility and solubility of the gases and water are ignored. A 3D control-volume finite element simulator, Hydrogeosphere (HGS) (Aquanty, 2015a, 2015b) is used to simulate the water saturation variations during precipitation changes. The results are converted to the air saturation variations and the soil gas emission are estimated. The combined modeling results are evaluated from the perspective of the transient mobility of soil gas and potential exchanged of GHGs between the atmosphere and the soil profile under a wide range of typical conditions that would be encountered within the Ontario agricultural landscape.

Chapter 2

Background

2.1 Greenhouse Gas Transport in Soil

Greenhous gases in soils are generated through chemical reactions and metabolism of plants, animals, and microbes (Oertel et al, 2016). For example, CO_2 is formed through root respiration and microbial respiration. NO and NO_2 are generated by microbial nitrification and denitrification process, while CH_4 is produced through methanogenesis. Generally, soil gas contains higher GHG levels than the atmospheric air. Vermoesen, Ramon and Cleemput (1991) measured the composition of gases in different soils and reported that the CO_2 content in soil is 3~6 times higher than that in the atmosphere. They also measured soil CH_4 concentrations and suggested that the magnitudes are of 10^5 to 10^6 ppb in silty and clay soil samples, which is significantly higher than the average atmospheric CH_4 concentration of 1803 ppb in 2011(IPCC, 2013).

Soil gas emissions are considered to be important sources of the atmospheric GHG. The gas exchange between the soils and the atmosphere resembles breathing. During such exchange, the GHG-rich soil gases is released to the atmosphere and contributes to the increase of atmospheric GHG levels. It is reported that soil degassing contributes 35% CO_2, 47% CH_4, 53% N_2O, and 21 % NO to the global GHG emission (IPCC, 2013). In 2016, the agricultural soils are estimated to contribute 24 Mt CO_2 eq of N_2O emission to the environment (ECCC, 2018). Hence, it is necessary to investigate the mobility of gases in soil and find approaches to diminish the GHG soil emission.

The molecule diffusion and advection are two important mechanisms of gas transport in soils. The molecule diffusion is described by the Fick's Law. Multiple factors can influence the gas diffusion rate including the gas pressure and thermal conditions. Most studies focus on gas diffusion under static water saturation conditions. Neira al. (2015)

investigated the movement of O_2 in soils and suggested that the soil gas movement is dominated by diffusion under static hydraulic conditions. Pourbakhtiar et al. (2017) studied the influence of wind action on gas diffusion with different but constant moisture conditions in porous media. They indicated that the air filled porosity and soil air permeability varies with the soil water content. Such properties are considered to be positively related with the gas diffusivity in soil (Hamamoto et al, 2009). Healy et al. (1996) predicted the soil-air gas exchange rate and investigated its influence factors using a static-chamber method. They assigned hypothetical field conditions to the experiments and simulations and assumed that the gases moved only by the diffusion in the soils. Although most previous studies have investigated various influence factors on the soil gas diffusion, little work has been done to consider the influence of transient climatic events on the mobility of soil gas or to assess the role of soil gas advection.

Advection refers to the bulk motion of the soil gases in response to the total gaseous pressure gradient caused by external forces (Scanlon, Nicot, and Massmann, 2002). The volume of the gases and water in soil pores varies during infiltration and exfiltration. As the water volume increases, the gases are pushed out from the soil pores and may redistribute within the soil pore network or enter the atmosphere. Because soil gases are rich in GHG, the advection may lead to instant and transient contributions to the atmospheric GHG levels. So far, there are few studies focusing on the soil gas advection and its role on the release of GHGs from soil surfaces, especially the advection driven by the soil moisture variation.

Oertel et al (2016) stated that the soil moisture is the most important driver for soil gas emission to the atmosphere. However, they were focused more on the variation of the redox conditions caused by the moisture variation rather than the physical movement of the soil gas. Sponseller (2007) measured the change of the soil CO_2 efflux under different precipitation rates. Again, in this study, the variation of the soil redox conditions as soil water contents changed was considered to be the main cause of the difference in the CO2 emission rate, rather than the soil gas advection. Costanza-Robinson and Brusseau (2002) performed a

phase miscible displacement experiment to evaluate the contribution of diffusion and advection on gas transport in natural porous media under unsaturated conditions. It was suggested that the mechanical mixing and gas displacement contributes more to the overall soil gas mobility than the gas diffusion when the soil water content is higher than 0.2 for non-reactive gases like methane. However, the experiment was conducted under constant prescribed infiltration rates. To understand the soil gas mobility under variable climatic conditions, an evaluation of soil gas mobility under varying precipitation conditions would be required.

Precipitation is a potential driver for the soil gas advection. In the current research, soil gas advection resulting from transient infiltration during variable precipitation events is investigated. However, the gas flow is different from the water flow in several aspects (Scanlon, Nicot, and Massmann, 2002). Firstly, the density of the soil gases may vary significantly and may influence the soil gas pressure. In addition, the high compressibility of gas may result in non-linear gas flow phenomena in soil. The low pneumatic conductivity and viscosity enables soil gases to move under low gradients. When the temperature increases, the viscosity of the soil gases increases but that of water decreases. Another difference between water and gas flow is that the gas will have stronger slip flows, also known as Klinkenberg effect. Due to the low viscosity, soil gases are less likely to adhere on the pore walls like the water does. Hence, the velocity of soil gases on the pore wall is not zero and slip flows occur. Finally, the diffusion is more significant for gas than for water due to the high molecular diffusion coefficients of gases.

The effective diffusion coefficient for molecular diffusion in soil environments decreases sharply when the water saturation increases. Precipitation events generally lead to strong and rapid water saturation variations. Hence, the diffusion might be limited during storms. Meanwhile, soil gas diffusion may be negligible compared with soil gas advection when external forces like seasonal and climate changes are applied. Nicot, and Massmann (2002) stated that the advective gas flux might exceed the diffusive gas flux even under small

total pressure gradients. Gas advection is the dominate transport process when the mean free path of gas molecules (λ) is significantly lower than the pore radii (λ_p) and the soil particle radii (r_p), because the intermolecular collision exceeds the collision between gas molecules and pore walls in this condition. The mean free path of gas molecules is reversely related with the mean pressure of gas in soils. Thus, the unsaturated soils that have high gas saturation and high mean gas pressure tend to have significant advection flow due to the pressure gradient, because λ in the unsaturated zones is small and more likely to be smaller than λ_p and r_p. Consequently, advection becomes the main gas transport mechanism at the beginning of precipitation events, when the water saturation is low and the gas saturation is high in the soils, especially for permeable soils. In considering soil GHG emission, the early stage of storms is the period when soil gases rich in GHG are released to the atmosphere.

2.2 Factors Affecting GHG Mobility in Soil

Soils are porous media that can act as sources or sinks for greenhouse gases. The gases escape from the soils when barometric pressures change or precipitation occurs and infiltrating water saturates the pore space that was previously occupied by the soil gases. When the precipitation ceases and the water drains downward, atmospheric air can be drawn back into the soil. The gas transport efficiency, which is related to the water drainage capacity, is associated with the bulk soil porosity that consists of the matrix porosity and macroporosity, and the soil water retention characteristics.

2.2.1 Soil Matrix

The gas transport parameters vary with the soil texture, which is an intrinsic property of the porous medium that generally considered a constant characteristic. Hamamoto et al (2009) indicate that the gas diffusivity and soil air permeability are positively related with the air-fill porosity. Meanwhile, the air-filled porosity is higher in soil matrixes with coarse grain size and low bulk density. According to the size distribution of mineral grains, soils can be

divided into different textural classes. Sandy soil is considered to have grain size mostly between 0.075 mm and 4.75 mm in diameter (American Society for Testing and Materials, 1985). Silty soil and clayey soil has smaller grain size that is less than 0.075 mm. Generally, silty soil has lower plasticity than clayey soil. Meanwhile, loam describes soil with relatively even distributions of these three different grain size categories. Due to the high conductivity and relatively large pore diameter of sandy materials, gas emission from sandy soils are expected to be greater than that from clayey soils under partially saturated conditions.

In the current research, the water movement is utilized as an inverted surrogate of the gas movement. Hence, the hydraulic parameters for the soil matrix are considered instead of the pneumatic parameters. To quantify the variation of water saturation, two soil characteristics are required, which include the soil water retention curve and hydraulic conductivity.

The soil water retention curves (SWRC) describe the water storage capacity of the soil. It represents the relationship between the soil moisture or soil water content θ [dimensionless] and the soil water potential ψ [L]. The soil water retention curve is an intrinsic characteristic of soil that seldom varies although it may have hysteretic properties. Generally, the residual saturation for sandy soils is lower than that for clayey soils. The saturation in sandy soils is more sensitive to soil water potential variation than that in clayey soils. Various empirical models have been developed to represent the soil water retention curve, including the Brooks and Corey model and the van Genuchten (VG) function (Ghanbarian-Alavijeh et al, 2010). In this research, the van Genuchten function is adopted.

The hydraulic conductivity K describes the drainage capacity of the soil. Generally, soils with coarse textures tend to have higher K and as such, sandy soils have higher drainage capacity than silty and clayey soils. K is a constant when the soil is saturated (K_{sat}), but is a function of the water saturation under unsaturated conditions. SWRC information is required to determine K for partially saturated sediments.

2.2.2 Macroporosity

In addition to soil texture, the soil structure also influences the gas mobility in soil. Soil structure refers to the way that the soil textural particles (sand, silt, and clay) assemble (American Society for Testing and Materials, 1985. Poorly-structured soils do not have obvious aggregation, while well-structured soils have granular aggregates that are durable. McCarthy and Brown (1992) suggested that poorly-structured soils are less air-permeable than well-structured soils, because well-structured soils tend to have larger inter-aggregate flow channels. In addition, the soil structural complexity is enhanced by the presence of macrospores and agriculture drainage tiles. Macropores and tiles can act as conduits for water to migrate rapidly through the bulk soil, which potentially lead to significant changes on the soil water saturation. Consequently, the soil gas permeability and degassing rate will be affected by the soil macroporosity.

Macropores are large pores where preferential flow can occur (Soil Science Society of America, 2020) and refer to soil pores with diameter larger than 0.075 mm. Macropores can be formed through various mechanisms including the soil-animal-plant interactions including root and worm holes, animal behaviors, and soil matrix erosion and cracking (Beven and Germann, 1982). Generally, macropores play important roles in conducting rapid, non-equilibrium flow through soil. Panday and Nkongolo (2015) investigated the effect of the soil porosity and water content on greenhouse gas emission in a silt loam soil in Jefferson City, Missouri. They collected soil gas samples in the field using static and vented chambers and found that more GHGs are released as the pore space increases with a correlation coefficient of 0.27~0.53.

The macropore system is influenced by multiple factors. Beven and Germann (1982) suggested that the land use has the most pronounced influence on the soil macroporosity. Plowing may cut the natural macropores and lead to the vertical discontinuity of pore networks. Soil compaction by traffic and heavy machines may also destroy macropores. On the other hand, the installation of the agricultural tiles can enhance the macroporosity. Frey et

al. (2012) suggested that macroporosity above the tiles is greater than that at the middle between tiles in clay under high water saturation conditions. The tiles can create unsaturated soil condition that is favored by earthworms and physical processes of macropore formation. However, the influence of tile on soil macroporosity is limited by the strength and depth of earthworm activities, the amount historical burrows that are abandoned by earthworms, and the change of seasons. Meanwhile, the installation and backfilling of tiles may also alter the soil structure and change macroporosity. Besides the land management, extreme weather conditions like drought may promote the formation of soil cracks through dessication, which can lead to an increase in macroporosity. In addition, changes in ecological systems resulting from various land management systems may influence macroporosity by affecting the nature of both the population and activity of soil wildlife (Beven and Germann, 1982).

The hydraulic properties of macropores will influence soil gas mobility. Due to the nature of their formation, most macropores impart significant hydraulic anisotropy within natural soils due to the higher degree of vertical orientation and continuity of most macropore features as opposed to the horizontal and transverse directions. However, low permeability linings or coating that may develop on the interface between macropores and soil matrix, may impede lateral flows and enhance the hydraulic anisotropy.

The preferential flow in macropores starts when the applied water pressure exceeds the water entry pressure (Jarvis, 2007). The water entry pressure is determined by the surface tension of water, radius of the meniscus between the water and air, and the contact angle of the meniscus with the pore wall. For macropores that have equivalent cylinder diameter around 0.3~0.5 mm, the water entry pressure is -100~-60 mm of water, which equals to 0.0097~0.0058 atm.

Jarvis (2007) stated that macropore flow starts when the water pressure on the surface exceeds the water entry pressure. The water entry pressure is controlled by the surface tension of water, the radius of curvature of the air–water interface, and the contact angle between the air-water interface and macropore wall. Figure 1 illustrates the influence of

macropore flow on water infiltration in soils. Point A indicates the initial stage of percolation. The macropores are filled with gases and hydraulically impermeable. The non-equilibrium flow in macropores starts when the pressure potential increases to reach the water entry pressure of small macropores at point B. The macropore flow becomes significant when the pressure potential reaches the water entry pressure of large macropores during the late stage of percolation at Point C. In this stage, macropores that have equivalent cylindrical diameter larger than 0.3–0.5 mm and vertical continuity become highly conductive in transporting water. The uneven wetting of soils is observed and the flow. The macropore flow enables water to reach the lower part of the soils more rapidly than it travels through the soil matrix.

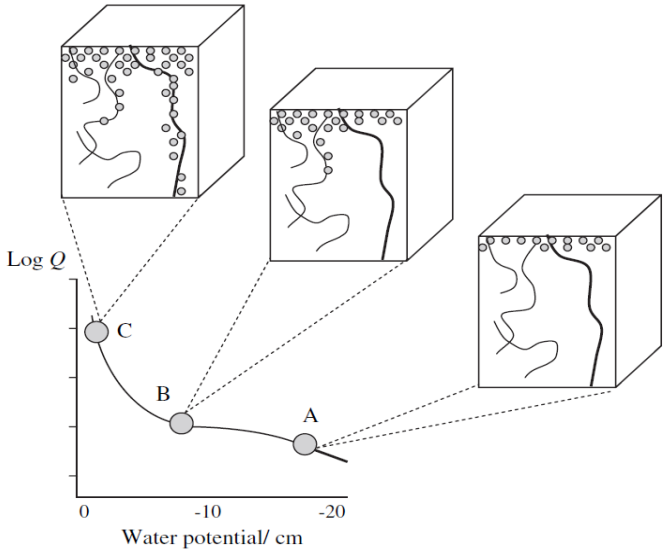

Figure 1. Movement of water under differing water potentials in macropores. The cubes represent soil cells and the thick lines indicate large macropores while the thin lines indicate small macropores. The gray dots in cubes represent water. From Jarvis (2007).

The macropore flow rate is related with the rainfall intensity and duration, the initial soil moisture content, and the saturated hydraulic conductivity of soil matrix (Jarvis, 2007). For example, significant macropore flow may occur during heavy precipitation events. However, very intense rainfall may cause the sealing of macropore openings on the surface

of silty soils and reduce the macropore flow (Beven and Germann, 1982). Cultivated arable land tends to have lower macropore flow than non-cultivated grasslands due to the disruption of macropore continuity during soil tillage (Jarvis, 2007). However, not all macropores are involved in water transport. Jarvis (2007) suggested that only about 10~50% of the total macropores transport water during water infiltration events.

2.2.3 Agriculture Drainage Tiles

Agriculture tiles are permeable drainage tubes that are installed beneath cultivate farm fields to enhance subsurface drainage to facilitate crop growth (Welling, 1997) (Figure 2). Tile drainage is being implemented in nutrient contamination extensively throughout North America and Europe in recent years (Frey et al., 2012). Excessive moisture may accumulate in soils under moist and cool climatic conditions, which may degrade field conditions and lower crop productivity. Once the water table reaches the base of the tile drain, groundwater is discharged through the pipes, usually to a lateral surface water drainage system, which increases soil drainage improving crop growth potential.

The agricultural tiles can be considered as artificial macropores. Unlike natural macropores that are vertically conductive, the tiles are laterally connected (Figure 2). Tiles may receive water from both soil matrix and natural macropores overlying the tile or from the raising water table below the tile pipe invert.

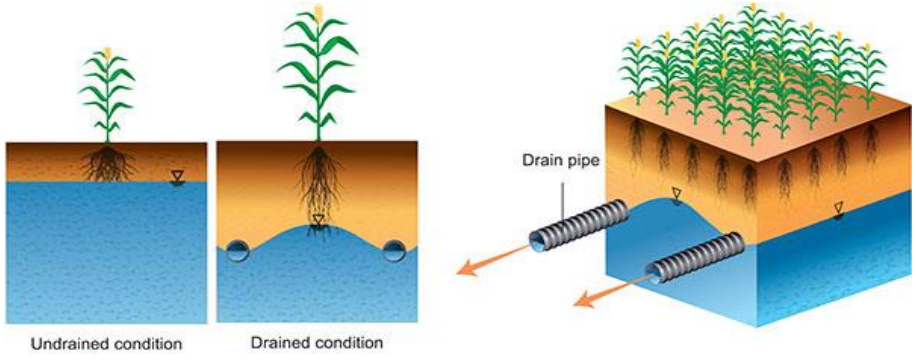

Figure 2. Schematic diagram of agricultural tiles in the field. Retrieved from Ghane (2018).

2.2.4 Precipitation and Evapotranspiration

Due to the variability in seasonal precipitation, water tables can fluctuate considerably during and between precipitation events. As the water table rises, soil GHG can be displaced from the partially saturated soils and released to the atmosphere. As the water table drops, the fresh atmospheric air can re-enter the soil pores at ground surface.

Precipitation events tend to increase soil GHG emission. Yan et al. (2018) summarized previous research on the effects of precipitation on the soil GHG emission rates. They stated that an increase in precipitation will lead to the promotion of N_2O (+154.0 %) and CO_2 (+112.2 %) emission. Meanwhile, a decrease of precipitation will result in lower N_2O (−64.7 %) and CO_2 (−8.6 %) emissions. Fatumah et al. (2019) recorded the variation of soil GHG emission with daily precipitation and soil temperature in banana–coffee farms in the Wakiso District, Uganda. In that work, it was suggested that the soil degassing is enhanced by daily precipitation. They also suggested that the effect of precipitation is stronger than the co-effect of precipitation and temperature on the soil GHG emission. However, like much of the previous literature on this topic, this research focused more on the influence of precipitation variation on the soil chemical and microbial conditions, rather than on precipitation impacts on physical soil gas mobility. It will be meaningful to investigate influence of precipitation intensity on soil gas convection and transient distribution within the context of the fate of soil GHG.

Evapotranspiration (ET) is the sum of water flux through evaporation and plant transpiration. ET acts as a sink for soil water and will influence some of the mechanisms influencing GHG emissions from soils. It can diminish the amount of infiltrated water and result in less variation of water storage in soil, which corresponds to less potential GHG emission. However, the consumption of water by ET may reduce the water saturation and enable the soil to accept more water during precipitation, which may elevate the soil GHG emission.

ET has been shown to vary with plant type and growth cycle. Oertel et al, (2016)

suggested that the wetlands have the highest absolute soil GHG emission potential, followed by forestlands, grasslands, croplands and barren lands. However, they also indicated that the soil GHG emission associated with the same vegetation type might vary significantly and is influenced by the local climate and soil management methods. Overall, ET plays a complex role in soil GHG emission.

Chapter 3

Field Study Area

Data collected during recent field investigations conducted on active agricultural fields, which are part of Agriculture and Agri-Food Canada's (AAFC) Watershed Evaluation of Beneficial Management Practices (WEBs) program for sustainable agriculture, were utilized for the current study (I. Widurska, personal communication, March 28th, 2021). These field sites are located located approximately 45 km east of the city of Ottawa, Ontario, Canada (Figure 3a). Information collected from two different landscape positions within the agricultural fields, which are labelled as Site 11 and Site 5 (original AAFC designations) in Figure 3b, is considered for this work. Site 11 represents cultivated farm land (Figure 3c) and Site 5 is situated within a riparian area adjacent a surface water drain (Figure 3d).

The field data that were collected by I. Widurska (personal communication, March 28th, 2021) included soil composition and texture, hydraulic parameters, and macropore information. As part of the Widurska (2020) study, field investigation campaigns were conducted during spring (May and June 2018), summer (July and August 2018), and fall (October and November 2018). Figure 4 shows the soil profile from the agricultural land through the riparian zone, perpendicular to the surface water drain.

Figure 3. WEBS site map. Retrieved from I. Widurska (personal communication, March 28th, 2021). (a) Location of WEBS field site with respect to the City of Ottawa, Ontario, (b) location of Site 11 and 5, (c) location of data collection plots in Site 11, (d) location of data collection plots in Site 5. Retrieved from Google, 2019.

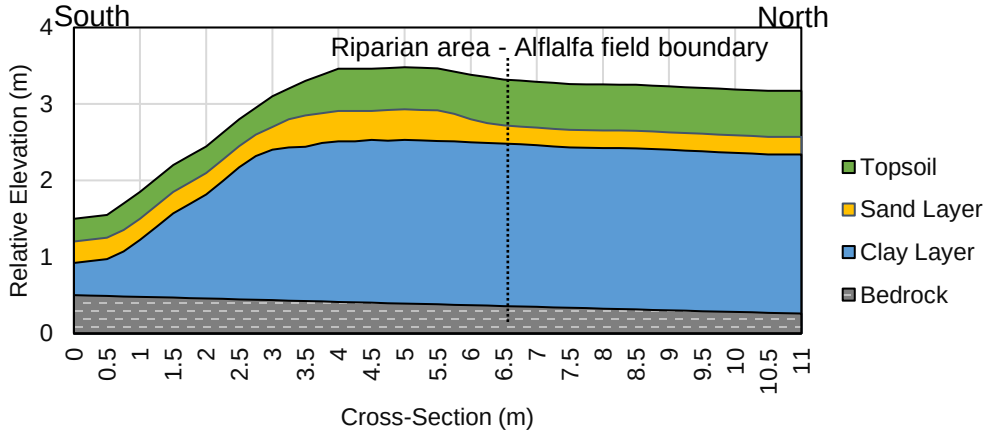

Figure 4. Soil profile of the WEBS site map. Retrieved from I. Widurska (personal communication, March 28th, 2021).

Chapter 4

Methods

The research undertaken in this study involves the development of a series of numerical experiments conducted at several different scales, to explore the influence of precipitation events, transient seasonal weather conditions, and soil characteristics on the mobility and potential emissions of GHG from the agricultural landscape. The study employs the numerical model Hydrogeosphere (HGS) (Aquanty, 2020) and utilizes extensive field and laboratory data collected from previous and concurrent studies at the WEBS field site, described earlier. A variety of scenarios based on 1D, and 3D simulations were used to derive insight into climatic and soil controls on soil GHG movement in shallow agricultural soils.

4.1 Hydrogeosphere Model

Hydrogeosphere (HGS) is a 3D control-volume finite element/finite difference model developed by Aquanty (2020). One unique feature of HGS is that it fully integrates groundwater and surface water flow and transport, including variably saturated and macroporous subsurface conditions. It implicitly calculates water flow and solute transport in both surface, subsurface, and macropore flow regimes simultaneously, instead of performing separate calculations for the surface and subsurface as is common with loosely coupled hydrologic models (Harter and Morel-Seytoux, 2013) like GSFlow (Regan and Niswonger, 2020) and Integrated Water Flow Model (California Department of Water Resources, 2021). HGS uses Richard's equation to solve for variably saturated 3D subsurface flow (Therrien and Sudicky, 1996) and the 2D diffusion wave equation to solve overland flow.

HGS uses a dual continuum formulation to simulate preferential flow through macropore features (Gerke and van Genuchten, 1993). The primary continuum (m) refers to the porous media (soil matrix flow), while the secondary continuum (d) refers to the dual (macropore flow) region. The primary and secondary continuums are typically

parameterized differently in order to represent the contrast between soil matrix and macropore flow conditions. A modified form of Richard's equation is used to describe the 3D variable-saturated flow in the soil matrix and macropores (Aquanty 2020), as follows:

$$-\nabla(\omega_m q_m) + \Gamma_{ex} \pm Q_m = \omega_m \frac{\partial}{\partial t}(\theta_{s,m} S_{w,m}) \quad (1)$$

$$-\nabla(\omega_d q_d) + \Gamma_d \pm Q_d = \omega_d \frac{\partial}{\partial t}(\theta_{s,d}\ S_{w,d}) \quad (2)$$

ω is the volume fraction [dimensionless] of total porosity occupied by soil matrix or macropores. The sum of ω_m and ω_d equals to 1. q is the fluid flux [LT^{-1}] and Γ_{ex} denotes the sum of fluid exchange [$L^3L^{-3}T^{-1}$] between the matrix and all other domains. Similarly, Γ_d represents the sum of fluid exchange between the dual continuum (macropores) and other domains. Q represents external fluid sources and sinks [$L^3L^{-3}T^{-1}$]. Potential sources include precipitation and irrigation, while the potential sinks includes evaporation, transpiration and groundwater pumping. On the right hand side, t is time [T], θ_s is the saturated water content [dimensionless] assumed equal to porosity. S_w is the water saturation [dimensionless], which ranges from 0 to 1.

The fluid flux q in each continuum is expressed using the Darcy equation as:

$$q = -K_{sat} * k_r \nabla(\psi + z) \quad (3)$$

K_{sat} is the saturated hydraulic conductivity [LT^{-1}], ψ is the pressure head [L], and z is the elevation head [L]. k_r is the relative permeability [dimensionless] and is a function of S_w. The relationship between k_r, S_w and ψ can be expressed by the van Genuchten (1980) function:

$$S_W = \begin{cases} S_{Wr} + (1 - S_{Wr})\left[1 + |\alpha\psi|^{\beta}\right]^{-v}, & \psi < 0 \\ 1, & \psi \geq 0 \end{cases} \quad (4)$$

$$v = 1 - \frac{1}{\beta} \qquad \beta > 1 \quad (5)$$

with the derived kr:

$$k_r = S_e^{(l_p)}\left[1 - \left(1 - S_e^{\frac{1}{v}}\right)^v\right]^2 \quad (6)$$

$$\mathbf{S_e} = \frac{\mathbf{S_W} - \mathbf{S_{Wr}}}{\mathbf{1} - \mathbf{S_{Wr}}} \quad (7)$$

S_{wr} is the residual water saturation [dimensionless], α is the inverse of the air-entry pressure head [L^{-1}], l_p is the pore connectivity parameter [dimensionless], and β is the pore-size distribution index [dimensionless]. The values of S_{wr}, α, and β represent intrinsic soil-specific water retention characteristics and define the shape of a soil water retention curve. In this study, the pore connectivity parameter l_p is set to be 0.5 based on Mualem's (1976) model.

Water exchange between the soil matrix and macropores is governed by the difference in pressure head between the two continuums according to:

$$\boldsymbol{\Gamma} = \boldsymbol{\alpha}_{\omega d} K_a k_{r,a} (\boldsymbol{\psi_d} - \boldsymbol{\psi}) \quad (8)$$

Where $\boldsymbol{\Gamma}$ is the inter-continuum exchange [T^{-1}], α_{wd} is the first-order fluid exchange coefficient for subsurface-macropore coupling [L^{-2}]. K_a is the hydraulic conductivity of the interface between the soil matrix and macropores [LT^{-1}], and $k_{r,a}$ is the corresponding relative permeability. $k_{r,a}$ is determined using the van Genuchten (1980) formulation with parameters configured for the interface, which in this case were set equal to those of the soil matrix. K_a was set at 1/12 according to guidance provided by Gerke and Kohne (2002).

Meanwhile, the right hand side of the Richard's equation can be simplified as:

$$\frac{\boldsymbol{\partial}}{\boldsymbol{\partial t}}(\boldsymbol{\theta_s S_w}) \approx \mathbf{S_W S_S} \frac{\boldsymbol{\partial \psi}}{\boldsymbol{\partial t}} + \boldsymbol{\theta_s} \frac{\boldsymbol{\partial S_w}}{\boldsymbol{\partial t}} \quad (9)$$

Hence, the modified Richard's equation only concerns two variables including S_w and ψ. In each continuum, a certain water saturation S_w can be determined once the pressure head is given.

Overland flow is described by the 2D Saint Venant equations, per Aquanty (2020):

$$-\nabla \cdot (d_o q_o) - d_o \boldsymbol{\Gamma}_o \pm Q_o = \frac{\partial \emptyset_o h_o}{\partial t} \quad (10)$$

Where:

$$q_o = -K_o \cdot k_{ro} \nabla (d_o + z_o) \quad (11)$$

d_o is the depth of flow [L]. Γ_o is the water exchange between the surface and subsurface

domains [LT^{-1}]. Q_o is the volumetric flow rate per unit area from external water inputs or outputs [LT^{-1}].$\emptyset_o$ is the surface flow domain porosity [dimensionless], which varies from 0 at the ground surface to unity at the top of flow obstructions. h_o is the water surface elevation [L]. t is time [T]. K_o is the surface conductance [LT^{-1}] and k_{ro} is a factor that describes the reduction in horizontal conductance from obstruction storage exclusion [dimensionless]. z_o is the land surface elevation [L].

The water exchange term Γ_o [T^{-1}] is calculated by:

$$\mathbf{d_o\Gamma_o} = \omega_m \frac{k_{r,m}K_{zz,m}}{l_{exch}}(h_m m - h_o) + \omega_d \frac{k_{r,d}K_{zz,d}}{l_{exch}}(h_d - h_o) \quad (12)$$

Again, m and d denote the porous medium (soil matrix) and dual medium (macropore) respectively. k_r is the relative permeability [dimensionless], while K_{zz} is the vertical saturated hydraulic conductivity [LT^{-1}]. l_{exch} is the coupling length. h_m and h_d are the subsurface porous medium (matrix) and dual (macropore) head respectively [L]. In the surface-subsurface water exchange, the relative permeability k_{ro} may vary with the flow direction:

$$k_{ro} = \begin{cases} {S_{exch}}^{2(1-S_{exch})}, & d_o < H_s \\ 1, & d_o \geq H_s \end{cases} \quad (13)$$

$$S_{exch} = \frac{d_o}{H_s} \quad (14)$$

H_s is the sum of the height of rill storage and the height of surface obstruction [L] per Aquanty (2020).

The Hazen Williams empirical equation (HWE) is adopted to describe the agriculture tile flow, which is treated as 1D flow in subsurface pipes in HGS program (Aquanty, 2015).

Evaporation in HGS is calculated using a formulation derived from (Kristensen & Jensen, 1975). In HGS, the rate of transpiration T_p [L^3T^{-1}] is calculated according to (Aquanty, 2020):

$$T_p = f_1(LAI) * f_2(\theta) * RDF(t) * [E_P - E_{can}] \quad (15)$$

Where,

$$f_1(LAI) = \max\{0, \min[1, (C_1 + C_2 * LAI)]\} \quad (16)$$

$$f_2(\theta) = \begin{cases} 0 & \text{for } 0 \le \theta \le \theta_{wp} \\ f_3 & \text{for } \theta_{wp} \le \theta \le \theta_{fc} \\ 1 & \text{for } \theta_{fc} \le \theta \le \theta_o \\ f_4 & \text{for } \theta_o \le \theta \le \theta_{an} \\ 0 & \text{for } \theta_{an} \le \theta \end{cases} \quad (17)$$

$$f_3 = 1 - \left[\frac{\theta_{fc} - \theta}{\theta_{fc} - \theta_{wp}}\right]^{C_3} \quad (18)$$

$$f_4 = \left[\frac{\theta_{an} - \theta}{\theta_{an} - \theta_o}\right]^{C_3} \quad (19)$$

LAI is the leaf area index [dimensionless]. θ is the moisture content [dimensionless], which can be converted from the pressure head using SWRC. For the subscripts, wp stands for the wilting point, fc stands for the field capacity, o stands for the oxic limit, while an stands for the anoxic limit. RDF is the root density function that varies with time. E_p is the reference evapotranspiration [LT^{-1}]. E_{can} is the canopy evapotranspiration [LT^{-1}] that is derived from LAI and a canopy storage parameter. C_1, C_2, and C_3 [dimensionless] are user defined fitting parameters for which additional information is provided by Kristensen & Jensen (1975). RDF is the time-varying root density function that is influenced by root depth (Aquanty, 2015).

Evaporation from the ground surface E_{olf} and the subsurface soil E_s are calculated by:

$$E_{olf} = \alpha^*_{olf}\left(E_p - E_{can} - T_p\right) \quad (20)$$

$$E_s = \alpha^*\left(E_p - E_{can} - T_p - E_{olf}\right)EDF \quad (21)$$

Where,

$$\alpha^*_{olf} = \begin{cases} \left(\frac{d_o}{h_s}\right)^{2\left(1-\frac{d_o}{h_s}\right)} & \text{for } 0 \le d_o \le h_s \\ 1 & \text{for } h_s < d_o \end{cases} \quad (22)$$

$$\alpha^* = \begin{cases} \frac{\theta - \theta_{e2}}{\theta_{e1} - \theta_{e2}} & \text{for } \theta_{e2} \le \theta \le \theta_{e1} \\ 1 & \text{for } \theta_{e1} < \theta \\ 0 & \text{for } \theta < \theta_{e2} \end{cases} \quad (23)$$

θ_{e1} is the moisture content at the end of the energy-limiting stage, while θ_{e2} is the

limiting moisture content. When θ is higher than θ_{e1}, full evaporation will occur. When θ is lower than θ_{e2}, no evaporation will occur. EDF is the evaporation distribution function, which varies with depth.

For estimating the volume of gas emitted from the soil during a wetting cycle it is assumed that the total pore space in soil is occupied by water or air ($S_a + S_w = 1$, S_a is air saturation). For the purpose of this work, the assumption is made that the influence of compression and dissolution of the soil gases are considered to be negligible. Once the variation of water saturation S_w with time t is determined for both the primary and secondary continuums, the change of water volume ΔV_w and of air volume ΔV_a in the simulated domain can be estimated by:

$$\Delta V_w = -\Delta V_a = \left(\omega_m \phi_m \Delta S_{w,m} + \omega_d \phi_d \Delta S_{w,d}\right) * V_T \tag{24}$$

Hence, the average soil gas emission rate is:

$$v_{emitted} = -\frac{\left(\omega_m \phi_m \Delta S_{w,m} + \omega_d \phi_d \Delta S_{w,d}\right) * V_T}{\Delta t} \tag{25}$$

4.2 Hydraulic Parameter Selection

Two main sets of numerical experiments were conducted during the course of the current study. The first involved the establishment of typical conceptual conditions that would be encountered within an agricultural landscape and utilized model parameters derived from the literature. The objective of this conceptual study was to assess the sensitivity and significance of various soil parameters in controlling transient infiltration phenomena during discrete precipitation events and consequently the mobility of GHG. The second set of experiments build on the conceptual modeling and incorporate field measured information derived from the WEBS field site in order to investigate dynamic field infiltration and soil gas behavior at a monitored field site. The parameter sets adopted for both simulations experiments are described below.

4.2.1 Soil Parameters for Conceptual 1D and 3D Simulations

Conceptual 1 dimensional (1D) and 3 dimensional (3D) flow models were designed to simulate transient water mobility under variably saturated conditions within the near surface environment during specified precipitation events. The hydraulic and geological parameters used for the modeling were selected from the literature to represent general characteristics of common soil types within an agricultural setting.

4.2.1.1 Soil Matrix Parameters

Three conceptual soils are selected to represent typical soil matrix, including the sandy loam, silty loam, and clay loam. Table 1 shows the hydraulic data of conceptual soil matrix that were derived from literature sources. The van Genuchten (VG) function is adopted in the study to predict soil water retention capacity, which performs well for unsaturated soils (Ghanbarian-Alavijeh et al, 2010). It contains three shape parameters and assumes that the soil water curve is sigmoidal-shaped. This research adopts VG parameters from the Rosetta database (U.S. Department of Agriculture, 2019). The Rosetta database provides average hydraulic parameters for the twelve USDA textual classes (U.S. Department of Agriculture, 2019). Once the soil textual class is known, the VG parameters for the soil can be predicted. Figure 5a shows the soil water retention curves (SWRC) of the three conceptual soils using VG parameters obtained from the Rosetta database. Theses VG parameters are shown in Table 1. Overall, the SWRC of the conceptual silty loam and clay loam are similar to those of the soils sampled in the WEBS field site by Widurska (I. Widurska, personal communication, March 28th, 2021) (Figure 5b).

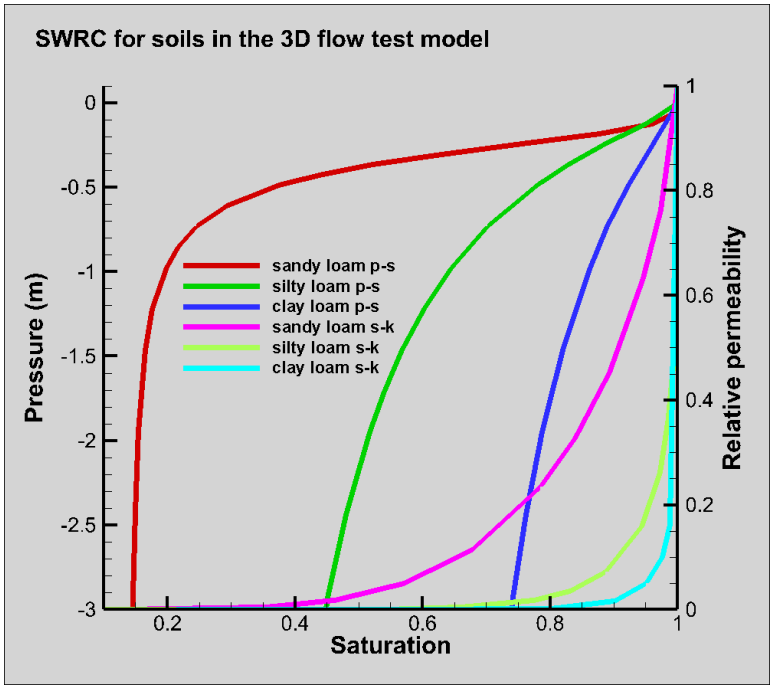

(a)

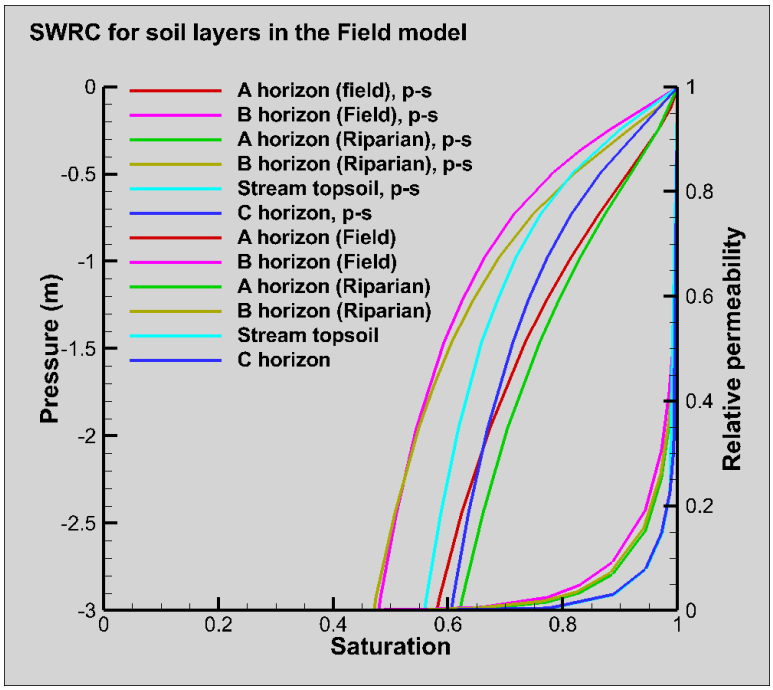

(b)

Figure 5. Soil water retention curves of the soil matrix of the sandy, silty, and clay loams in the conceptual models (a) and the soil matrix of different soil zones measured in WEBS

field site (b). Retrieved from Rosetta database (U.S. Department of Agriculture, 2019) and I. Widurska (personal communication, March 28th, 2021).

The hydraulic conductivity K of the soil matrix will significantly influence the mobility of water in the soil profile. When the soil is unsaturated and both water and gases exist in the soil pores, the Darcy equation for multiple-phase flow in the porous media is:

$$q_i = K_{sat} k_r * i \quad (15)$$

$$K = K_{sat} k_r \quad (16)$$

The subscript i indicates fluid i. q is the water flux [LT^{-1}]. K_{sat} is the saturated hydraulic conductivity [LT^{-1}]. k_r is the relative permeability [dimensionless] and i is the hydraulic gradient [dimensionless]. Generally, the hydraulic conductivity is a constant when the soil is saturated, but is variable when the soil is variably saturated. The saturated hydraulic conductivity K_{sat} for the conceptual soil matrix is obtained from the Rosetta database (U.S. Department of Agriculture, 2019), while the relative permeability k_r is predicted by the corresponding VG parameters.

The soil porosity values are also obtained from the Rosetta database (Table 1) (U.S. Department of Agriculture, 2019). Bulk densities for the different soils were obtained from Zeri et al (2018). The specific storage S_s is calculated by:

$$S_s = \rho_w g(\alpha_{aqf} + n\beta_w) \quad (17)$$

n is the porosity [dimensionless]. The water density ρ_w is 1000 kg/m^3. The acceleration of gravity g is 9.8m/s^2. The compressibility of water β_w is $4.4*10^{-10}$ m*s^2/kg. The compressibility of aquifer α_{aqf} [LT^2M^{-1}] for different soil types is predicted by Younger (1993) (Table 1). The calculated S_s values are also shown in Table 1.

Table 1. Soil matrix hydraulic parameters used in conceptual models

Conceptual soil type	Sandy loam	Silty loam	Clay loam
K_{sat} (m/s)[1]	7.44E-05	4.43E-06	1.71E-06
S_s (m^{-1})[1]	9.96E-05	9.82E-04	9.80E-03
Porosity (dimensionless)[1]	0.375	0.387	0.459
S_{wr} (dimensionless)[1]	0.141	0.1	0.214
α (m^{-1})[1]	3.53	2.67	1.5
β[1]	3.18	1.45	1.25
bulk density (kg/m^3)[2]	1550	1500	1450
aquifer compressibility ($m*s^2/kg$)[3]	1.00E-08	1.00E-07	1.00E-06

[1] Retrieved from Rosetta database (U.S. Department of Agriculture, 2019)

[2] Retrieved from Zeri et al (2018)

[3] Retrieved from Younger (1993)

4.2.1.2 Macropore Parameters

The hydraulic parameters for both the macropores and the interface between the macropores and the soil matrixes are required for simulation.

Frey (S. Frey, personal communication, March 28th, 2021) measured the variation of the volumetric fraction of macropores ω_d within the cropped and riparian soils at the WEBS field during different seasons and reported that ω_d varies from 0.002 to 0.034. Generally, ω_d is greater in fall but smaller in spring. In order to simplify the simulation, ω_d is set to be 0.005 for all conceptual models unless stated otherwise.

Unlike the soil matrix, the macropores have strong hydraulic anisotropy. Macropores tends to extend vertically and may have greater influence on the water movement in vertical direction than in the horizontal or transverse direction. To simplify the simulation, the

saturated hydraulic conductivity K_{sat} in vertical direction is assumed to be 10 times of that in the horizontal or transverse direction The hydraulic parameters for the macropores are shown in Table 2 (Frey et al., 2016; S. Frey, personal communication, March 28th, 2021), which are identical among the three conceptual soils.

Table 2. Macropore parameters used in conceptual models

Macropore parameters		default value
	$K_{sat, x}$	1
K_{sat} (m/s) [1]	$K_{sat, y}$	1
	$K_{sat,z}$	10
S_s (m^{-1}) [1]		1.00E-04
θ_s (dimensionless) [2]		0.9
S_{wr} (dimensionless) [2]		0.05
α (m^{-1}) [2]		25
β (dimensionless) [2]		3.5
bulk density (kg/m3) [1]		265
tortuosity (dimensionless) [1]		0.76
first-order fluid exchange coefficient α_{wd} ($m^{-1}s^{-1}$)[2]		50

[1] Retrieved from S. Frey (personal communication, March 28th, 2021)

[2] Retrieved from Frey et al. (2016)

For the hydraulic properties of the interface between the macropores and soil matrix, the VG parameters and interface hydraulic conductivity K_a are considered (Table 3). In this research, the interface VG parameters are assumed to be the same as the soil matrix VG

parameters. Meanwhile, the linings of the macropores may impede lateral water flow. Hence, the interface hydraulic conductivity K_a is set to be 1/10 of the saturated hydraulic conductivity K_{sat} of the soil matrix.

Table 3. Interface hydraulic parameters used in conceptual models

Conceptual soil type	Sandy loam	Silty loam	Clay loam
$S_{wr,\ interface}$ (dimensionless)[1]	0.141	0.1	0.214
$\alpha_{interface}$ (m^{-1})[1]	3.53	2.67	1.5
$\beta_{interface}$ (dimensionless)[1]	3.18	1.45	1.25
K_a (m/s)	7.44E-06	4.43E-07	1.71E-07

[1] Retrieved from Rosetta database (U.S. Department of Agriculture, 2019)

4.2.1.3 Surface Parameters

The ground surface roughness coefficients and surface storage of water are considered in the simulations. For the current research, the overland domain is divided into four zones with different hydraulic and geological properties, including the Stream bed, Bank riparian, Edge of field riparian, and Field surface. The corresponding surface parameters are shown in Table 4 (S. Frey, personal communication, March 28th, 2021).

Table 4. Surface hydraulic parameters used in conceptual models

	Stream Bed	Bank Riparian	Edge of Field	Field Surface
x friction [$L^{-1/3}T$]	0.01	0.11	0.08	0.03
y friction [$L^{-1/3}T$]	0.01	0.11	0.08	0.03

obstruction storage height (m)	0.0001	0.001	0.001	0.001
rill storage height (m)	0.0001	0.001	0.001	0.001
coupling length (m)	0.02	0.02	0.02	0.02

Retrieved from S. Frey (personal communication, March 28th, 2021)

4.2.2 Soil Parameters for Field Model

Widurska (I. Widurska, personal communication, March 28th, 2021) measured the soil matrix and macropore parameters in the WEBS field site. Unlike the conceptual 1D and 3D models, the Field model has soil matrix and macropores that are divided into zones with different hydraulic properties. The soil matrix of the Field models is divided into 6 zones, including A horizon (corn), A horizon (riparian), B horizon(corn), B horizon (riparian), C horizon, and Stream bed topsoil (Figure 24). The soil matrix parameters for each zone are shown in Table 5 and are based on the field investigations completed at the WEBS site by Widurska (2020). The SWRC of different soil zones in the WEBS site are shown in Figure 5b. Generally, the soil matrix in the Field model is similar with that of the clay loam selected for the conceptual 3D and 1D flow model, but with higher values of hydraulic conductivity and Van Genuchten alpha values.

Table 5. Soil matrix parameters used in the Field model

Field model parameters	C Horizon	B Horizon (Riparian)	B Horizon (corn)	Stream topsoil	A Horizon (Riparian)	A Horizon (corn)
Hydraulic conductivity, K_{iso} (m/s)	4.00E-06	4.00E-06	2.70E-06	5.60E-06	7.00E-06	4.00E-06

Specific storage (m^{-1})	1.00E-04	1.00E-04	1.00E-04	1.00E-04	1.00E-04	1.00E-04
Porosity (dimensionless)	0.53	0.47	0.39	0.8	0.61	0.5
Van Genuchten Residual Saturation, Θ_r	0.1	0.06	0.04	0.12	0.09	0.09
Van Genuchten alpha, α (m^{-1})	0.02	0.02	0.03	0.03	0.01	0.01
Van Genuchten beta, β (dimensionless)	1.31	1.45	1.35	1.31	1.44	1.51
Bulk Density (kg/m^3)	1200	1400	1600	600	1070	1320

Retrieved from I. Widurska (personal communication, March 28th, 2021)

Similarly, the macropore network is divided into 5 zones including Surface (field), Surface (riparian), Bench (field), Bench (riparian), and the Sandy layer. Bench refers to an excavated face during field data collection. I. Widurska (personal communication, March 28th, 2021) measured the volumetric fraction and suggested interface hydraulic conductivity values for each macropore zone in the field, which are shown in Table 6. The other macropore parameters used in the Field model are the same as the HGS default values presented in Table 2.

Table 6. The macropore parameters used in the Field model

Field model macropore	Bench (Riparian)	Bench (Field)	Surface (Riparian)	Surface (Field)	Sandy layer
Volume fraction dual medium (dimensionless)	0.012	0.007	0.011	0.007	0.004
Interface K (m/s)	1.41E-07	1.41E-07	1.41E-07	1.41E-07	1.41E-07

Retrieved from I. Widurska (personal communication, March 28th, 2021)

The ground surface of the Field model is divided into 4 zones, which include Stream bed, Slope riparian, Main riparian, and Field. Generally, the surface domain of the Field model has similar hydraulic properties with the conceptual 3D flow model (Table 4). One exception is the Main riparian zone, whose Manning roughness coefficients in x and y directions, are both elevated to 0.11 $m^{-1/3}s$.

4.2.3 Agricultural Tile Parameters

The agricultural tiles are treated as 1D horizontal pipes without pipe sidewall thickness in the HGS model. The tile diameter is set to be 0.1 m in this research, which is the conventional standard for the inner diameter of an agricultural tile (Welling, 1997). The coupling length and coupling conductivity for 1D pipe flow are required when performing dual continuum calculation. According to HGS default database, the coupling length is 10^{-4} m and coupling conductivity is 1 m/s, which is a conceptual length required by HGS program to calculate tile fluxes.

In this research, the agricultural tiles do not reach the bank slope and intersect with the ground surface. A conceptual discharge node is set manually at the end of the tile near the bank. The boundary condition is set to be simple drain in HGS program, which refers to the drain flux drainage boundary condition (Aquanty, 2015).

4.2.4 Precipitation and Evapotranspiration Data

Three transient precipitation scenarios are considered in this research. The first scenario is the wet weather during spring, which is represented by a conceptual 10-day storm event. The second scenario is the dry weather in summer, which is represented by a conceptual 21-day storm event. The third scenario is the long-term field precipitation condition, which is recorded in WEBS site over the spring, summer and fall seasons. The conceptual 10-day storm event and 21-day storm event are used to study the mechanism of water and gas transport in soil under single precipitation events. In order to simplify the analysis, only the 10-day storm simulation is performed in the investigation of different factors that may influence soil degassing. The 21-day storm simulation is performed to investigate the difference of water and gas transportation under wet and dry weather. The precipitation rates in the conceptual 10-day and 21-day storm events are set manually. S. Frey (personal communication, March 28th, 2021) reported the precipitation in WEBS site from May to October in 2018. It is suggested that the magnitude of the average precipitation rate is 10^{-8} m/s and that of the peak precipitation rate is 10^{-6} m/s. In order to observe an obvious variation in water saturation, the precipitation rate in the Initial stage in the 10-day storm event is set to be $8*10^{-8}$ m/s, which is about 1/6 of the precipitation rate in the Storm stage. Table 7a and 7b show different weather stages and their corresponding precipitation rates for the conceptual 10-day and 21-day storm events. The evapotranspiration was considered to be negligible in the single event scenarios but was incorporated into the long-term field precipitation simulations.

Table 7. The variation of precipitation rate in the conceptual 10-day and 21-day storm events

(a) 10-day storm event

Stage	Time duration	Precipitation rate (m/s)
Initial stage	Day 1	$8*10^{-8}$

Storm stage	Day 2~3	$4.6*10^{-7}$
Recover stage	Day 4~8	$8*10^{-8}$
Drainage stage	Day 9~10	0

(b) 21-day storm event

Stage	Time duration	Precipitation rate (m/s)
Initial drainage stage	Day 1~10	0
Storm stage	Day 11	$4.6*10^{-7}$
Drainage stage	Day 12~21	0

To maintain a relatively high initial soil water saturation at the start of the 10-day storm event, an initial simulation period was required before the 10-day storm simulation. The purpose of the initial simulation is to make sure the soil is in hydraulic equilibrium at the beginning of the storm simulation. In the initial simulation, the initial hydraulic head is set to be 2 m in elevation. The precipitation rate and the duration are set to be $8*10^{-8}$ m/s and 10 days respectively. At the end of the initial simulation, all modeled domains reach hydraulic equilibrium with 0 net water exchange. The hydraulic condition from the last run of the initial simulation is used as the initial condition in the 10-day storm simulation.

The same initial simulation is also performed before the 21-day storm simulation, which provides initial water saturation condition for the later storm simulation. The Initial drainage stage (Table 7b) is set to permit the soil profile to drain and create drier soil conditions to represent the summer weather. Unlike in the 10-day storm simulation, the Storm stage may start when the soil has not yet reached complete hydraulic equilibrium in the 21-day storm event.

Besides the conceptual 10-day and 21-day storm events, a field precipitation record in the WEBS field site is used to estimate the soil gas emission during a long period with multiple and highly variable precipitation events. I. Widurska (personal communication,

March 28th, 2021) reported that the temperature as measured at the WEBS field site between November and April in 2018 is generally lower than 0 °C (Figure 6). Hence, the soil may freeze during winter and spring, which would likely impede the gas exchange between the soil and the atmosphere. In this research, only the soil GHG emission from summer and fall are considered for the long-term simulation using the field precipitation and evapotranspiration record.

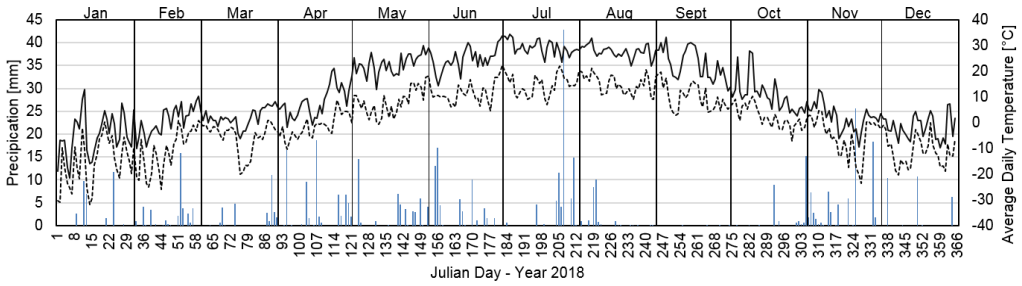

Figure 6. Precipitation and temperature records for the WEBS site in 2018. Retrieved from I. Widurska (personal communication, March 28th, 2021). The solid black line refers to the maximum average daily temperature. The dashed black line refers to minimum average daily temperature. The blue bars refers to the precipitation.

The precipitation and potential evapotranspiration (PET) data reported by S. Frey (personal communication, March 28th, 2021) from May to October 2018 are used in the long term simulation (Figure 7a and 7b). The leaf area indices (LAI) provided by Kross et al. (2013) and Mitchell et al. (1998) are used to estimate the transpiration with corn vegetation and riparian vegetation respectively (Figure 7c).

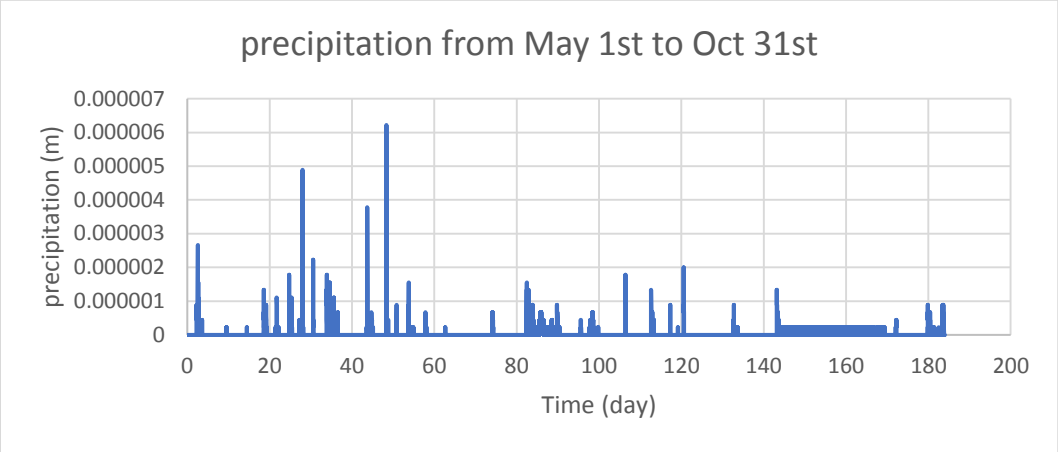

(a)

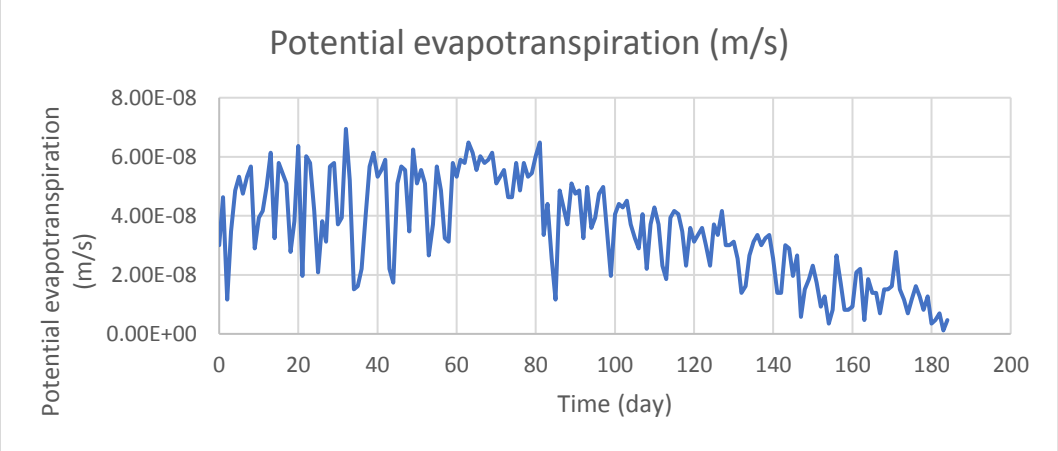

(b)

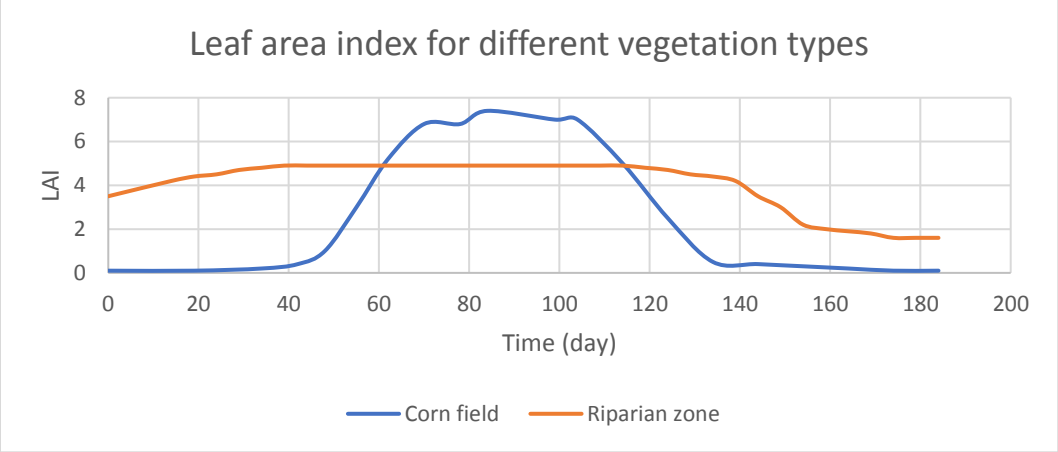

(c)

Figure 7. Precipitation and evapotranspiration parameters used in the Field model. (a) Precipitation record in WEBS site. Retrieved from S. Frey (personal communication,

March 28th, 2021). (b) Potential evapotranspiration record in WEBS site. Retrieved from S. Frey (personal communication, March 28th, 2021). (c) Leaf area index data for corn fields and riparian zones. Retrieved from Kross et al. (2013) and Mitchell et al. (1998). Day 1 refers to May 1st, 2018 and Day 184 refers to October 31st, 2018.

Except for the LAI data and root growth parameters, the other parameters used in the evapotranspiration calculation for two vegetation types are the same (Table 8). In the simulation, the corn is treated as temporary vegetation that has root growth from the beginning of the simulation to the end of September (Day 152).The riparian zone is considered as a steady system that has less variation on root depth. Overall, it is meaningful to consider the vegetation types in the simulation, which may have influence on the water saturation variation and soil GHG emission.

Table 8. Evapotranspiration parameters for different vegetation types

Parameters		Corn field	Riparian zone
pressure head (m)	wp	-150	-150
	fc	-3	-3
	o	-0.1	-0.1
	an	-0.01	-0.01
	e1	-0.2	-0.2
	e2	-2	-2
L_m (m)		0.9	0.9
L_0 (m)		0.1	0.9
C_1		0.19	0.19
C_2		0.19	0.19
C_3		1	1

canopy storage parameter		

Retrieved from S. Frey (personal communication, March 28th, 2021)

Chapter 5

Results and Discussions

This research includes four numerical models, which are different in size, surface landform and soil zone division. The first is a conceptual 3D flow test model (3D model) that is designed to provide a general view of the soil responses to the specified precipitation events driving the simulations. The second is a conceptual 1D-flow model (1D model) that is used to investigate the influence of the macropores on soil water and GHG mobility under a variety of conditions. The third is a 3D Field model, which represents the WEBS field site conditions. The fourth is a 3D Flat-surface field model (Flat Field model) that is modified from the original 3D Field model. The Flat Field model is specifically designed to investigate the influence of land surface topography.

5.1 Conceptual 3D Flow Test Model

5.1.1 Model Description

The initial conceptual 3D flow test model (3D model) was based on an HGS model developed by Dr. Steve Frey and provided as the starting point for the current simulations. The length of the model is 100 m and the width is 14 m. The variation of the height of the model surface is shown in Figure 8. The modelled domain receives precipitation along the top surface and discharges laterally through an exit boundary from x=0 m to 10 m.

Figure 8a shows the 3D flow test model domain. The model is divided into 801 columns and 61 rows. Figure 8b, c, and d show the geometry of the soil matrix, macropores, and overland domains. Unlike the soil matrix and macropore domains that are treated as unstructured domains, the overland domain is subdivided into four zones with different hydraulic properties, including the Stream bed, Bank riparian, Edge of field riparian, and Field riparian (Figure 8d). An agricultural tile is included in the original 3D flow test model. It is situated in the middle of the domain and is 0.1 m in radius.

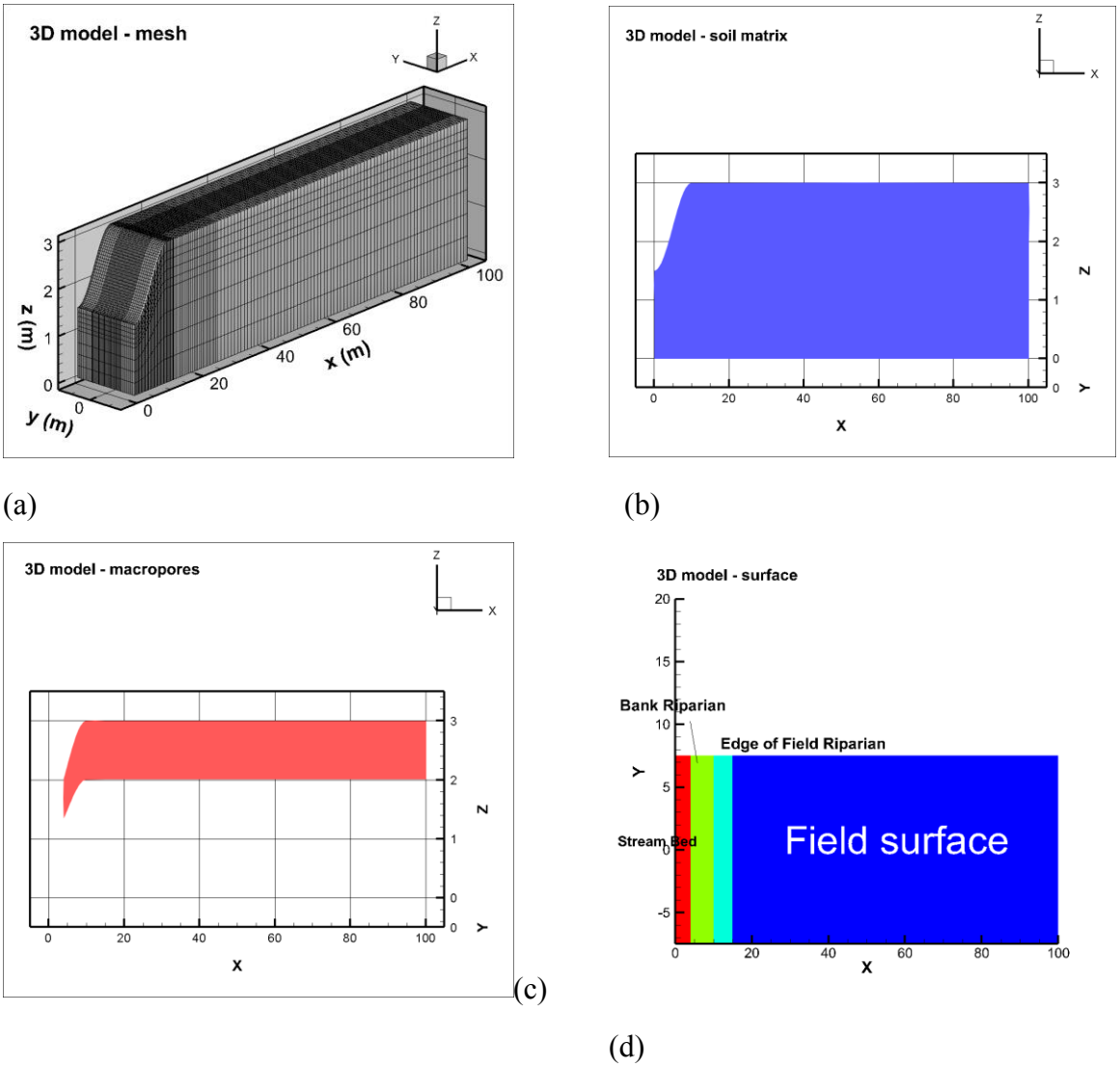

Figure 8. Finite element grid (a) and the zonation for soil matrix (b), macropores (c) and ground surface (d) for conceptual 3D flow test model. All graphical units are in (m).

Three common soil types with different hydraulic properties are used in the 3D flow test model, which include the sandy loam, silty loam, and clay loam. Several different combinations of the soil matrix, macropores, and agriculture tile positioning are tested in the simulation experiments to investigate the effects of each soil system component on soil water and gas occurrence and mobility.

5.1.2 Model with Only Soil Matrix

In this first set of simulations, the soil profile is considered to consist of a massive and homogeneous soil matrix with neither the macropores nor tiles being considered in the numerical experiments.

During the conceptual 10-day storm simulation, the silty loam and the clay loam remain fully saturated. The water saturation only varies in the sandy loam. The variation rate of the water volume (m3/s) in the soil matrix (PM) are plotted respectively in Figure 9a. When the Storm stage starts, PM does not reach the peak value immediately in the sandy loam. Similarly, the discharge of water in the soil matrix is retarded when the precipitation drops to the rate before the storm (Recover stage). When the precipitation ends, PM starts to drop at a relatively constant rate.

Figure 9b indicates the variation of water accumulation rate in the overland domain (OVERLAND) and the water discharging rate through the outer boundary (OUTBC). Generally, the silt loam behaves the same as the clay loam. For these two soils, OVERLAND and OUTBC values increase sharply when the precipitation event begins. Later, the OVERLAND value falls back to zero while OUTBC value remains high and constant. As the precipitation rate drops back to the initial value, OVERLAND curve decreases to negative values, which indicates that water discharges out from the overland domain reducing stored surface water. In the Recover stage, both OVERLAND and OUTBC tend to return to their original levels. Finally, when the precipitation ends, the overland domain discharges again and the OUTBC value decreases progressively for the silty loam and clay loam. For sandy loam, similar variation tendencies on OVERLAND and OUTBC curves are observed. However, there are two peaks in the OVERLAND curve and a delay on the increase of OUTBC curve in the Storm stage in the permeable sandy loam.

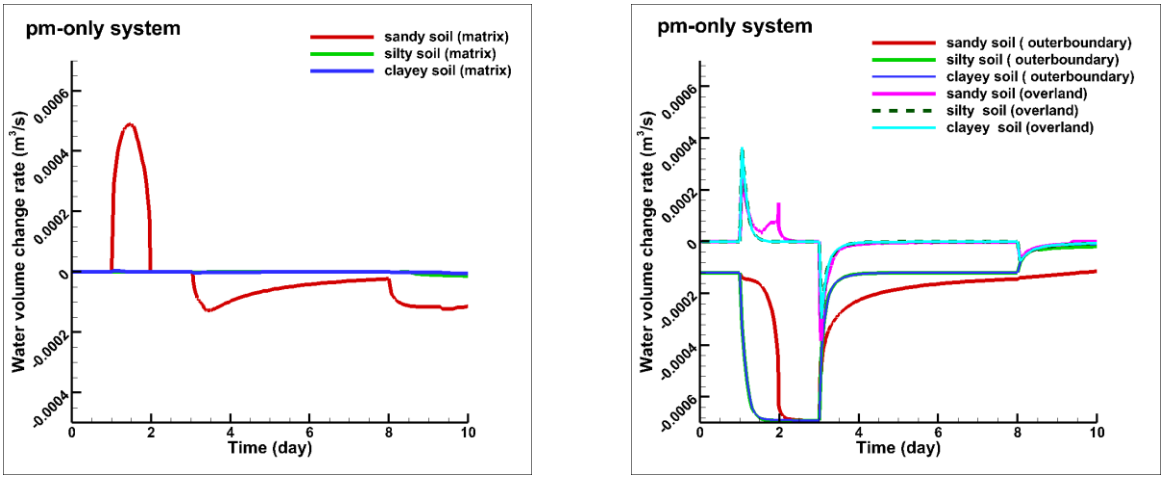

(a) (b)

Figure 9. (a) Water storage variation in soil matrix when only considering the soil matrix during the 10-day storm simulation. (b) Overland storage variation and the outer boundary flow variation when only considering the soil matrix during the 10-day storm simulation.

Under the imposed initial conditions, there is no change is storage within the subsurface for the silty loam and the clay loam scenarios because the matrix is essentially fully saturated throughout the simulation. The lag of PM variation in the sandy loam might result from the low hydraulic conductivity in the unsaturated zone, which impedes the water movement through soil matrix. After reaching the peak, PM curve drops due to the decrease of the pore space that can accept water. Figure 10 shows the variation of the soil wetting curve with time. Freeze and Cherry (1979) suggested that the water saturation change does not increase linearly with time or depth. During the late stage of wetting, few voids are left in the soil matrix. Subsequently, as the shallow soil becomes fully saturated, the downward infiltration of water may be retarded and the water storage in the Overland domain may increase. Hence, there is a second peak of the PM curve in sandy loam.

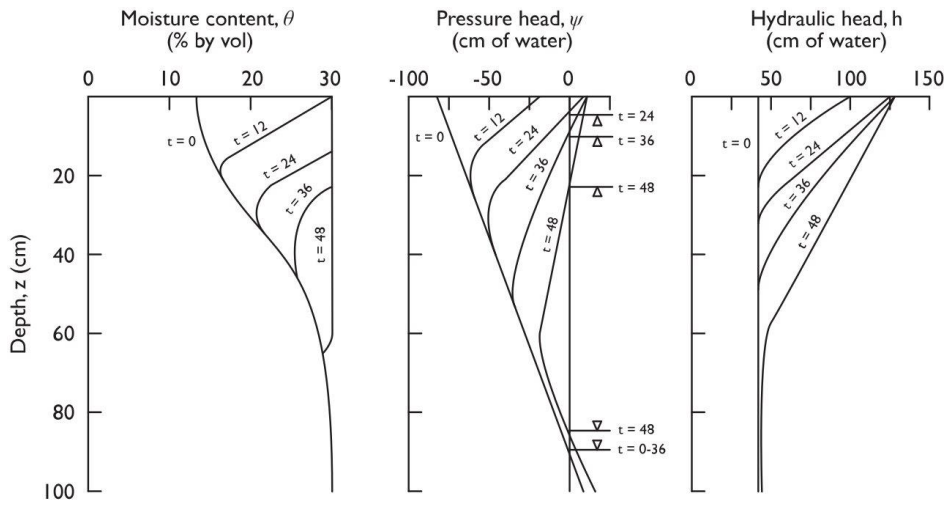

Figure 10. Soil wetting curves. Retrieved from Freeze and Cherry (1979).

The results of the conceptual 21-day storm simulation are shown in Figure 11a and 11b, which imitates a drier soil condition during summer. In this simulation, the water saturation varies dramatically in permeable soil like sandy loam, but only slightly in less permeable soils like silty loam and clay loam.

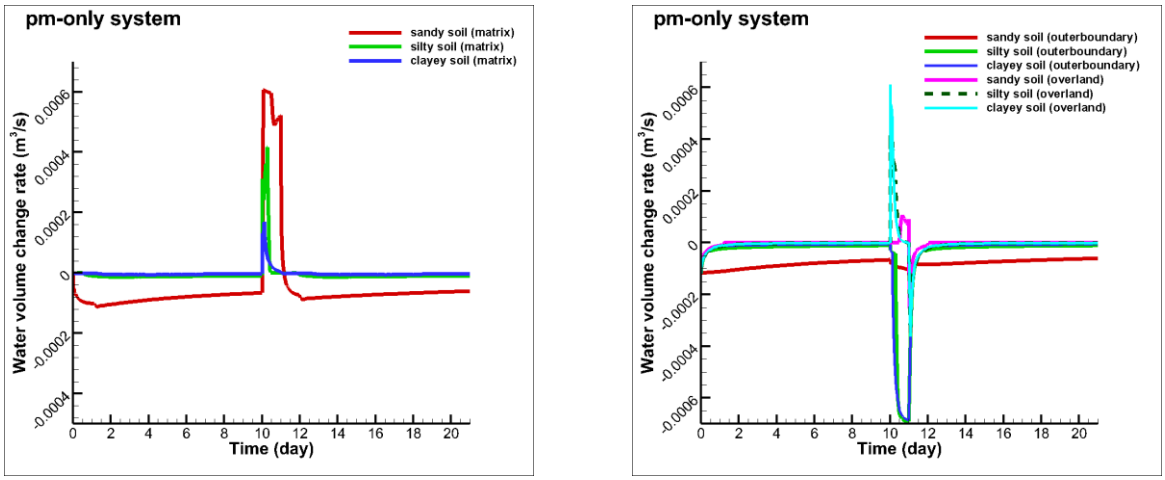

(a) (b)

Figure 11. (a) Water storage variation in soil matrix when only considering the soil matrix during the 21-day storm simulation. (b) Overland storage variation and the outer boundary flow variation when only considering the soil matrix during the 21-day storm simulation.

Like the results of the 10-day storm simulation that represents wetter soil conditions, the sandy loam has the greatest water storage variation. Delays of the increase of OVERLAND curve and the decrease of OUTBC curve for the sandy loam curve are also observed. Meanwhile, the OVERLAND curve of the sandy loam has two peaks during the Storm stage. The mechanism of soil water transport under dry soil conditions is similar to that under the wetter conditions. Although the storms last for 1 day in both the 10-day and 21-day simulations, the soil tends to have lower water saturation in the 21-day simulation because there is more open pore space for the soils to accept the infiltrated water, which leads to greater water storage increase under these drier conditions.

5.1.3 Model with Soil Matrix and Macropores

In this second set of simulations, macropores are included within the upper 1 m of the domain as indicated in Figure 8c. Again, no tiles are included. During the 10-day storm simulation, all modelled profiles are initially partially saturated as a result of the influence of the macropores and variations in water accumulation rate in both the soil matrix (PM) and macropores (DUAL) are observed for the three soil types.

PM and DUAL curves reach their peaks or valleys instantly after the precipitation rate changes (Figure 12a). Compared with PM curves, the Dual curves have negligible variations. Generally, the sandy loam tends to have a larger increase in PM and smaller increase in DUAL since water mainly passes through the matrix instead of the macropores in the more permeable soil. However, one exception is the PM value for the sandy loam when precipitation drops from peak value to the initial value. The valley of PM curve for the sandy loam is shallower than that for the silty loam or clay loam, which indicates that the sandy loam has the lowest initial discharging rate in soil matrix when precipitation is diminished. This likely reflects the rapid draining characteristics of the macropores that are very active within the silt and clay loams.

No water accumulation in overland domain is observed because all modeled domains

remain partially saturated and can accept all of precipitation during the course of the simulation periods (Figure 12b). In the Storm stage, OUTBC curves reach their lowest points when the precipitation rate begins to drop. Generally, the permeable soil has low absolute OUTBC values in the Storm stage, but high absolute OUTBC values in the Recover stage and drainage stage.

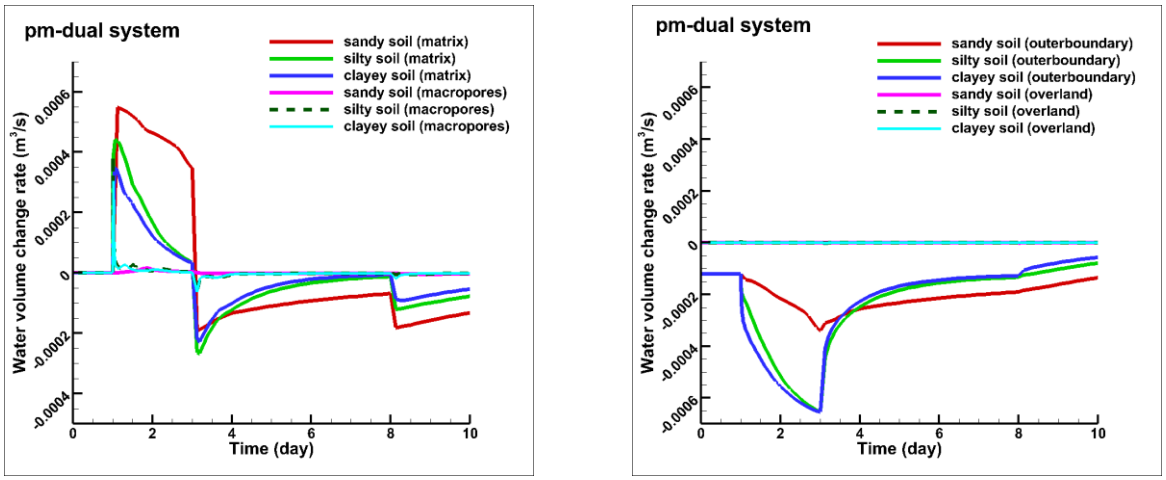

(a) (b)

Figure 12. (a) Water storage variation in soil matrix when considering both the soil matrix and macropores during the 10-day simulation. (b) Overland storage variation and the outer boundary flow variation when considering both the soil matrix and macropores during the 10-day simulation.

The fluctuations of DUAL curves may indicate the frequent water exchange between the soil matrix and macropores. They may also be simulation errors. Generally, the macropores occupy small volumetric space within the soil and have limited influence on the total water accumulation variation.

The instant responses of PM and DUAL to the precipitation change result from the elevated drainage capacity of the macropores. Macropores enhance the drainage capacity of the soil and enable more water to enter the soil instead of draining as surface flow. Subsequently, the PM peak is higher and the PM valley is deeper for the same soil in the

simulations that incorporate macropore flow.

The clay loam and silty loam are less permeable than the sandy loam and have less water storage variation during the Storm stage. However, even small changes in PM can result in significant variations in the water saturation and the water table location in less permeable soils. Hence, the silty loam and clay loam have higher water tables at the end of the Storm stage, which leads to higher lateral hydraulic gradients, which influences the discharge rates. Therefore, the magnitude of variability of both the PM and OUTBC curves for the silty loam and clay loam are higher than that for the sandy loam (Figure 12a and 12b). As the soils drain and the difference between the water table elevations in the different soils diminish, the drainage rate in the sandy loam surpass those in the silty loam and clay loam due to the high hydraulic conductivity of the sandy loam.

OUTBC values do not reach a constant rate during the Storm stage for the three soils, which is different from what was observed in the previous scenario without the macropores. The results show that all three soil types remain partially saturated in the soil matrix throughout the simulations. The precipitation infiltrates directly into the matrix and moves through the macropores so that there is no increase in surface water storage.

Similar behavior for the PM, DUAL, OUTBC, and OVERLAND rates are observed in the results of the 21-day storm simulation (Figure 13a and 13b). Under dry conditions, the sandy loam has the greatest water storage increase during storm, while the clay loam has the lowest. Compared with the results of the 10-day storm simulation, the amount of water storage increase in the Storm stage is greater in the 21-day storm simulation, which may be related with the lower initial water saturation of soil.

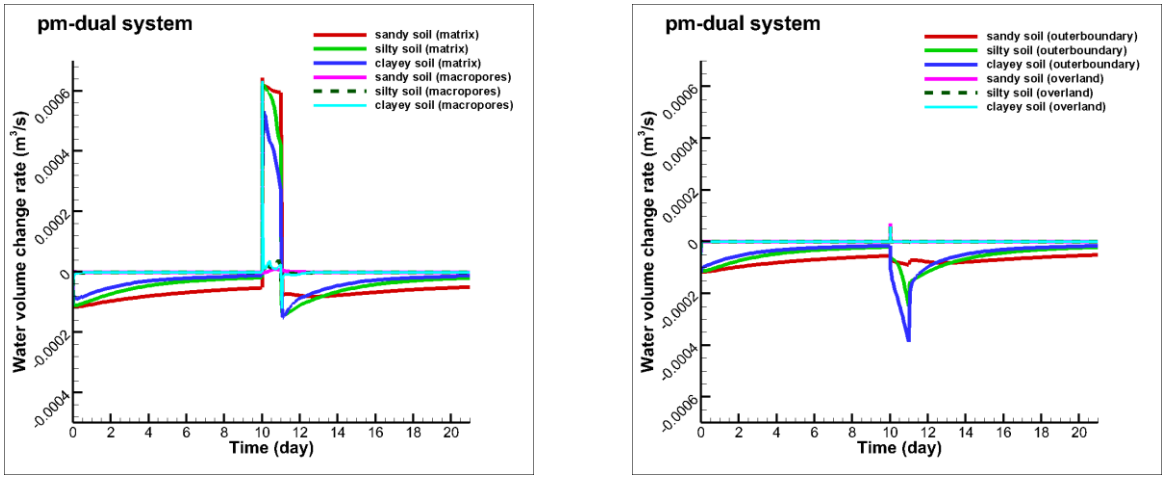

(a) (b)

Figure 13. (a) Water storage variation in soil matrix when considering both the soil matrix and macropores during the 21-day simulation. (b) Overland storage variation and the outer boundary flow variation when considering both the soil matrix and macropores during the 21-day simulation.

5.1.4 Model with Soil Matrix, Macropores, and an Agricultural Tile

In addition to both the soil matrix and macropores being represented in this scenario, an agricultural tile is set in the middle of the test domain at the elevation of 2 m (1 m deep). The tile extends from x = 20 m to x = 100 m.

During the 10-day storm scenario, all modeled domains remain partially saturated during the entire period of the the simulations. The initial water table is lower than those found in simulations without tiles. Generally, the PM, DUAL, OVERLAND and OUTBC curves behave similarly to those in the previous 3D model with soil matrix and macropores (Figure 14a and 14b) and the shape of PM curves are all convex. Dense fluctuations of PM curve in the clay loam is observed, which may be minor numerical instability.

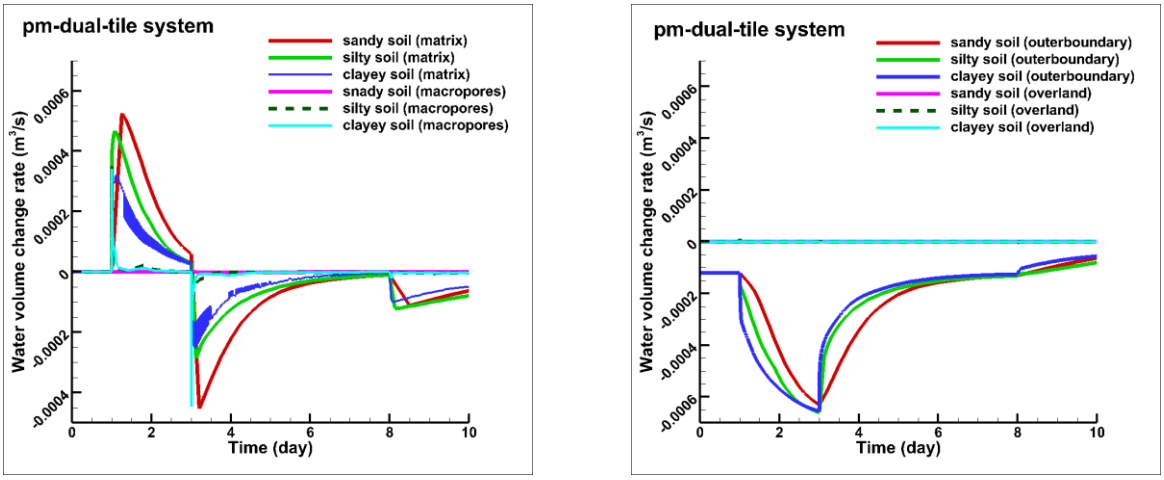

(a) (b)

Figure 14. (a) Water storage variation in soil matrix when considering the soil matrix, macropores, and agricultural tile during the 10-day storm simulation. (b) Overland storage variation and the outer boundary flow vitiation when considering the soil matrix, macropores, and agricultural tile the 10-day storm simulation.

The deepened valley for the sandy loam may be attribute to the enhanced soil drainage by the agricultural tile. The tile connects the vertical macropores and provides a pathway for the macropore flow to discharge and the water storage variation in the soil matrix is reduced since less water will be retained. Subsequently, the OUTBC value in the sandy loam during the Storm stage increases because less water is held in soil. The tile is able to control the water storage and may reduce the fluctuation of water saturation under wet weather (10-day storm simulation). Hence, the PM valley for the sandy loam becomes the deepest due to the strongest drainage capacity. Compared with the results of the pm-dual systems during the 10-day storm simulation, the influence of tile on the PM and OUTBC curves for silty loam and clay loam is negligible in the pm-dual-tile system, which might be due to the high water retention capacity of the soil matrixes.

Similar variation tendencies of the PM, DUAL, OUTBC and OVERLAND curves are found in the results of the 21-day storm simulation (Figure 15a and 15b). Under drier

conditions, the reduced soil water saturation before the storm enables the soil to absorb more infiltrated water. The tile appears to have a minor influence on the water storage variation in less permeable soils under dry conditions.

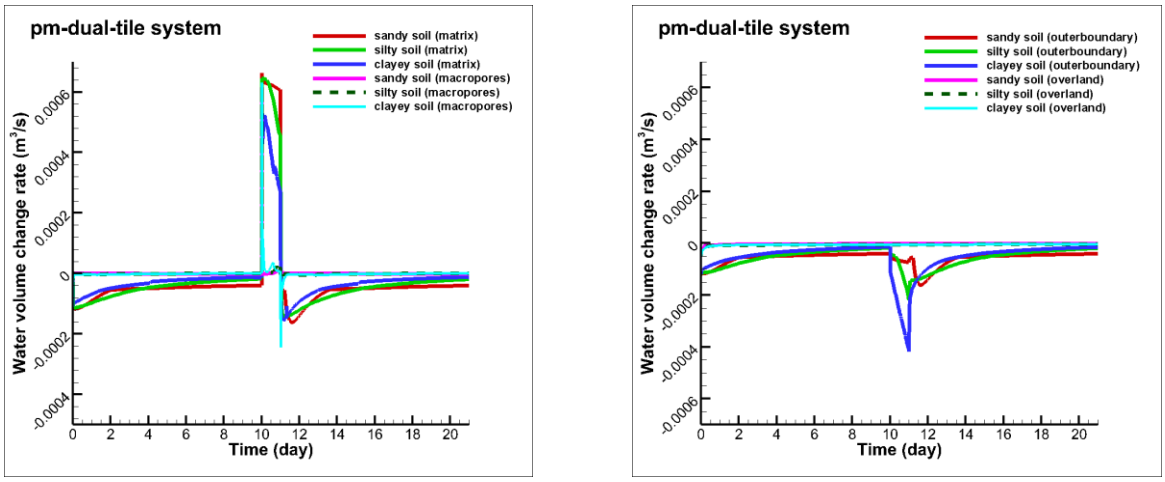

(a) (b)

Figure 15. (a) Water storage variation in soil matrix when considering the soil matrix, macropores, and agricultural tile during the 21-day storm simulation. (b) Overland storage variation and the outer boundary flow vitiation when considering the soil matrix, macropores, and agricultural tile the 21-day storm simulation.

5.1.5 General Comparison

The results of the 10-day storm simulation (wetter climatic conditions) and the 21-day storm simulation (drier climatic conditions) are plotted and compared by soil type in Figure 16 and 17.

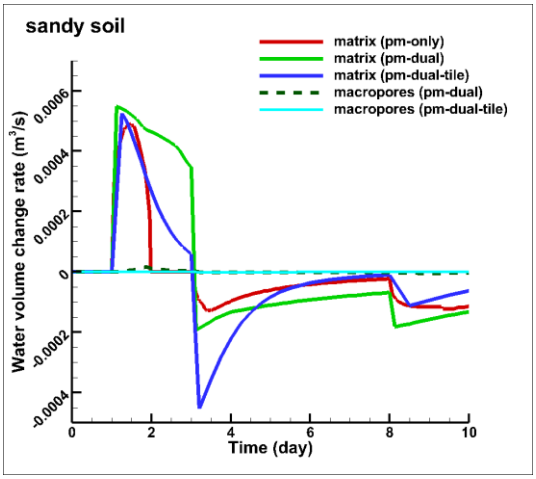

(a)

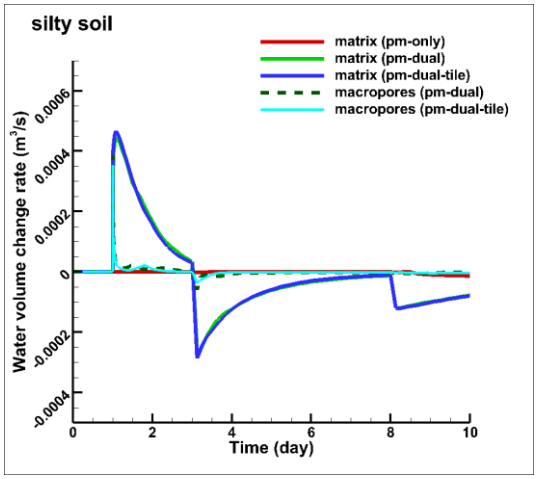

(b)

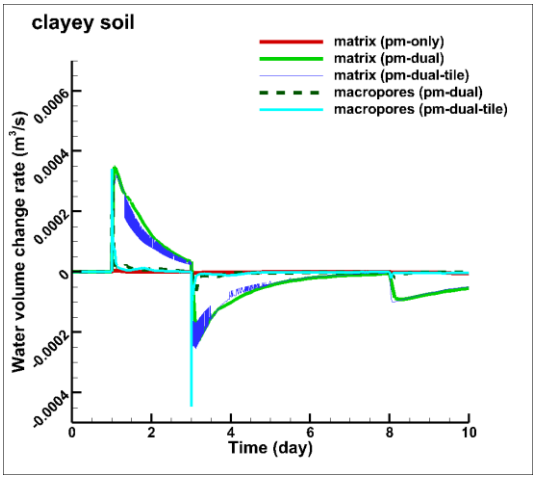

(c)

Figure 16. Comparisons of PM and DUAL curves between different soils during the 10-day storm simulation. (a) Sandy loam, (b) silty loam, and (c) clay loam.

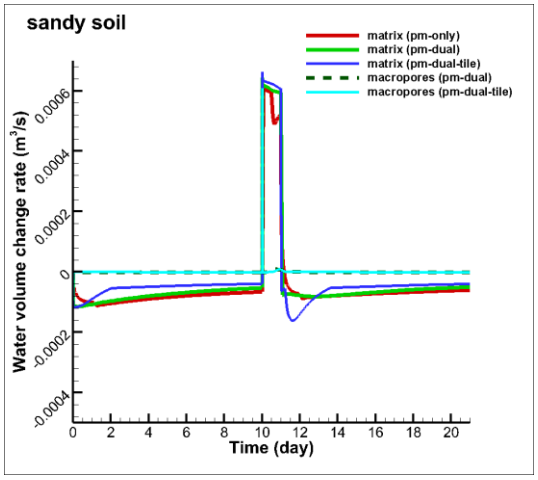

(a)

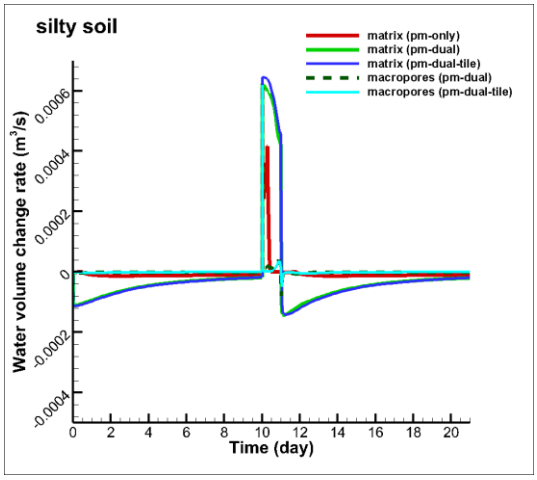

(b)

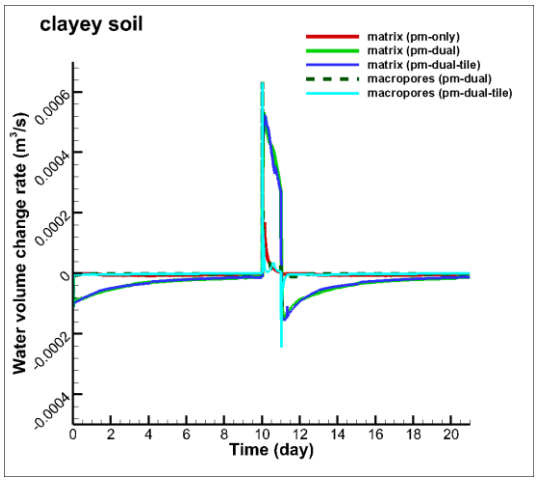

(c)

Figure 17. Comparisons of PM and DUAL curves between different soils during the 21-day storm simulation. (a) Sandy loam, (b) silty loam, and (c) clay loam.

In both the 10-day and 21-day storm simulations, the three soil scenarios (pm-only, pm-dual, and pm-dual-tile systems) with the sandy loam matrix have obvious water storage variation. These storage change trends are less obvious for the lower permeability soils due to the higher initial soil water contents. Overall, the macropores appear to enhance the water storage change during the precipitation events. More water enters the soil, more soil gas is released to the environment. Hence, it is predicted that the macropores can enhance the soil

GHG emission in all three conceptual soils.

Although the agricultural tile can be considered as an artificial macropore that can enhance soil drainage, it appears to play different roles in the two storm simulations. In the 10-day storm simulation, it diminishes the water storage increase during storms and leads to a weaker soil degassing in the pm-dual-tile system compared with the pm-dual system. In the 21-day storm simulation, however, a contrary condition occurs. The agricultural tile lowers initial soil water saturation and more space is available to accept infiltrated water during the storm event compared with the soil system without tile. Subsequently, higher soil degassing is expected for the pm-dual-tile system under the drier conditions.

The tile effect is more pronounced in permeable soils than in less permeable soils. For soils that are less permeable, no significant difference is observed among the PM curves in different soil systems. Hence, the promotion of water storage variation by the tile appears weaker in less permeable soils. Overall, the role that the agricultural tile plays in soil water and gas mobility is influenced by the water saturation condition and water drainage capacity of the soil.

5.2 Conceptual 1D Flow Model

5.2.1 Model Description

In order to further investigate the influence of the macroporosity on soil water and gas mobility, a conceptual 1D flow model is constructed using the HGS framework. .

Figure 18a shows the domain discretization. The conceptual 1D flow model is divided into 200 blocks in z-direction. Figure 18 b, c, and d show the geometry of the soil matrix, macropores, and overland domains of the conceptual 1D flow model. The agricultural tile is excluded in the model. Indeed, the 1D model represents a soil cell right above a tile, where the water movement is dominated by vertical flow. Only vertical flow is considered in this model. Incident precipitation enters through the top surface and leaves from the bottom boundary of the domain. No surface runoff is considered in the conceptual 1D flow model.

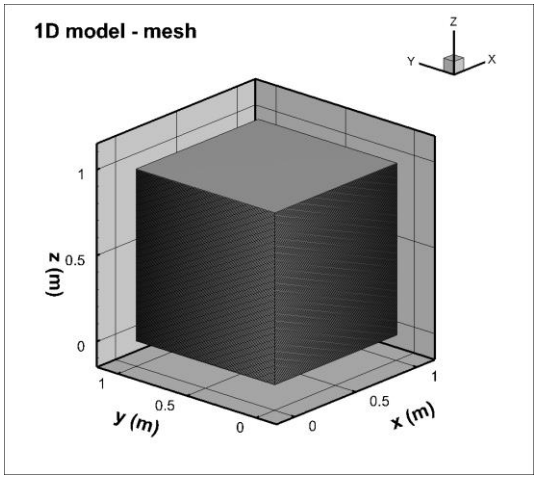

(a)

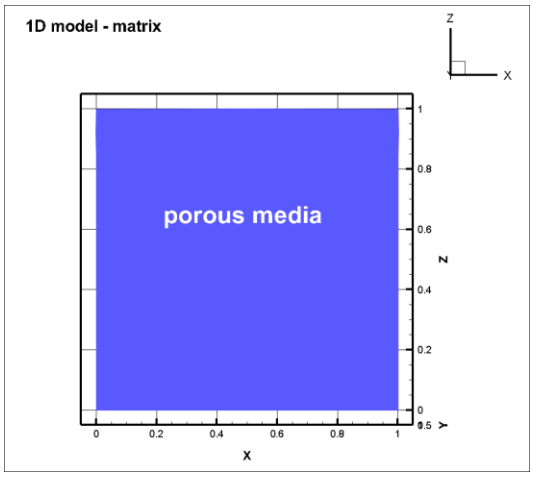

(b)

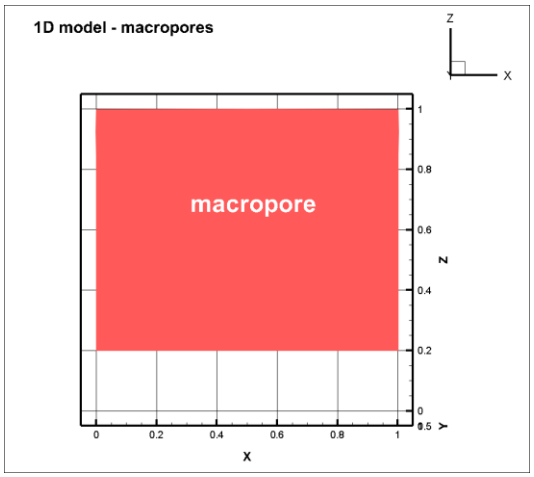

(c)

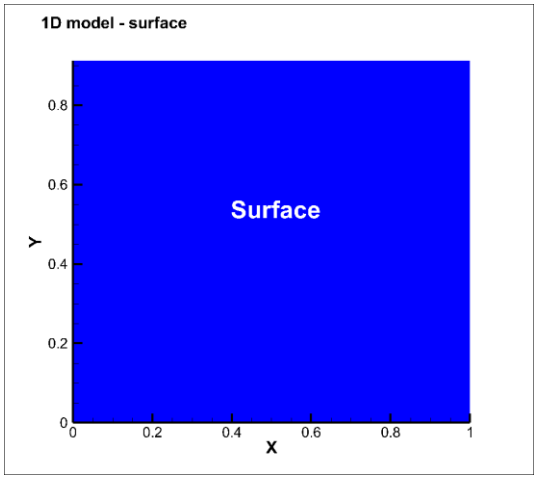

(d)

Figure 18. Finite element grid (a) and the zonation for soil matrix (b), macropores (c) and ground surface (d) for conceptual 1D flow model. All graphical units are in (m). The 1D flow model is a cubic.

Three soil types are used in the conceptual 1D flow model, including the sandy loam, silty loam, and clay loam, which are the same as those used in the 3D conceptual models. The influence of macropore volumetric fraction, which is the portion occupied by macropores by the total porosity, on soil gas mobility is investigated. I. Widurska (personal

communication, March 28th, 2021) suggested that the macropore volumetric fraction varies with the annual seasons from 0.005 to 0.03 in the WEBS field site. Generally, the macropore volumetric fraction is small in spring and larger in fall. In this research, three macropore volumetric fractions are considered including 0.005, 0.01, and 0.02, which are assumed to represent the macropore conditions in spring, summer, and fall respectively. To simplify the analysis, only the 10-day storm scenario is investigated with the 1D flow model. The simulation results of the 1D flow model may provide a general view of seasonal variation of macropore characteristics on soil gas mobility.

5.2.2 Model with Different Volumetric Fractions

Figure 19 indicates the water accumulation rate change with time in the 1D flow model for the three different macropore volumetric fractions and soil matrix types. In the 1D model simulations, the silty loam appears to show the most water volume change in the matrix when the precipitation rate changes. This finding contradicts with the results of the 3D test model, where the sandy loam had the greatest water volume change.

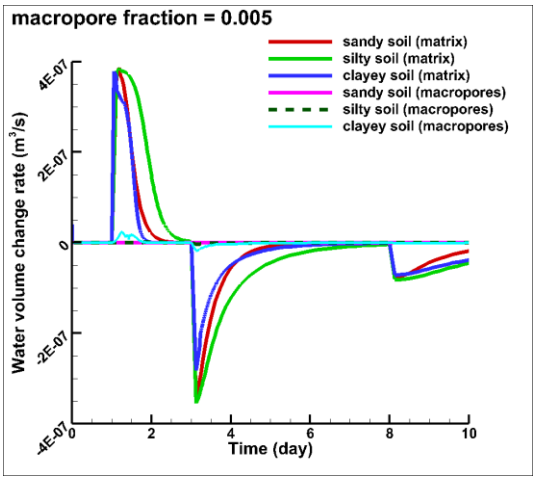

(a)

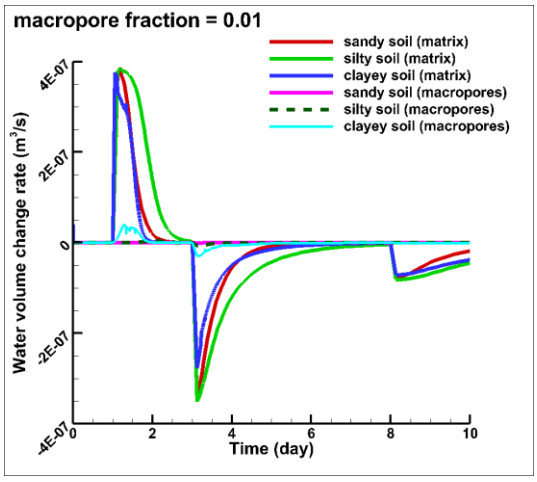

(b)

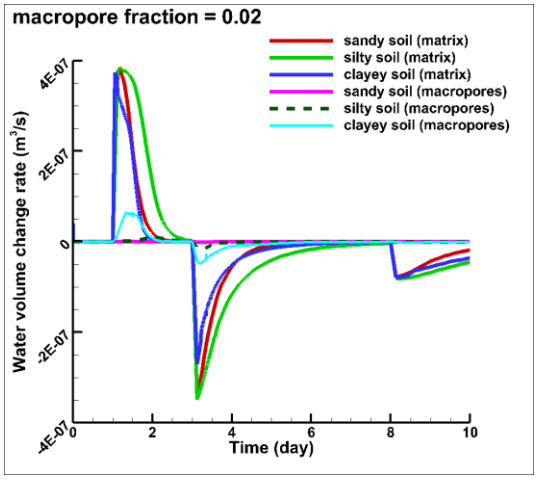

(c)

Figure 19. Comparison of PM and Dual curves for different soils under same macropore volumetric fraction. (a) Sandy loam, (b) silty loam, and (c) clay loam.

Such contradiction may be caused by the high drainage capacity of the sandy loam matrix. Figure 20 shows the seepage rate through different soils. For all three simulations with different macropore fractions, the sandy loam has higher seepage than the silty loam. The results suggest that water tends to drain more rapidly out of the sandy loam as expected and the increase in soil water storage small. The silty loam is less permeable, drains slower and is able to store more infiltrating water. Therefore, the increase of water storage in the silty loam is higher than that in the sandy loam during the storm. Though the clay loam has low drainage capacity as well, it has the highest water saturation before the storm. To simulate the water saturation condition in the 1D flow model, two observation points are set at x = 0 m and y = 0 m. The shallow point is at the depth of 0.15 m, while the deep point is at the depth of 0.45 m. Figure 21 suggests that the water saturation is high at both shallow and deep observation points in the clay loam. Meanwhile, the conceptual storm event has the smallest promotion of water storage in the clay loam. Hence, the clay loam has limit space to accept the infiltrated water and the soil degassing is weak.

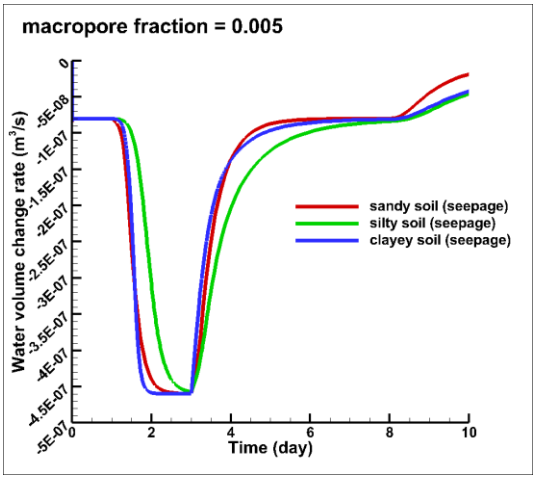

(a)

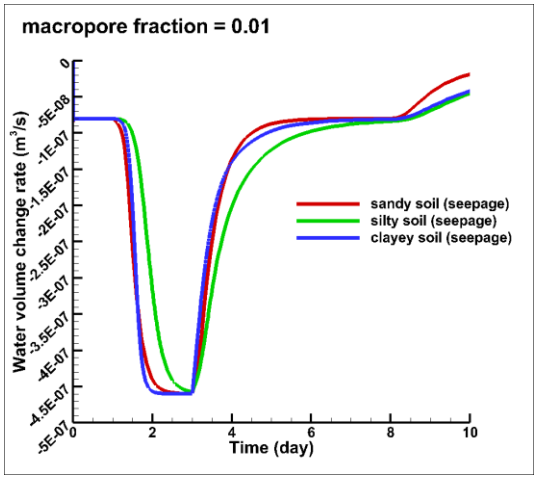

(b)

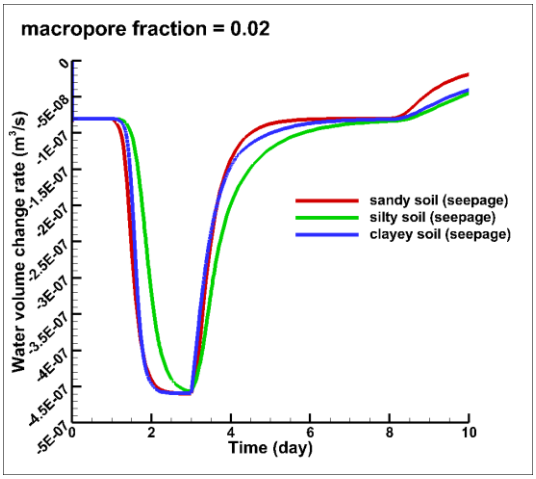

(c)

Figure 20. Comparison of seepage curves for different soils under same macropore volumetric fraction. (a) 0.005 macropore fraction, (b) 0.01 macropore fraction, and (c) 0.02 macropore fraction.

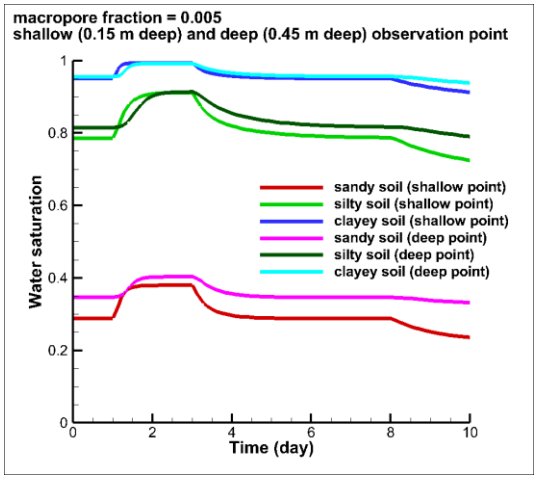

(a)

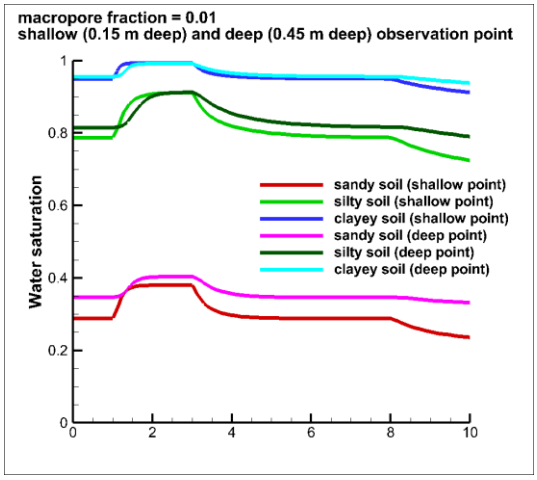

(b)

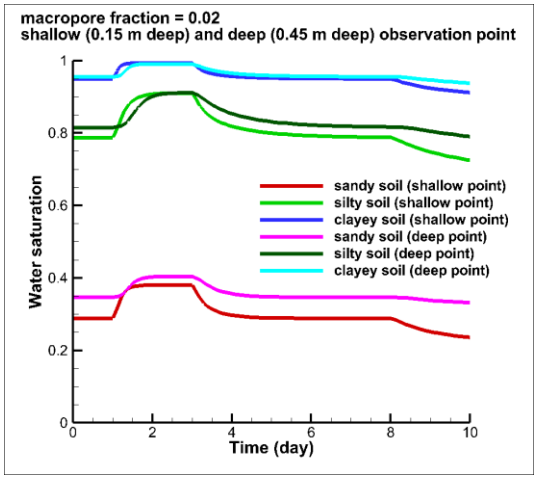

(c)

Figure 21. Soil water saturation at shallow (0.15 m deep) and deep (0.45 m deep) observation points in the conceptual 1D flow model. (a) 0.005 macropore fraction, (b) 0.01 macropore fraction, and (c) 0.02 macropore fraction.

Another factor that may contribute to the difference between the simulation results of the 3D and 1D models is the difference in the system size and complexity. In the 1D model, only the vertical flow is considered. The lateral and transverse transport of water is ignored, which may lead to the underestimation of the drainage capacity for soils. Meanwhile, the difference of the model shape and size may also influence the simulation results.

5.2.3 Model with Different Soil Matrixes

The water accumulation rate changes in the matrix and macropores with different macropore fractions in the same soil types are shown in Figure 22. For the sandy loam and silty loam, the influence of macropore fraction variation on water storage variation is negligible. For the clay loam, a slight increase of DUAL value is observed when the macropore fraction increases. However, the change in PM value with the macropore fraction is negligible.

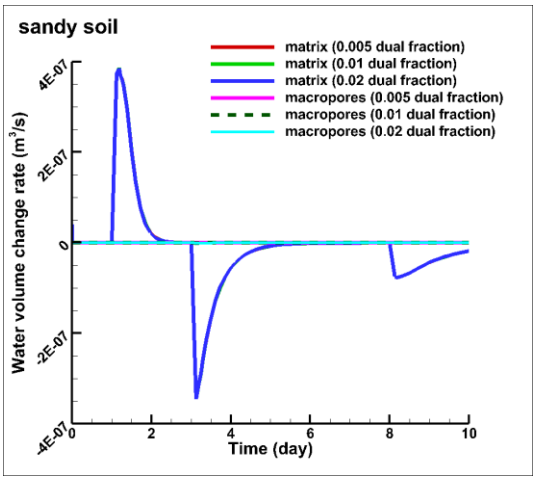

(a)

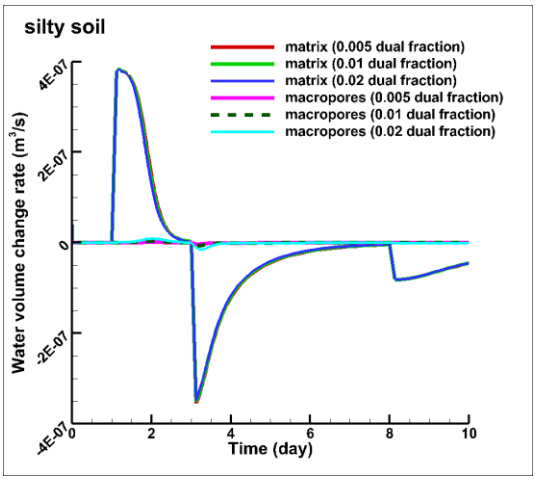

(b)

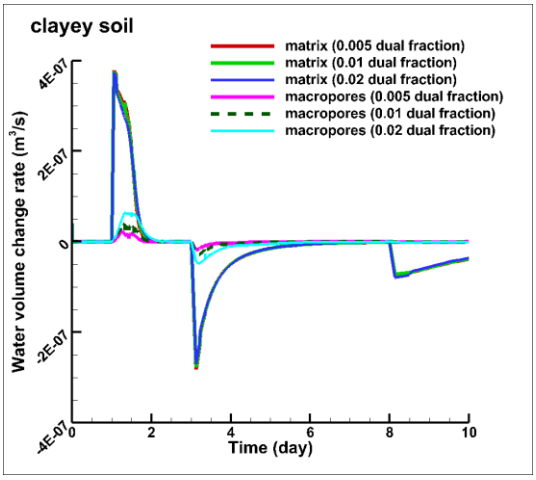

(c)

Figure 22. Comparison of PM and Dual curves for the same soil under different macropore volumetric fraction. (a) Sandy loam, (b) silty loam, and (c) clay loam.

Overall, the water accumulation rate in the matrix does not seem to be very sensitive to the macropore fraction changes between 0.005 and 0.02 for the three simulated soil types. The water accumulation rate in the macropores is more likely to be influenced by the change of macropore fraction. The less permeable the soil matrix is, the more significant such influence will be.

5.3 Field Model

5.3.1 Model Description

I. Widurska (personal communication, March 28th, 2021) built a 3D flow field model (Field model) based on the data measured at the WEBS field site. This model was adopted in the current research to examine a set of field-based simulations. The length of the field model is 30 m and the width is 14 m. Unlike the 3D flow test model that has a flat ground surface, the Field model has some surface topography as illustrated in Figure 23 and 24. The relative elevation for the flat field area is 3.17 m and a berm and drainage face are set along left side of the model (from x = 0 m to x = 10.5 m), with a relative elevation ranging from 1.5 m to 3.48 m. The surface topography represents measurements made at the WEBS field site. A tile is included in the Field model at y = 0 m and extends from extending from x = 6.5 m to 30 m, whose elevation is 2.5 m (about 0.67 m deep).

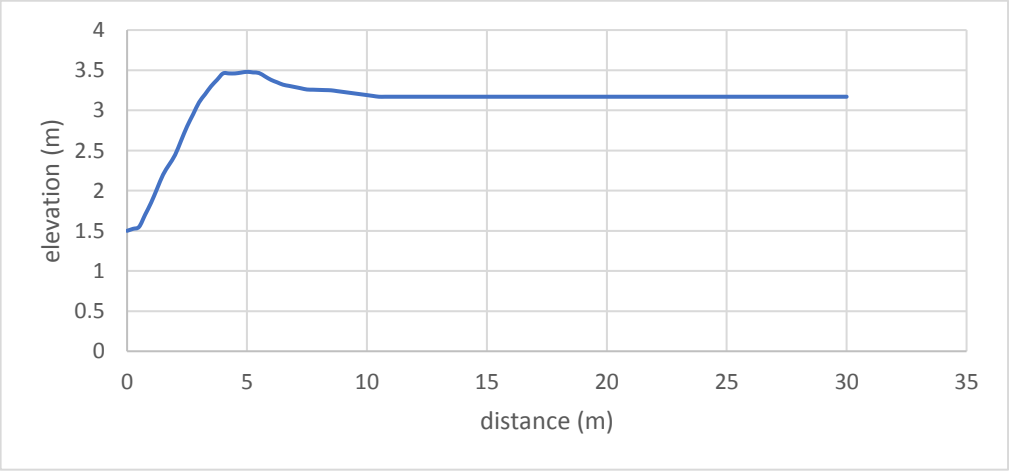

Figure 23. The field profile at WEBS field site. Modified from I. Widurska (personal

communication, March 28th, 2021).

The stratigraphic zonation adopted for the Field model is shown in Figure 24. The Field model is divided into 802 columns and 61 rows (Figure 24a). Based on field information obtained by I. Widurska (personal communication, March 28th, 2021) a thick clay layer (C horizon) forms the lower stratigraphic unit, overlain by the B and A soil horizons. The riparian area is also divided horizontally and vertically in the vicinity of the berm area and sloped left lateral boundary (Figure 24 b). The zonation adopted for the macropore representation is illustrated in Figure 24c, which also reflects field observations. The shallow subsurface is subdivided into Surface and Bench zones in both riparian and field area. The bottom of the macropore domain is a sandy unit. The surface domain has been subdivided into 4 areas with varying characteristics to represent the conditions observed in the field (Figure 24d).

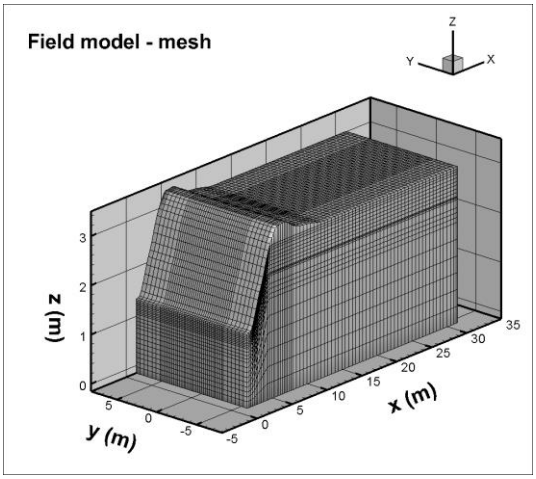

(a)

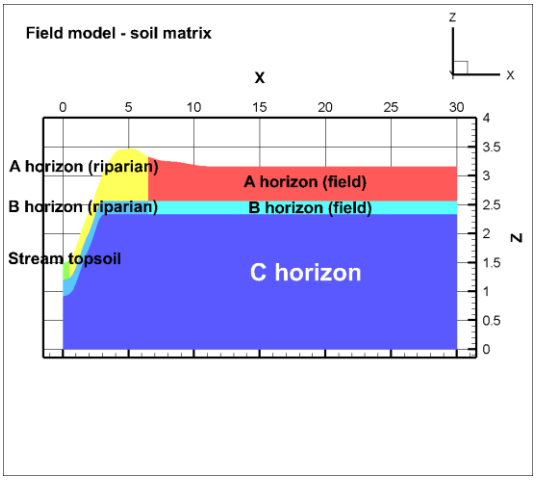

(b)

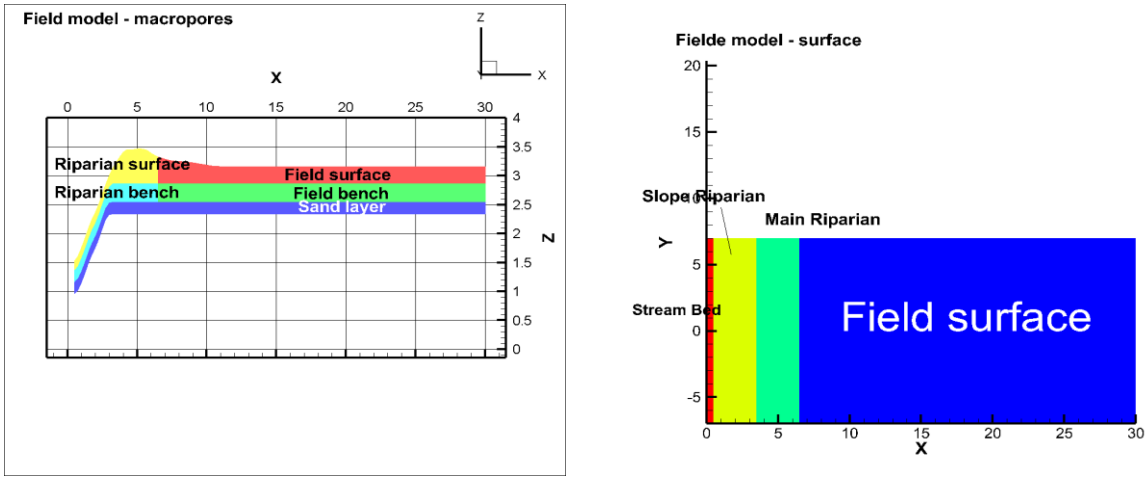

(c) (d)

Figure 24. Finite element grid (a) and the zonation for soil matrix (b), macropores (c) and ground surface (d) for 3D flow Field model. All graphical units are in (m).

The hydraulic parameters used in the Field model are either derived from measurements made by I. Widurska (personal communication, March 28th, 2021) at WEBS field site or derived from the literature as outlined in detail in the Methods section. The soil heterogeneity is considered in the Field model and each soil zone has different hydraulic properties.

5.3.2 Model with Soil Matrix, Macropores, and an Agricultural Tile

In the Field model, the hydraulic conductivity varies from $2.7*10^{-6}$ to $7*10^{-6}$ m/s (I. Widurska, personal communication, March 28th, 2021). The volumetric fraction of macropores varies from 0.004 to 0.012. Generally, the surficial zones in the Field model have greater hydraulic conductivity and macropore volumetric fraction (Table 5 and 6).

To simplify the analysis, only the 10-day storm simulation scenario is investigated with the Field model (Figure 25). Similar with the conceptual 3D flow test model, the water storage variation in the soil matrix is greater than that in the macropores. However, the fluctuation of total water storage variation in the Field model is weaker than that in the

conceptual 3D flow test model during the same storm event. Several differences appear between the results of the Field model and the 3D flow test model.

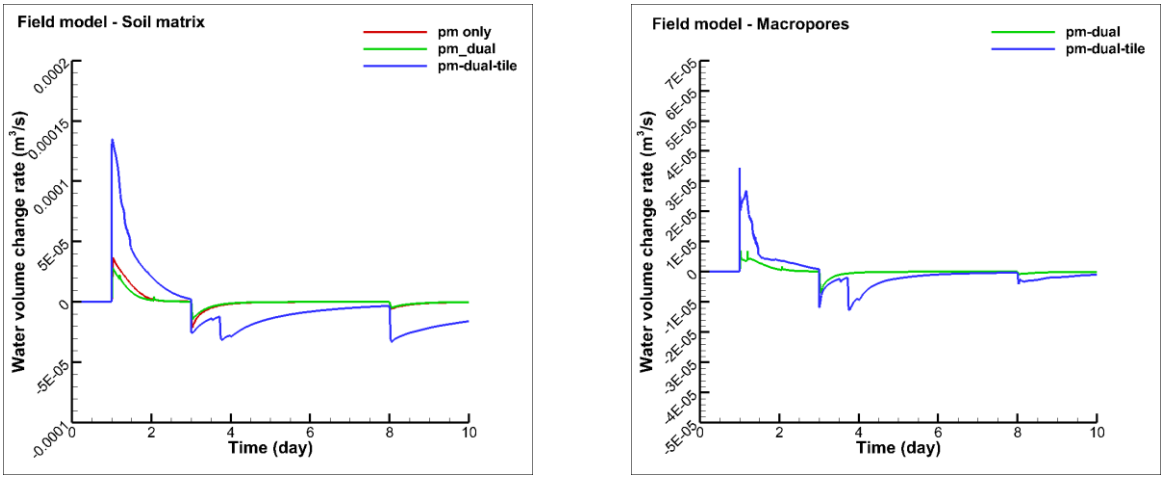

(a) (b)

Figure 25. Water storage variation in the soil matrix (a) and macropores (b) of the Field model in the 10-day storm simulation (wet weather).

First, water ponding appears in the soil matrix. Figure 26 shows the water saturation contours in the soil matrix before the conceptual storm event. The water saturation does not increase monotonically when the depth increases. The location of the less saturated interlayer corresponds to the interface between the A horizon (riparian) and the B horizon (riparian) in the Field model.

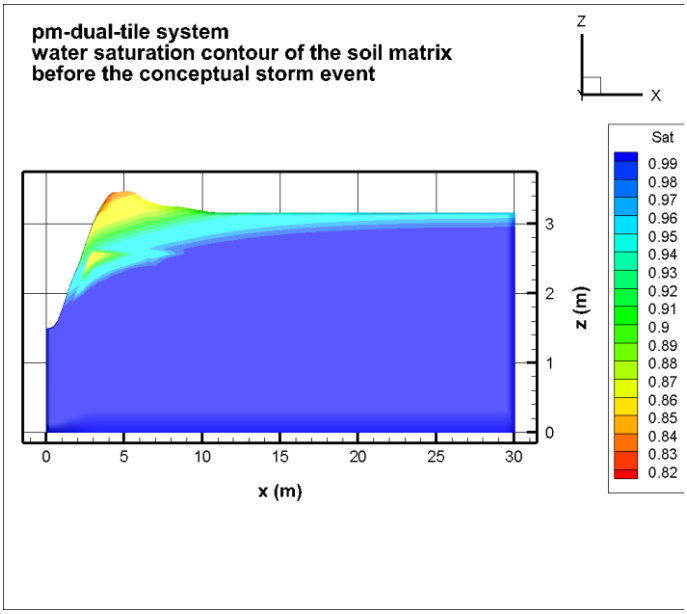

Figure 26. Water saturation contour in the soil matrix of the Field model before the Storm stage.

Second, the introduction of macropores to the soil system for the field case does not appear to enhance the water storage change in PM as greatly as it does in the 3D flow test model. The PM curves for the system with only soil matrix (pm-only system) and the system with soil matrix and macropores (pm-dual system) are close and overlap most of the time (Figure 25). On the contrary, the water storage variation in both the soil matrix and macropores increases greatly when the agricultural tile is added to the soil system (pm-dual-tile system). In the conceptual 3D flow test model, however, the agricultural tile does not significantly influence the water storage increase during the storm (Figure 16).

The water ponding may result from the soil heterogeneity. Since the underlying B horizon (riparian) has lower hydraulic conductivity than the A horizon (riparian), the infiltrated water may be impeded by the less permeable B horizon (riparian) and accumulate on the contact surfaces. Meanwhile, the water ponding may retard the water infiltration and create a higher water saturation in the surficial soil. Thus, the water infiltration may be impeded and the water storage variation in the Field model becomes smaller.

The addition of macropores to the system does not appear to enhance the water storage

variation in soil matrix greatly in the Field model, which may result from the co-effect by the water saturation condition and the soil heterogeneity. The simulation results suggest the majority of the soil matrix and macropores are saturated in the pm-only system and pm-dual system before the Storm stage. Such finding suggests that the addition of macropores to the soil system may not be enough to cause observable influence on the water storage variation.

The promotion of water storage variation in the soil matrix by the cooperation of macropores and agricultural tile is shown in the pm-dual-tile system for the Field model. In the pm-dual-tile system, the water saturation in both soil matrix and macropores before the storm is significantly lower than that in the pm-only and pm-dual systems. Obvious water saturation variation occurs during the storm. Generally, the tile provides an efficient and preferred pathway for the soil to drain. The low initial water saturation and enhanced drainage capacity lead to the greater water storage variation in the pm-dual-tile system.

However, it is hard to determine if a solo tile can increase or decrease the water storage variation. Either the promotion or the diminishment of water storage variation may result from the co-influence by the tile and macropores. Generally, the addition of a tile tends to enhance the water storage variation when the macropore zone has high water saturation, but reduce the water storage variation when the macropore zone has low water saturation and drains efficiently.

Generally, the Field model has lower water saturation variation and tends to release less soil GHG compared with the conceptual 3D flow test model during the conceptual 10-day storm simulation. The soil heterogeneity appears to lead to water accumulating on the interfaces between soil zones in the Field model, which may impede the water infiltration and diminish the water storage increase during the storm. The addition of macropores to the field soil system may have a limited influence on the water storage variation solely. However, the co-appearance of macropores and a tile can enhance the water storage variation greatly. Hence, it is significant to consider the soil heterogeneity when making soil GHG emission management plans.

5.4 Influence of Model Domain Structure

5.4.1 Surface Topography Effect

Besides the soil heterogeneity, the land surface topography may influence the mobility and interaction between surface water and groundwater during precipitation events. In the field case under consideration in this study, a small berm exists at the left lateral end of the modeling domain (Figure 24) and it is hypothesized that this topographic feature may influence water movement and distribution within the domain depending on the hydraulic scenario being evaluated.

To investigate the influence of this topographic feature, a modified field model without the berm is built (All-flat Field). In the All-flat Field model, the top surface beyond the bank slope is flat and equivalent to the elevation of the field surface in the original Field model (Figure 27). The All-flat model is divided into 802 columns and 61 rows. Other model components including the zone division, geological and hydraulic parameters and precipitation input remain unchanged.

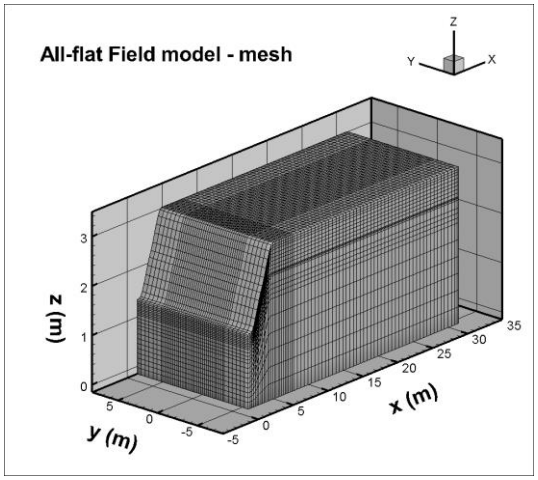

(a)

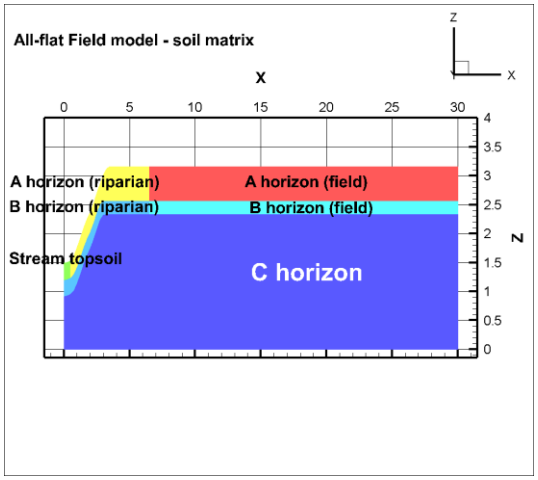

(b)

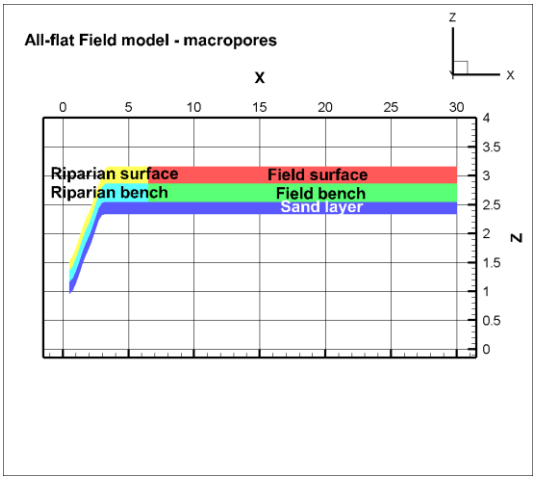

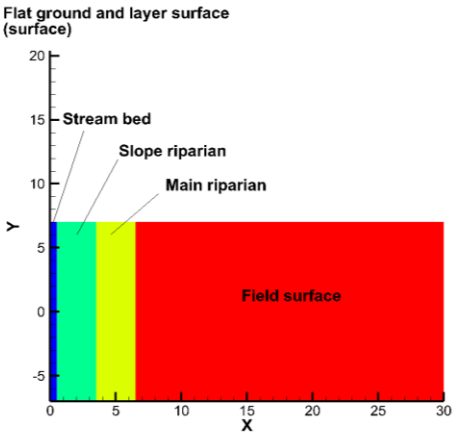

(c) (d)

Figure 27. Finite element grid (a) and the zonation for soil matrix (b), macropores (c) and ground surface (d) for 3D flow All-flat Field model. All graphical units are in (m).

The result of the original Field model and the All-flat Field model are compared in Figure 28. Generally, the All-flat Field models follow the drainage pattern of the original Field model. The water storage variation in the pm-dual-tile system is still much greater than that of the pm-dual and pm-only systems. As the field surface becomes flat, the water storage variation in all soil systems decreases.

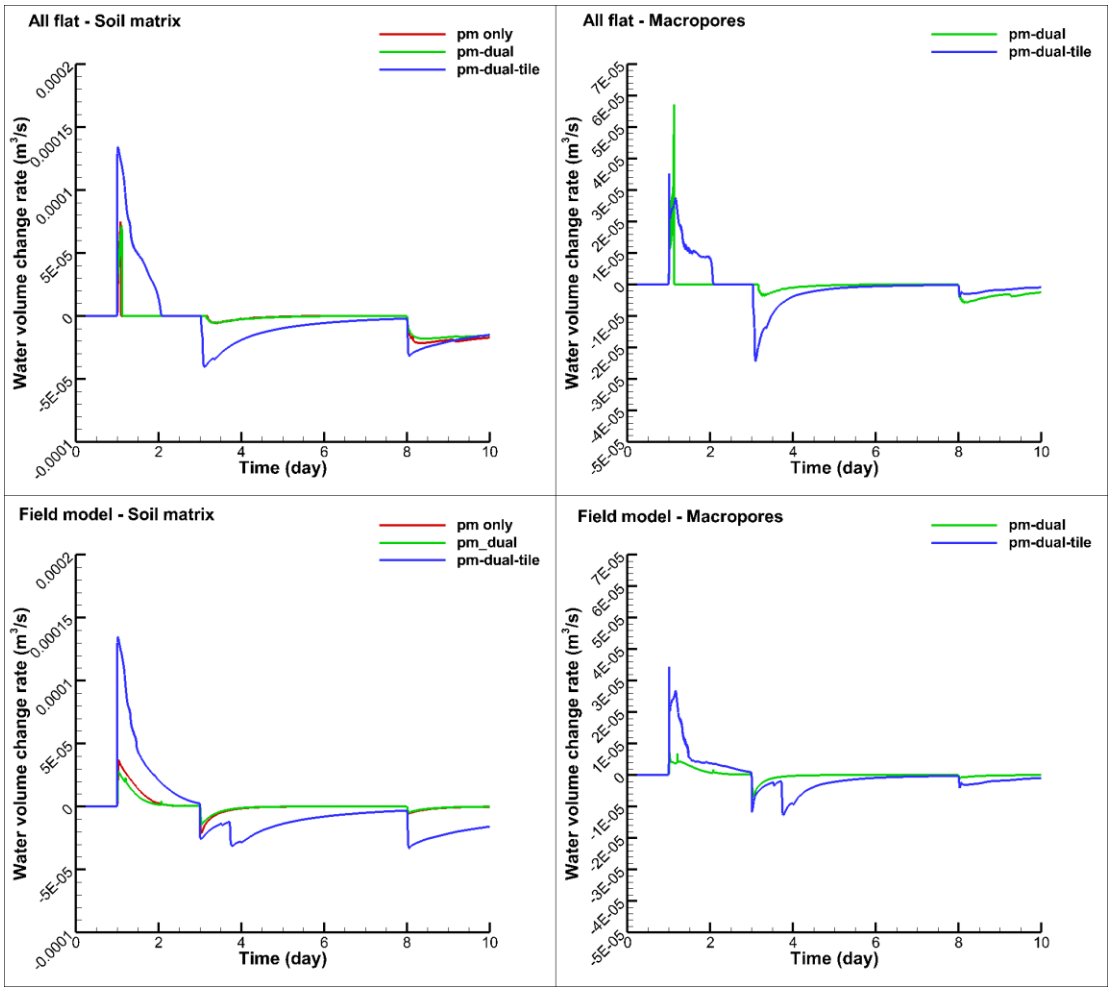

Figure 28. Comparisons of the water storage variations in the soil matrix and macropores in the pm-only, pm-dual, and pm-dual-tile systems of the original Field model and the All-flat Field model during the 10-day storm simulation.

For PM curves, the original Field model results included a second increase in both the pm-only and pm-dual systems during the Storm stage and a second decrease in the pm-dual-tile system during the Recover stage, while the All-flat model did not show this behavior. The second decrease of the DUAL curve is also shown in the pm-dual-tile system of the original Field model.

The berm may lead to the increase of water storage increase during the storm. Figure 29 shows water saturation contour in the soil matrix of the two Field models right after the

storm. At the late stage of the storm, the All-flat Field model is fully saturated and unable to accept more water. However, the original Field model is still unsaturated at the berm and able to absorb water.

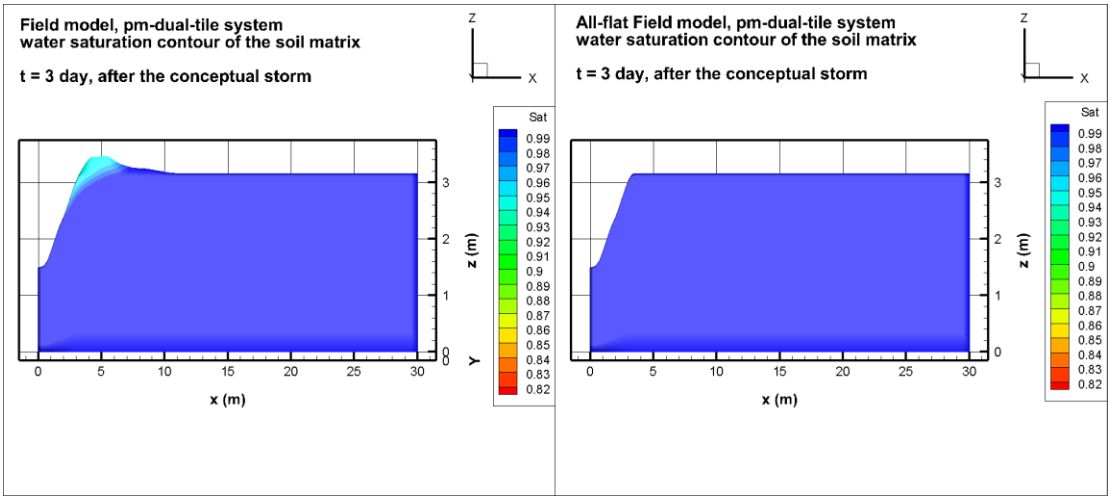

Figure 29. Water saturation contour in the soil matrix of the original Field model (a) and the All-flat Field model (b) right after the storm.

The second increase and decreases of PM and DUAL curves may also be attributed to the berm. When the storm starts, the rainfall accumulates on the ground surface behind the berm and forms surface water ponding. The berm enables the original Field model to have greater surface water ponding than the All-flat Field domain (Table 9). The surface water depth in the All-flat model is much smaller than that in the original Field model after the storm. As the surface water depth increases, the water exchange between the overland domain and the underground domains is enhanced. Hence, the secondary increase of PM is observed during the storm. When the storm ends and the precipitation rate drops to the level before the storm, the water ponded on the ground surface may replenish the soil and partially offset the water loss. Subsequently, the second decrease of PM and DUAL curves can be observed in models with great surface water ponding.

Table 9. Water depth in the overland domain right after the Storm stage in the 10-day storm

simulation for Field models

Soil system	In All-flat Field model (m)	In Field model (m)
Pm	0.005	0.143
Pm-dual	0.005	0.161
Pm-dual-tile	0.003	0.019

Generally, the soil with flat field surface tends to have smaller water storage variation and release less GHG. The topographic effect is more obvious in the soil systems that have low drainage capacity like the pm and pm-dual systems. However, the impact of the topographic effect is related with the surface water depth and the water saturation condition in soils. The surface topographic effect might be negligible when the soil is dry and there is no surface water ponding.

5.4.2 Soil Heterogeneity Effect

The comparison between the Field model and the 3D flow test model may provide a general view for differences between heterogeneous soils and homogeneous soils on water mobility and soil gas emission. However, the two models are different in size, shape, and hydraulic properties. To investigate the effect of the soil heterogeneity on the fate and mobility of water further, a homogeneous All-flat Field model (Homo Field) is built. All soil zones in the Homo Field model are set to have identical properties. The Homo Field model uses the arithmetic means of the parameters from the heterogeneous All-flat Field model (Hetero Field), which are shown in Table 10.

Table 10. Soil matrix and macropore parameters used in the Homo Field model

Parameters	Field model average
Matrix parameters	
Hydraulic conductivity, K_{iso} (m/s)	4.55E-06

Specific storage (m^{-1})	1.00E-04
Porosity (dimensionless)	0.55
Van Genuchten Residual Saturation, Θr (dimensionless)	0.083
Van Genuchten alpha, α (m^{-1})	2
Van Genuchten beta, β (dimensionless)	1.40
Bulk Density (kg/m^3)	1198
Macropore parameters	
Volume fraction dual medium	0.008
Interface K (m/s)	1.41E-07

Figure 30 shows the results of the Homo Field model and the Hetero Field model. Generally, the two model behave similarly. The water storage variation increases dramatically when the macropores and tile are added to the soil system. Both models have second increases of DUAL curve in the Storm stage.

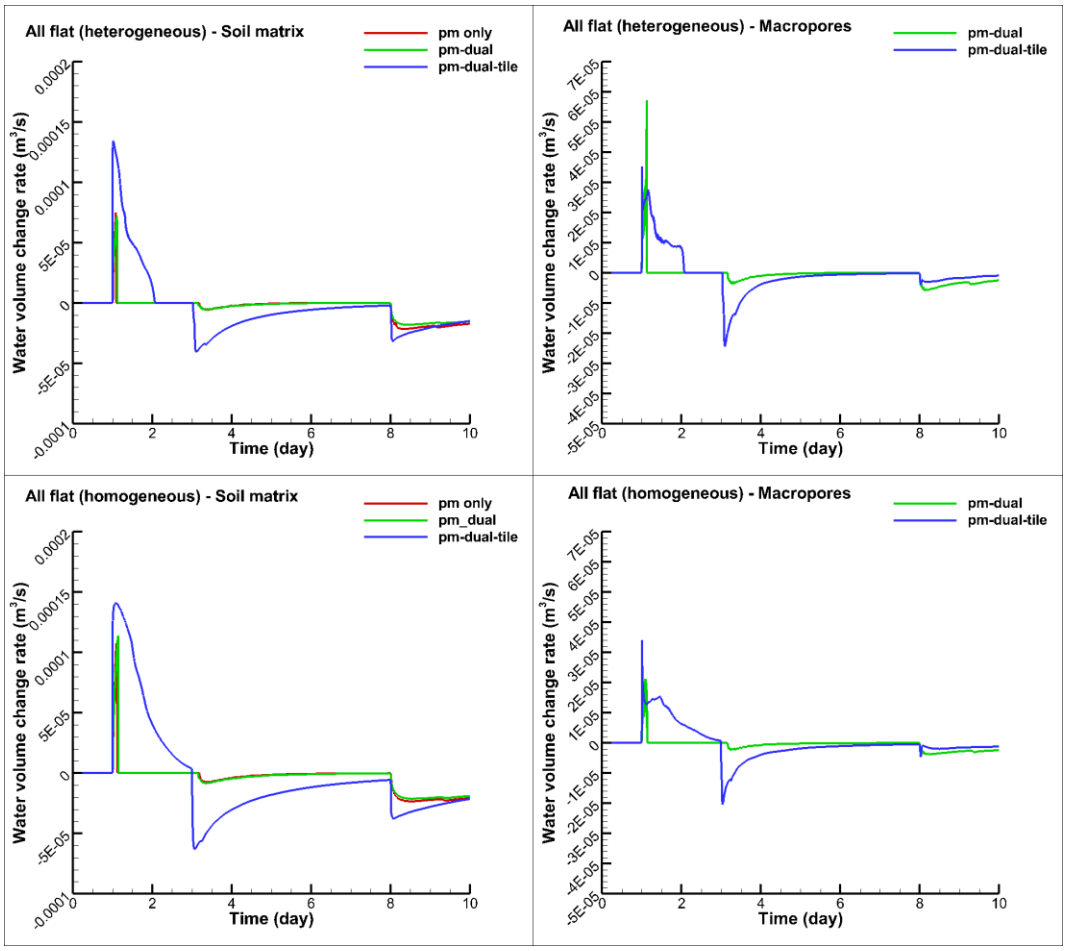

Figure 30. Comparisons of the water storage variations in the soil matrix of the pm-only, pm-dual, and pm-dual-tile systems for the Homo Field model and the Hetero Field model during the 10-day storm simulation.

In both the Homo and Hetero Field models, the soil matrix of the pm-only and pm-dual system is highly saturated during the most time of the 10-day storm simulation. Hence, the water storage capacity and the soil GHG emission capacity of the pm and pm-dual systems are low. In these systems, the addition of macropores has limited influence on the water storage variation regardless of the soil heterogeneity.

For the pm-dual-tile system, both the Homo Field model and the Hetero Field model become further unsaturated. Thus, the water storage increases greatly during the storm in the

pm-dual-tile system, because it has more space in the soil to accept rainfall compared with the pm or pm-dual system. In both the Homo Field model and the Hetero Field model, the co-influence of the macropores and tile results in an increase in water storage variations.

The Homo Field model tends to have greater water storage variation than the Hetero Field model, especially in the pm-dual-tile system that has high drainage capacity. This may be due to the soil heterogeneity. The comparison between the Homo and Hetero Field models suggests that the decrease of soil heterogeneity may diminish water ponding between soil zones and enhance the drainage capacity of soil. Hence, the Homo Field model will have lower water saturation before the storm and be capable to absorb more infiltrating water and release more soil gas.

However, such findings may not be universal. The soil heterogeneity can either enhance or reduce the drainage capacity and water retention capacity of soils, which leads to different water saturation conditions. Therefore, the influence of the soil heterogeneity on the water storage variation is uncertain. Still, it is significant to consider the role of soil heterogeneity in controlling both water and soil gas mobility in these types of systems.

5.5 Tile Depth Effect

5.5.1 Tile Depth Effect in Conceptual 3D Flow Test Model

The difference in tile depth may lead to a variation of soil drainage behavior. The relative elevations from the base of the model are 3m for the ground surface, 1.5 m for the steam bed, and 2m for the tile (1 m deep) in the 3D flow test model (Deep 3D)(Figure 24). An adapted 3D flow test model is built, with the tile installed at 2.5 m (0.5 m deep) (Shallow 3D). Other parameters remain unchanged and only one tile is considered in each soil system. The shallow and deep tiles both connect with the macropore network.

The same three common soil types utilized in the previous 3D test modeling are considered in these simulations including the sandy loam, silty loam, and clay loam. The matrix and macropore parameters of each soil type are also the same as those used in the

original 3D flow test model.

Figure 31 shows the comparison between the results of the Deep, and Shallow 3D models. The tile is lower than the highest water table in the Deep 3D model. However, the tile is higher than the water table throughout the 10-day storm event in the Shallow 3D model (Table 11).

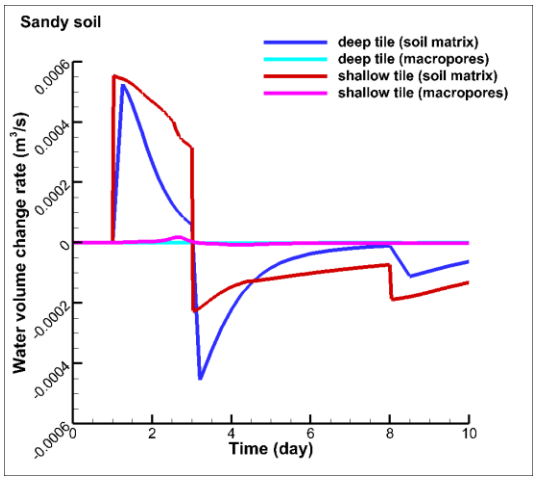

(a)

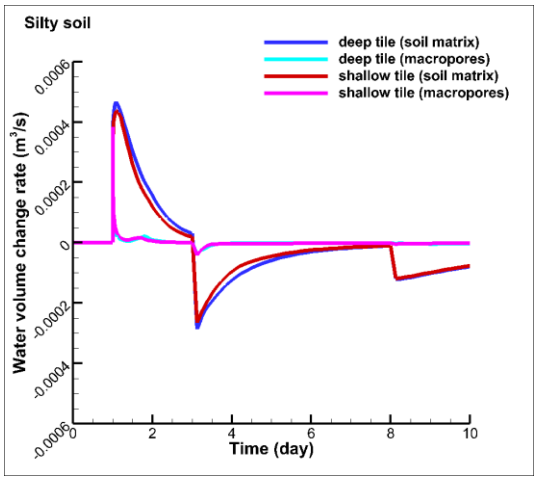

(b)

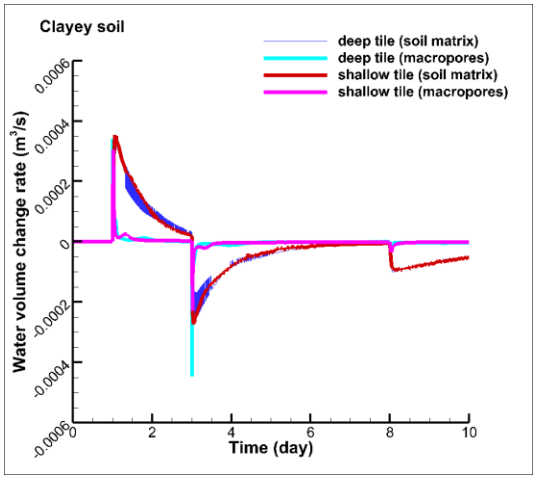

(c)

Figure 31 Comparisons of the water storage variation in systems with different tile depths.

(a) Sandy loam, (b) silty loam, and (c) clay loam.

Table 11. Elevation of water tables in the 3D flow test models (sandy loam) with different tile

depths

Time (s)	86400	259200	691200	864000
In shallow-tile system (m)	2.27	2.45	2.41	2.28
In middle-tile system (m)	2.09	2.2	2.09	2.08
In deep-tile system (m)	1.03	1.04	1.03	1.03

Within the soil matrix, the increase of tile depth results in slightly higher water storage variation for less permeable soils (Figure 31). The result suggests that soil system with a deeper tile has lower water saturation before the storm. Thus, more water is accepted in the deep-tile system during the storm.

However, the soil degassing from the matrix in the Shallow 3D model exceeds that in the Deep 3D model in the permeable sandy loam, likely due to the elevation of water table (Figure 31). In the Shallow 3D model for sandy loam, the tile is above the water table during the entire simulation. Hence, the shallow tile is less involved in groundwater movement and the drainage capacity of the soil is lower overall. Therefore, for the permeable sandy loam, the Shallow 3D model has greater water storage increase during the storm then the Deep 3D model.

In the macropores, the water storage variation is negligible for both Deep and Shallow 3D models. The influence of the tile depth variation is not obvious and may be influenced by multiple factors.

The tile depth influence may be weakened as the soil becomes less permeable. The clay loam tends to have high initial water saturation and strong water retention capacity. Hence, there are less space in the soil to accept water during the storm. Consequently, the promotion of soil degassing by increasing the tile depth is not significant.

Overall, the increase of tile depth can enhance the soil degassing slightly by increasing the water storage increase during storms. The deep tile is less efficient in draining the

infiltrated water compared with the shallow tile. Hence, more water may be retained in the deep-tile system and greater water storage variation may occur. Meanwhile, the deep-tile system tends to have lower water saturation than the shallow-tile system before the storm when the precipitation rate is steady. Therefore, the deep-tile system will have greater space to accept water when the storm begins, which may contribute to the promotion of water storage increase and soil degassing during storms. The more permeable the soil is, the stronger the tile depth effect. However, the tile depth effect is influenced by the elevation of water table. If the water table is lower than the tile during precipitation events, the tile may be less involved in the soil water redistribution. Thus, great water storage increase and soil degassing may occur. Therefore, the elevation of local water table also needs to be considered when setting agricultural tiles, considering their influence on soil gas mobility.

5.5.2 Tile Depth Effect in Field Model

The tile depth simulation is also performed using the All-flat Field model (Hetero Field model). The elevations are 3.17 m for the field surface, 1.5 m for the steam bed, and 2.5 m for the tile (0.67 m depth) in the All-flat Field model (Shallow Field). To investigate the tile depth effect at field, a modified All-flat Field model (Deep Field) was constructed with the tile elevation increased to 2.04 m (1.13 m depth). The bottom surface of the macropore domain at the field area is also lowered to the elevation of 2.04 m, so that the tile is connected with the macropores. Other parameters remain unchanged. Only one agricultural tile is involved in each model.

Figure 32 shows the comparison between the results of the Deep and Shallow Field models. Throughout the simulations, all tiles are deeper than the highest water table. Hence, the tiles are effectively involved in groundwater transportation during the Storm stage.

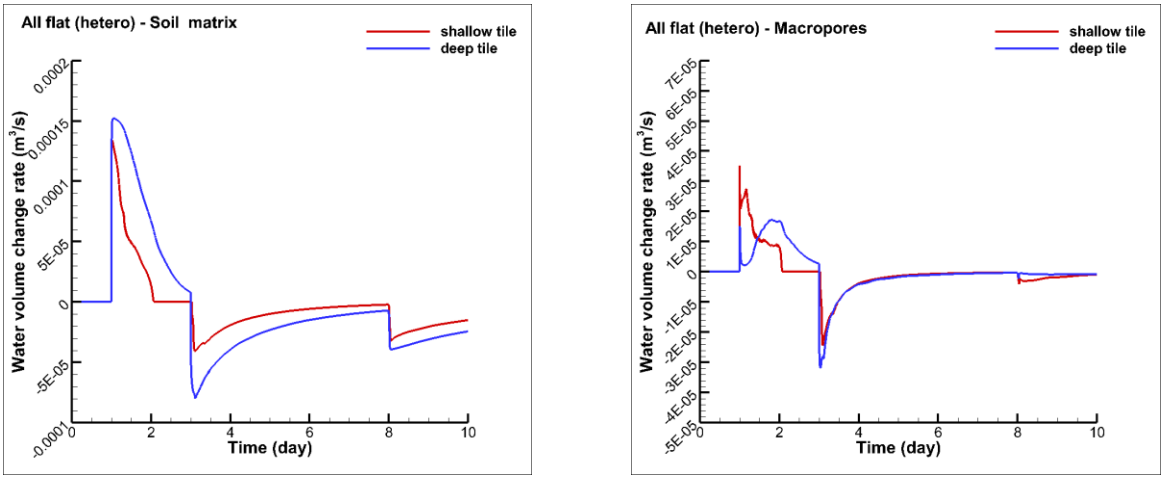

(a) (b)

Figure 32. Water storage variations in the soil matrix (a) and macropores (b) in Field models with different tile depths in the 10-day storm simulation.

In the soil matrix, the water storage variation increases as the tile depth increases. In the macropores, a delay of the peak of DUAL curve is observed for the Deep Field model.

Although the spacing between shallow tile and deep tile in the Field model and 3D model are similar and all tiles are connected with macropores, the tile depth effect is stronger in the Field models. Such difference might result from soil water ponding along stratigraphic boundaries caused by soil heterogeneity. The infiltrated water may be retained and pond above the tile. Hence, the deep tile may perform more poorly in draining water in heterogeneous soils than in homogeneous soils. Thus, the increase of tile depth may promote the water storage increase and soil degassing more significantly in the heterogeneous soils than in the homogeneous soils during storms. However, the strong tile effect in the Field models may also relate with the differences on model size and hydraulic and geological properties between the Field model and 3D flow test model.

Overall, the installation of shallow tiles may decrease the soil GHG emission, because shallow tiles enhances the drainage capacity and leads to high water saturation before storm events. Besides, the soil heterogeneity should also be considered since it may influence the

efficiency of shallow tiles in diminishing soil GHG emission.

5.6 Tile Number Effect

5.6.1 Tile Number Effect in Conceptual 3D Flow Test Model

Besides the depth, the number of the agricultural tiles may also influence the soil drainage behavior. In this research, the 3D flow test models with 1 tile (1-tile 3D model) and 3 tiles (3-tile 3D model) are considered. All tiles extend from x=20m to 1000m at the elevation of 2 m (1 m deep). In the 1-tile 3D model, the tile is at the middle of the model with y = 0 m. In the 3-tile 3D model, the tiles are distributed symmetrically at y = ±3.5 m and 0 m. Other parameters of these 3D models are the same as those of the original 3D flow test model.

Figure 33 shows the results for the 1-tile and 3-tile 3D. All tiles are deeper than the highest water table and are in contact with the macropores. Hence, the tiles are effectively involved in groundwater transportation during the Storm stage.

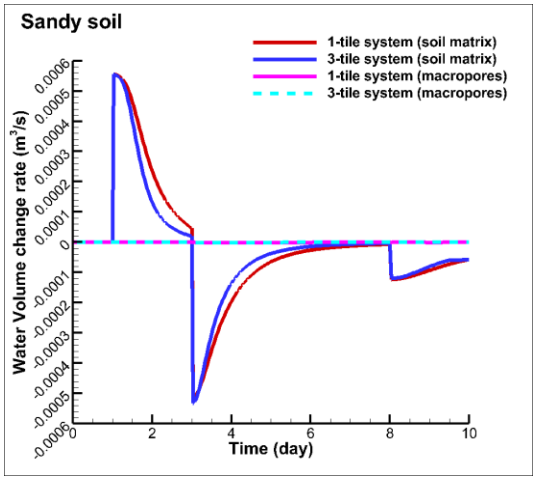

(a)

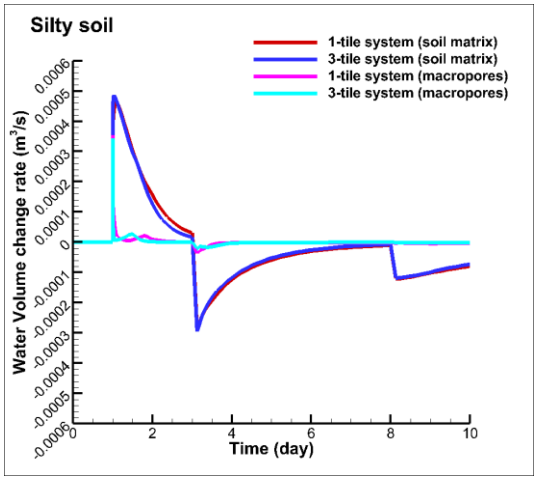

(b)

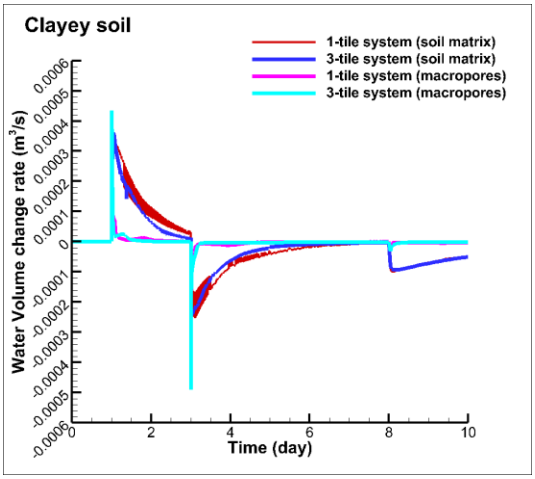

(c)

Figure 33. Comparisons of the water storage variation in systems with different tile numbers. (a) Sandy loam, (b) silty loam, and (c) clay loam.

For the soil matrix, the increase of tile number appears to result in a decrease of water storage variation and soil degassing during precipitation events. By installing more agricultural tiles, the drainage capacity of the soil profile is enhanced and although soil systems with multiple tiles tend to have lower initial water saturation in the matrix than those with a single tile, they appear to also have less variation of water saturation in matrix during the storm. In the 3-tile 3D models, the tiles control the water table fluctuation and diminish water storage changes. Hence, less soil degassing is expected for soil systems with multiple tiles.

For the macropores, the amount of water storage variation and soil degassing is negligible. The second peaks of DUAL curves in 3-tile 3D models appear more rapidly than those in 1-tile 3D models. Such early peaks may relate with the enhanced drainage capacity by increasing tile numbers.

Similar with the tile depth effect, the tile number effect is also reduced when the soil is less permeable. Hence, it may be more efficient for people to install more tiles to diminish soil GHG emission in permeable soils.

5.6.2 Tile Number Effect in Field Model

The 1-tile and 3-tile conditions are considered in the All-flat Field model (Hetero Field model). All tiles are at 2.5 m elevation (~ 0.67 m depth) and extend from x = 6.5 m to 30 m. The distribution of tiles are symmetrical. For the 1-tile Field model, the tile locates in the center of the system (y = 0 m). In the 3-tile system, the tiles locate in y = ±3.5 m and 0 m. Other parameters of these field models are the same as the original Field model and the tiles connect with the macropores.

Figure 34 shows the results of the Field models with different tile numbers. Generally, the more the tiles, the smaller the water storage variation. All tiles are deeper than the highest water table. Hence, the tiles are effectively involved in groundwater transport during the Storm stage.

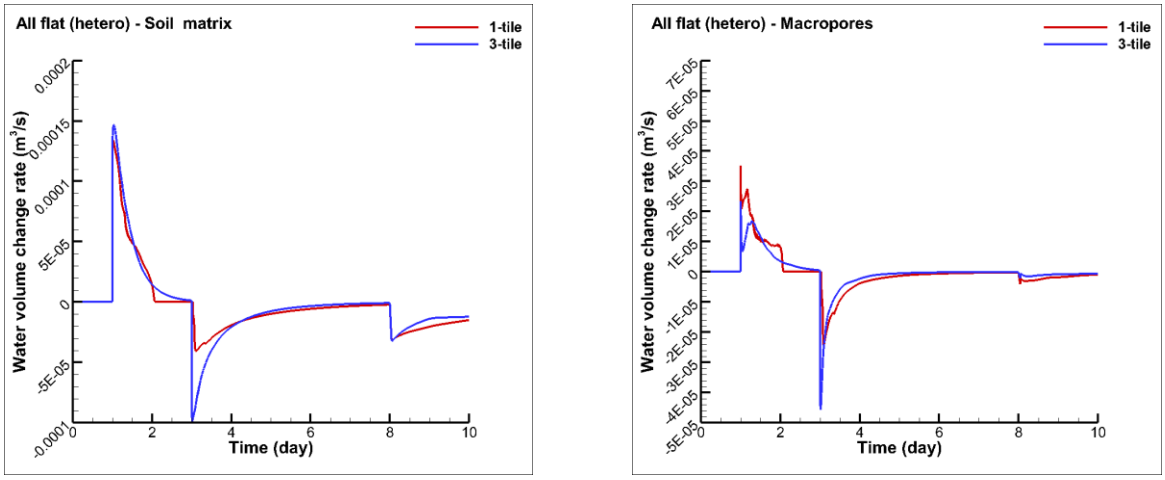

(a) (b)

Figure 34. Water storage variations in the soil matrix (a) and macropores (b) in Field models with different tile numbers.

During the storm, the water storage increase in the 3-tile Field model is greater than that in the 1-tile Field model, which contradicts with the results in the 3D-flow test models. Such difference may be related to the water saturation conditions. In the 1-tile and 3-tile 3D model and the 3-tile Field model, the water storage in the soil matrix keep increasing during

the Storm stage, as the PM values are positive. However, the water storage in the soil matrix stops to increase in the middle of the Storm stage in the 1-tile Field model, as the PM values drops back to zero after its initial increase at the beginning of the storm. Such finding suggests that the soil matrix of the 1-tile Field model is fully saturated and not able to release more gas. Hence, the 3-tile Field model will have more soil degassing than the 1-tile Field model.

Overall, the change of tile number influences not only the drainage capacity but also the initial water saturation of soils. It is necessary to consider the water saturation condition in the field when deciding the number of agricultural tiles to be installed.

5.7 Storm Intensity Effect

Besides the soil hydraulic and geological characteristics, the soil GHG emission will also be influenced by the precipitation intensity. In this research, 10-day storm simulations with varied storm intensity are performed to assess the water drainage capacity and degassing capacity of soils.

The All-flat Field models that are used in the tile depth and tile number effects are selected for the storm intensity simulation. Three storm rates are considered besides the original rate of $4.6*10^{-7}$ m/s (1x storm intensity), which are the 0.5x storm intensity ($2.3*10^{-7}$ m/s), 1.5x storm intensity ($6.9*10^{-7}$ m/s), and 2x storm intensity ($9.2*10^{-7}$ m/s). Except for the change of the storm intensity, other parameters remain unchanged.

Figure 35 shows the results for the storm intensity simulation. Generally, the water storage variation increases as the storm intensity increases. Consequently, the soil GHG emission is also elevated. For all models, the tiles are deeper than the highest water table position in the 10-day storm simulation.

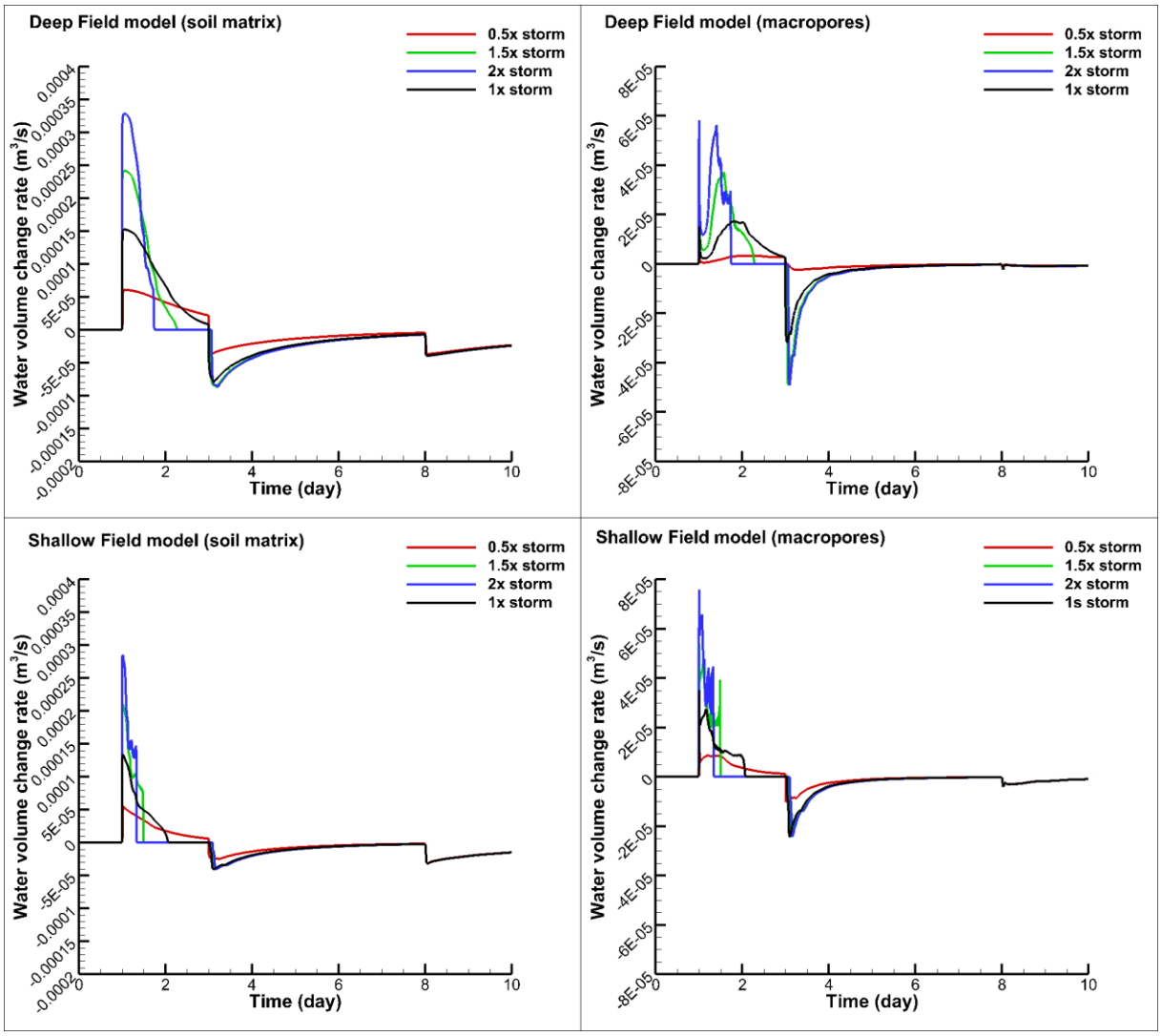
Deep Field model (soil matrix)
0.5x storm
1.5x storm
2x storm
1x storm
Water volume change rate (m3/s)
Time (day)
Deep Field model (macropores)
0.5x storm
1.5x storm
2x storm
1x storm
Water volume change rate (m3/s)
Time (day)
Shallow Field model (soil matrix)
0.5x storm
1.5x storm
2x storm
1x storm
Water volume change rate (m3/s)
Time (day)
Shallow Field model (macropores)
0.5x storm
1.5x storm
2x storm
1s storm
Water volume change rate (m3/s)
Time (day)

(a)

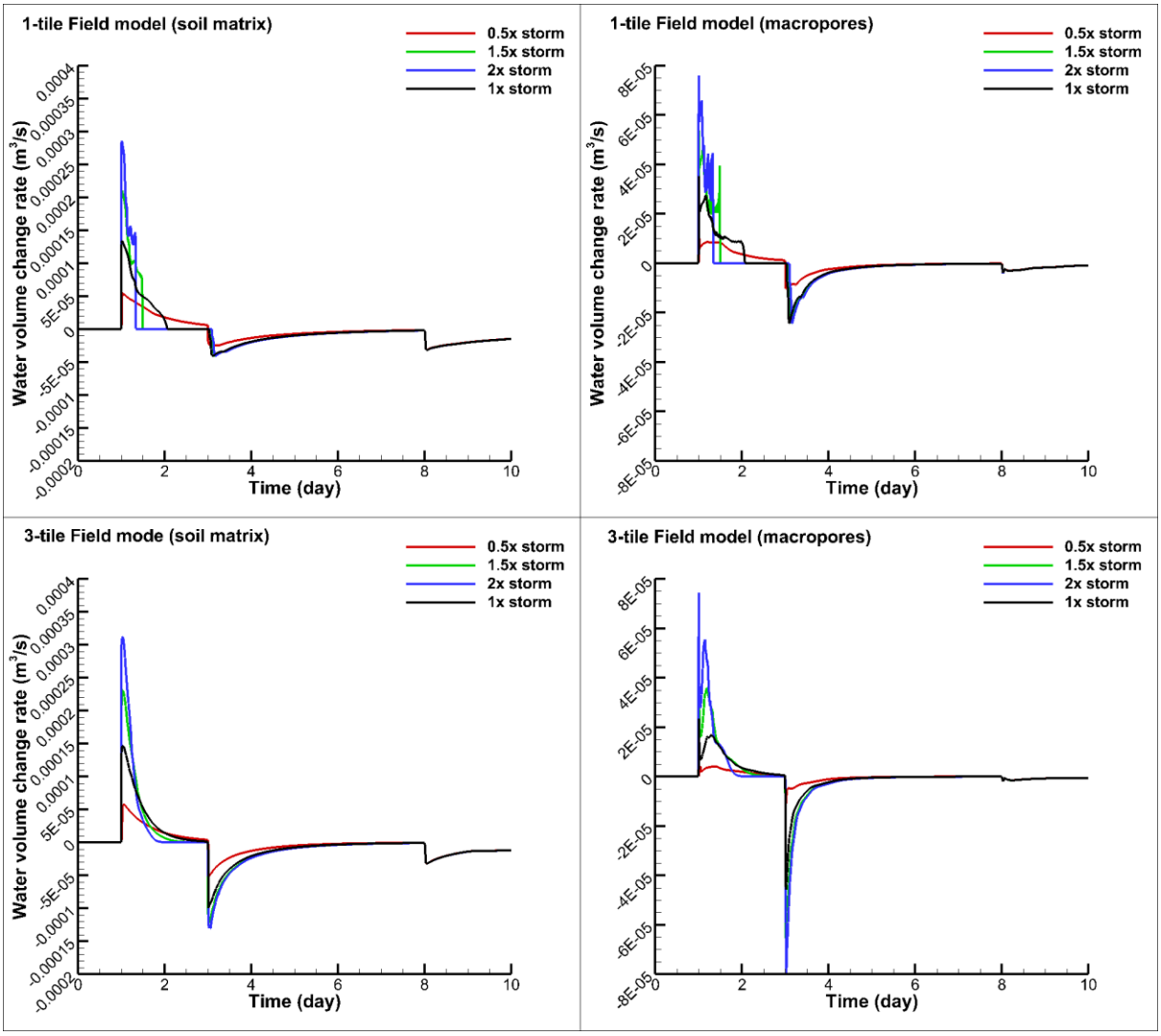

(b)

Figure 35. Comparisons of the water storage in the soil matrix of Field models with different tile depths (a) or tile numbers (b) under varying storm conditions.

The peak rate of water storage increase during the storm varies linearly with the storm intensity. A more rapid soil degassing is expected during a greater storm. However, the relationship between in the gas emission and storm intensity is not linear because the soil degassing is also controlled by the water saturation. The water saturation conditions before the storm are identical in the same model for different storm tests. Hence, the accumulative

soil gas emissions during the storm should also remain identical in the same model unless the storm intensity is too small to make the soil fully saturated (like Deep Field model, 0.5x storm).

Overall, the elevation of storm intensity may increase soil degassing. However, the storm intensity effect becomes negligible once the soil becomes fully saturated during the storm event. The storm intensity effect is influenced by the water drainage capacity and water saturation condition of soils. Soil systems like the deep-tile system and 1-tile system, which have low drainage capacity and low initial water saturation, may require heavy storms to become fully saturated. Hence, their soil degassing may be less during small storms.

5.8 Long-Term Simulation with PET

The precipitation data used in the previous conceptual model are set manually. The rain duration is 8 days and the precipitation rate is not 0 m/s at the beginning of the simulation. Such 10-day storm event is less likely to occur in nature. In reality, the precipitation is discontinuous. A single precipitation event may not last for a long time. Hence, it is significant to introduce long-term precipitation data to the model to investigate the response of the soil.

Besides precipitation, the evapotranspiration may also play an important role in the water mobility and soil degassing, which acts as a water sink. Although the influence of evapotranspiration is considered to be insignificant and is ignored in the 10-day storm simulations, it may be a critical parameter to consider in the long-term simulation. The precipitation and potential evapotranspiration (PET) data used in the long-term simulation are obtained by Frey (2020) at the WEBS field site from May 2018 to Oct 2018. PET provides boundary conditions, which is used by HGS program to calculate the actual evapotranspiration. Two vegetation types are considered in the estimation of transpiration, which are the corn field and the riparian zone. The corresponding evapotranspiration scenarios are noted as Corn ET and Riparian ET.

Only the positive parts of the PM and DUAL curves are considered to investigate the soil GHG emission, because they correspond to the water storage increase and relate with soil degassing process. The amount of gas released from the soil is estimated by integrating the positive PM and DUAL values with respect to time.

Both the homogeneous 3D flow test model and the heterogeneous Field model are used in the long-term simulations. Except for the difference on the precipitation and PET data, other parameters remain unchanged for these models.

5.8.1 Long-Term Simulation in Conceptual 3D Flow Test Model

Different combinations of the soil matrix type, macropores and agricultural tile configurations are investigated in the 3D flow test model for the long-term simulation (Long 3D model). The Long 3D model is homogeneous and only one tile is considered at the elevation of 2 m (1 m deep). Similarly, three soil types are involved including the sandy loam, silty loam, and clay loam. The soil parameters are the same as those used in the original 3D flow test model.

5.8.1.1 Gas Emission from Soil Matrix

Figure 36 shows the variation of positive PM integration with time. The gas emission from the soil matrix of the PM only system is significantly lower than that from the PM-dual system and PM-dual-tile system, especially in impermeable soils like the clay loam.

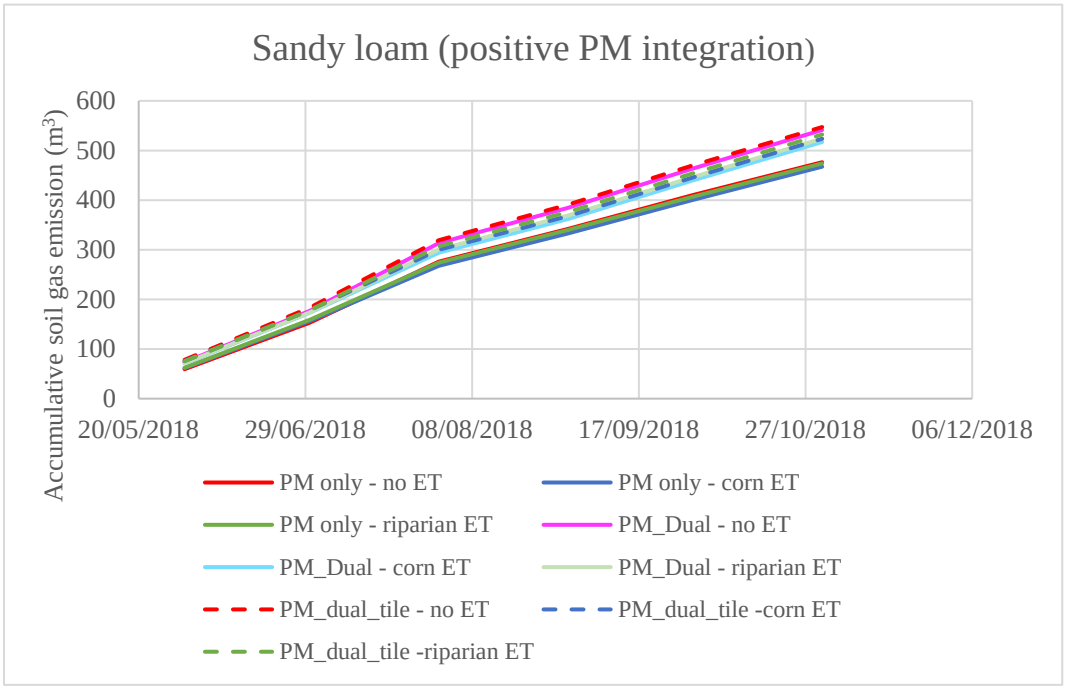
Sandy loam (positive PM integration)
Accumulative soil gas emission (m3)
600
500
400
300
200
100
0
20/05/2018
29/06/2018
08/08/2018
17/09/2018
27/10/2018
06/12/2018
PM only - no ET
PM only - corn ET
PM only - riparian ET
PM_Dual - no ET
PM_Dual - corn ET
PM_Dual - riparian ET
PM_dual_tile - no ET
PM_dual_tile -corn ET
PM_dual_tile -riparian ET

(a)

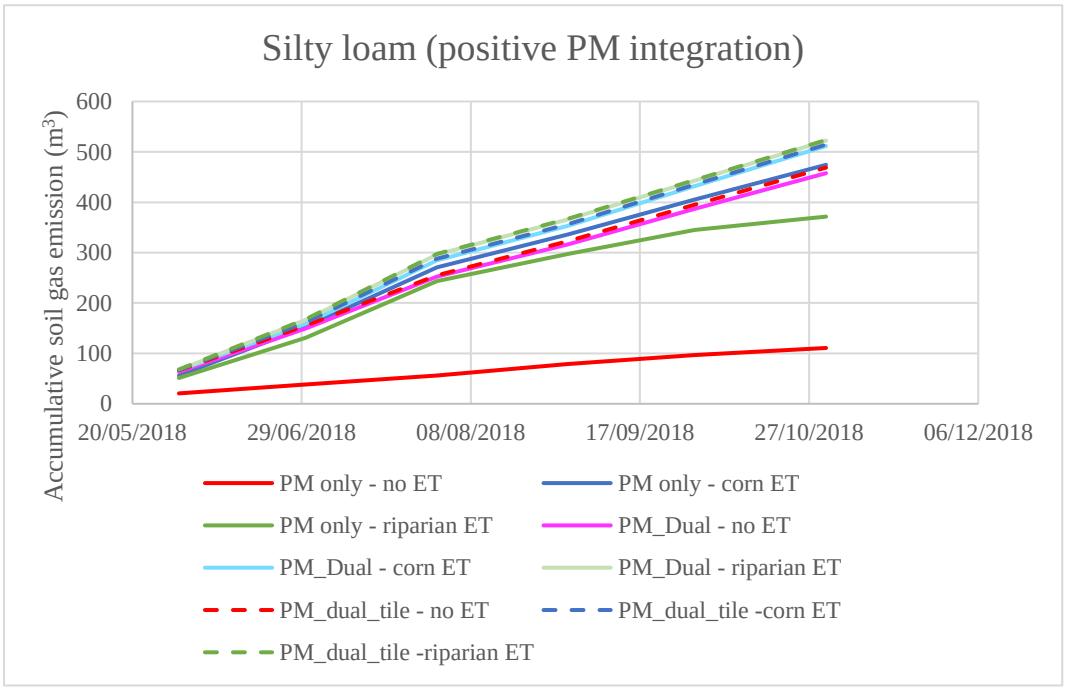
Silty loam (positive PM integration)
Accumulative soil gas emission (m3)
600
500
400
300
200
100
0
20/05/2018
29/06/2018
08/08/2018
17/09/2018
27/10/2018
06/12/2018
PM only - no ET
PM only - corn ET
PM only - riparian ET
PM_Dual - no ET
PM_Dual - corn ET
PM_Dual - riparian ET
PM_dual_tile - no ET
PM_dual_tile -corn ET
PM_dual_tile -riparian ET

(b)

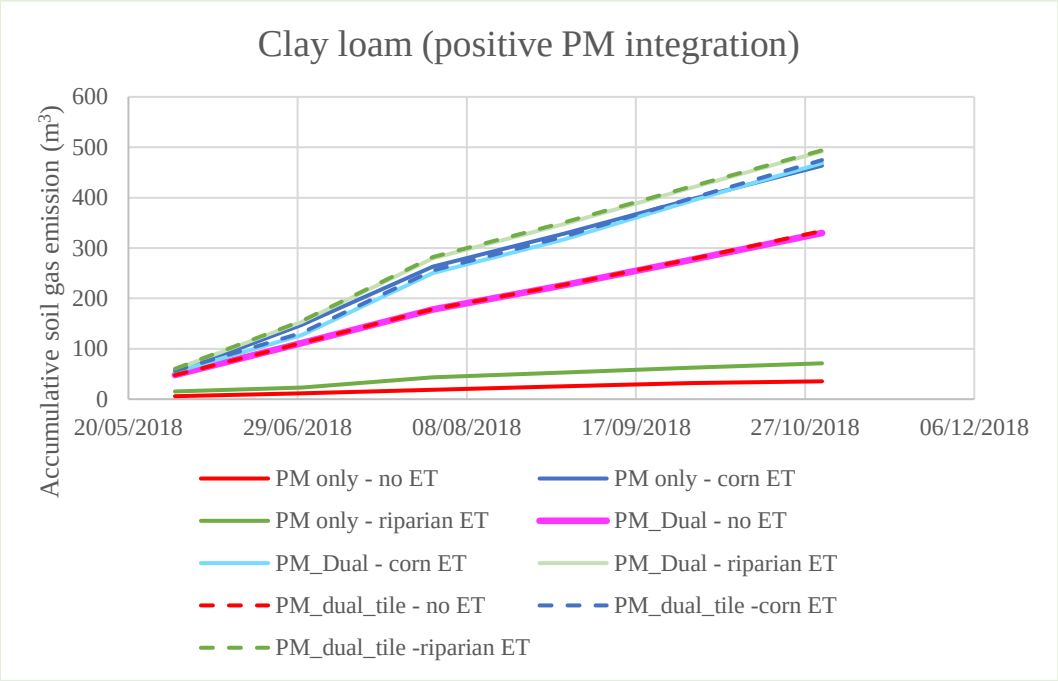

(c)

Figure 36. Variation of positive PM integration with time in the 3D flow test models of different soil types under different evapotranspiration conditions. (a) Sandy loam, (b) silty loam, (c) clay loam.

In permeable soils like the sandy loam, the introduction of PET data to the Long 3D model has limit influence on the gas emission. The gas emission from the soil matrix under a no-ET condition is slightly larger than that under riparian-ET condition or under corn-ET condition, whether the macropores and tile are considered in the model or not (Figure 36).

On the contrary, ignoring the PET component in the Long 3D model with lower permeability soils may lead to significant underestimation of gas emission from the soil matrix. In silty loam and clay loam, the gas emission from the soil matrix under corn-ET condition is larger than that under riparian-ET condition or under no-ET condition when only considering the soil matrix in the system. As the macropores are added to the system, the gas emission under riparian-ET condition exceeds that under the corn-ET condition. The addition of an agricultural tile appears to have little influence on soil gas emission behavior.

The permeable soil tends to have lower water saturation and may be less dependent on evapotranspiration to influence available storage. Evapotranspiration appears to play a relatively minor role in the case of the sandy loam soils in influencing the changes in water storage and GHG emission during precipitation events. In addition, soil water mobility in permeable soils are influenced less by the presence of macropores and tile drains than the less permeable soils.

Overall, the lower permeability soils generally have higher levels of water saturation and the mobility of the soil water and gas in these soil types depend greatly on the macropores and tile for water transportation. Evapotranspiration consumes the higher available water in these soils increasing storage available to accept infiltrating water and promote soil degassing during precipitation events When macropores and tiles are included in the system, the gas emission is enhanced significantly.

The increase of gas emission become slower after the beginning of August. The cause of such transition might be due to the decrease in precipitation beginning in July and the higher PET values during summer. When the precipitation becomes less frequent and weaker and the PET becomes stronger, the variation of water table will be diminished and less gas will be released from the soil.

5.8.1.2 Gas Emission from Macropores

Figure 37 shows the variation of positive DUAL integration with time. The gas emission from the macropore of the Ppm-dual system is higher than that of the pm-dual-tile system, which is opposite to the sequence of the gas emission magnitude in the soil matrix. Meanwhile, the amount of soil degassing from the soil matrix is of the same magnitude among different soil types. However, the magnitude of soil degassing from macropores may varies greatly with soil type. The less permeable soil will have significantly greater soil degassing compared with the permeable soil.

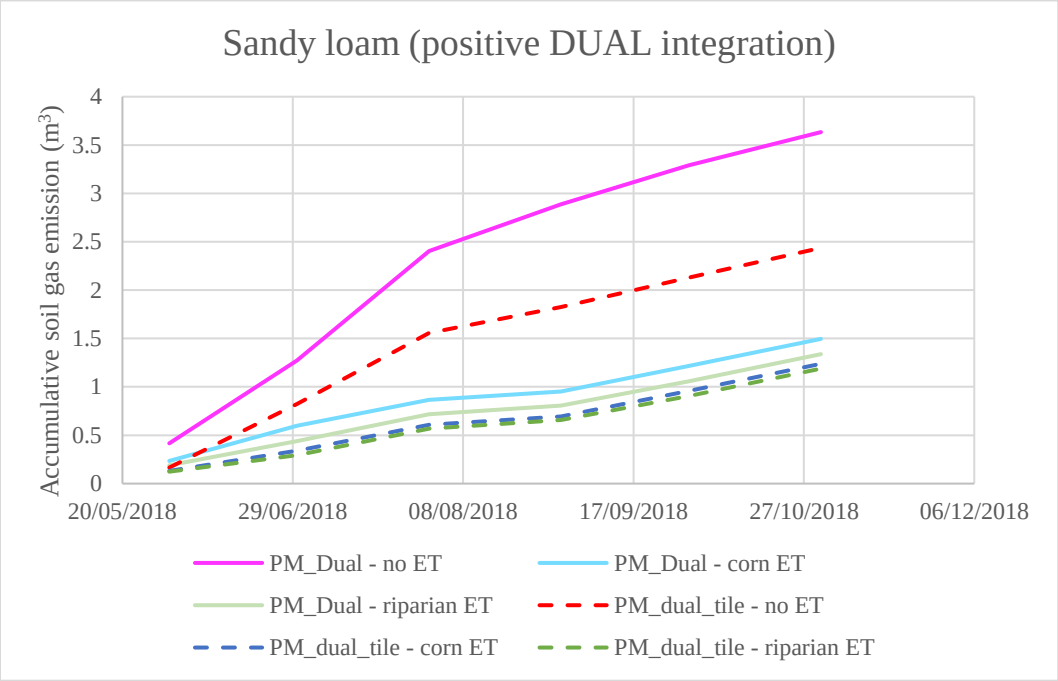
Sandy loam (positive DUAL integration)
Accumulative soil gas emission (m3)
4
3.5
3
2.5
2
1.5
1
0.5
0
20/05/2018
29/06/2018
08/08/2018
17/09/2018
27/10/2018
06/12/2018
PM_Dual - no ET
PM_Dual - corn ET
PM_Dual - riparian ET
PM_dual_tile - no ET
PM_dual_tile - corn ET
PM_dual_tile - riparian ET

(a)

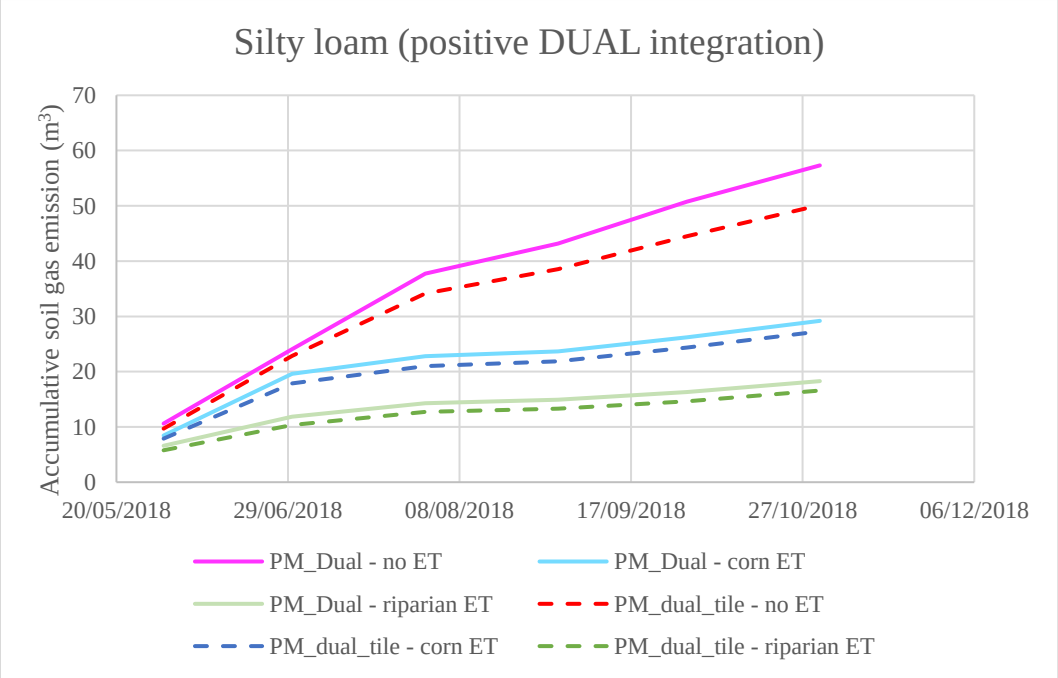
Silty loam (positive DUAL integration)
Accumulative soil gas emission (m3)
70
60
50
40
30
20
10
0
20/05/2018
29/06/2018
08/08/2018
17/09/2018
27/10/2018
06/12/2018
PM_Dual - no ET
PM_Dual - corn ET
PM_Dual - riparian ET
PM_dual_tile - no ET
PM_dual_tile - corn ET
PM_dual_tile - riparian ET

(b)

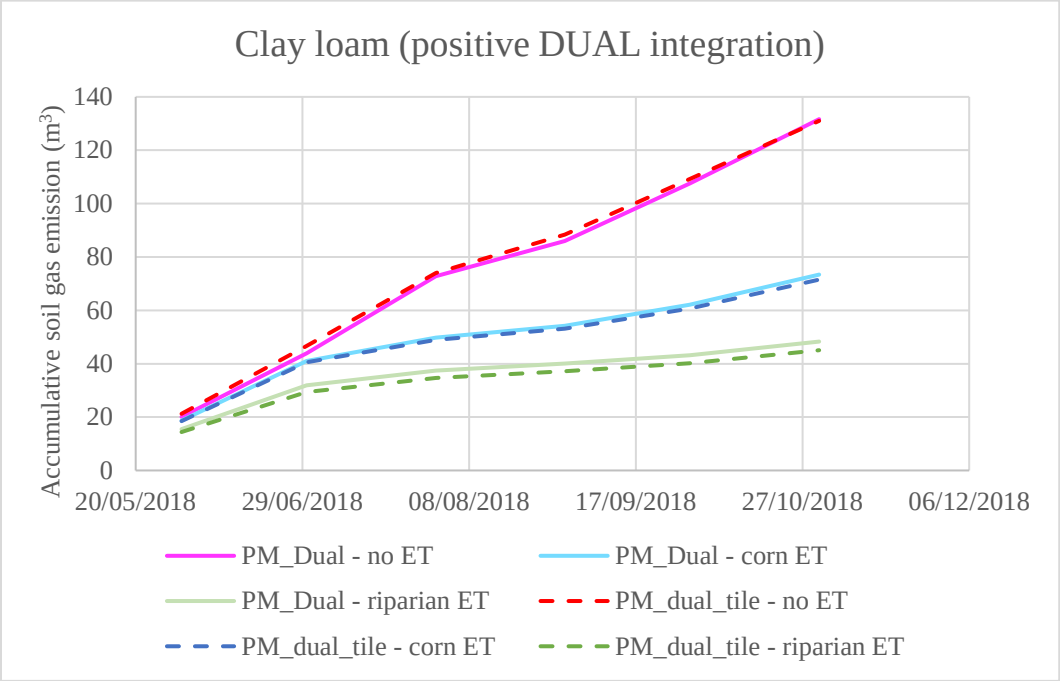

(c)

Figure 37. Variation of positive DUAL integration with time in the 3D flow test models of different soil types under different evapotranspiration conditions. (a) Sandy loam, (b) silty loam, (c) clay loam.

In each soil type, the gas emission from the macropores under no-ET conditions is larger than that under corn-ET condition or riparian-ET condition. Meanwhile, the sandy loam has the smallest gas emission from the macropores, while the clay loam has the highest. The addition of a tile to the system tends to reduce the gas emission, especially in permeable soils. The rate of soil gas emission reduces during August and increase again in September.

The high rate of soil gas emission from the macropores in the silty and clay loam soils is likely due the major role these features play in controlling soil water movement during transient precipitation events. Unlike the soil matrix, the macropores generally has low water saturation regardless of soil types. Evapotranspiration, however, acts to reduce the water from entering the macropores leading to less gas emission during precipitation events. The introduction of tile to the system enhances the drainage capacity further and limits the water

table fluctuation, which also helps to reduce the gas emission especially in permeable soils that drain rapidly. The low gas emission rate observed during August may result from the decreased precipitation intensity and frequency and the enhanced PET. Although the intensity of precipitation remains low beginning in September, the frequency increases and PET decreases. Thus, the water storage variation is promoted and the gas emission becomes rapid again. Therefore, both the increase of the rain intensity and frequency may lead to the increase of soil gas emission.

5.8.2 Long-Term Simulation in Field Model

The long-term simulation is also performed in the original Field model (Long Field model). The Long Field model is heterogeneous and represents the WEBS field site. An agricultural tile (elevation = 2.5 m) and macropores are included in the model (pm-dual-tile system). Except for the difference on the precipitation and PET data, other parameters used in the Long Field model are the same as those used in the original Field model.

Figure 38 shows the variation of positive PM and DUAL integrations with time. The gas emission from the soil matrix is greater than that from the macropores. However, the macropore flow contributes more to the total soil GHG emission in the Long Field model compared with in the Long 3D model. The amount of gas released from the macropores comprises about 40% of the total soil gas emission in the Long Field model, but is negligible in the Long 3D model.

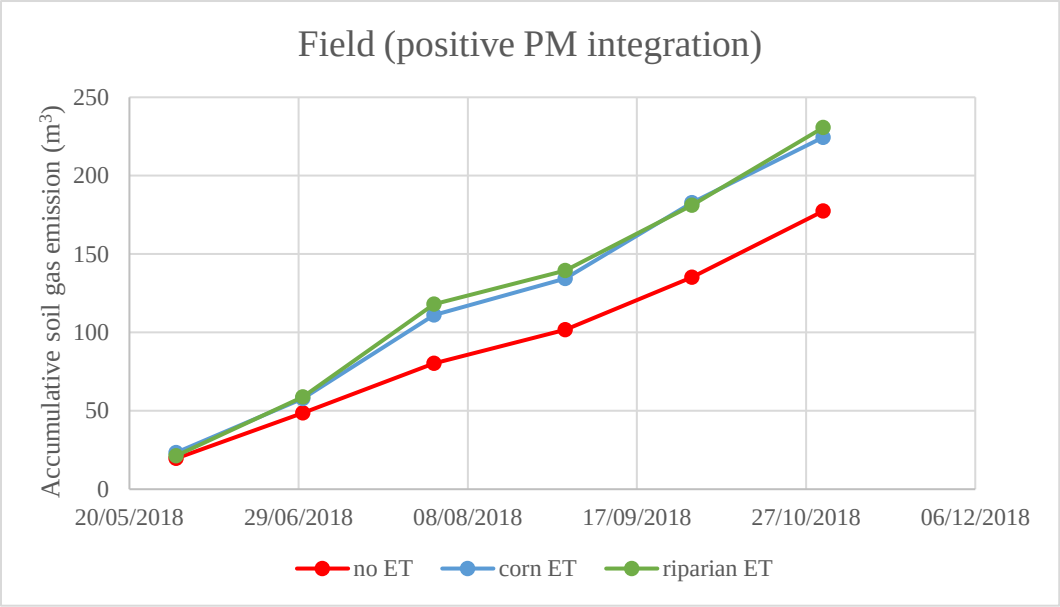

(a)

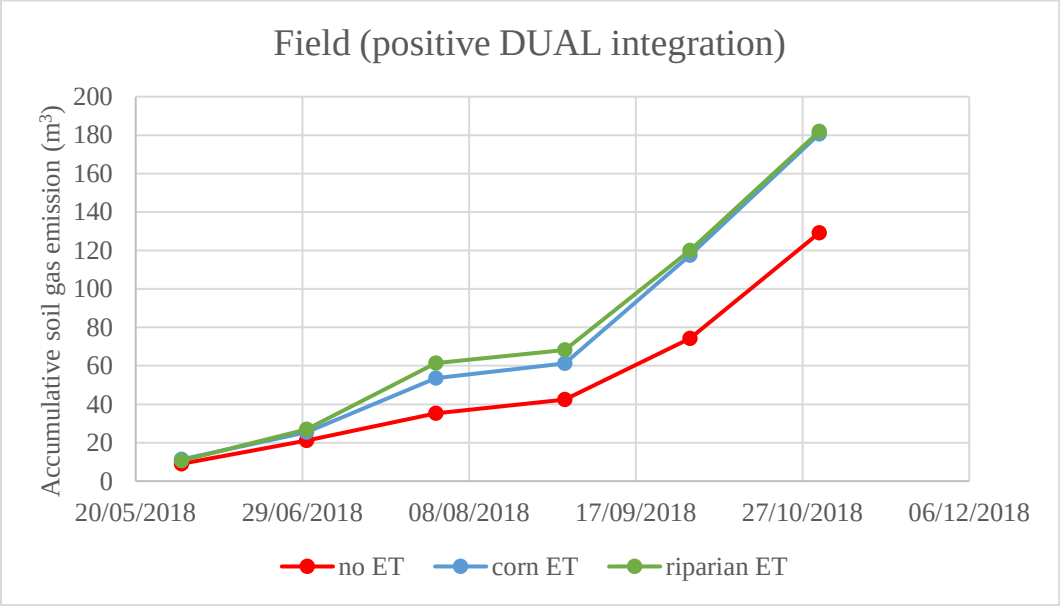

(b)

Figure 38. Variation of positive PM (a) and DUAL (b) integrations with time in the Field model under different evapotranspiration conditions.

The gas emission from soil matrix under the riparian-ET condition is higher than that under the corn-ET or no-ET condition, which corresponds to the results of the Long 3D

model (pm-dual-tile system, clay loam). Similarly, the transition of gas emission curves for the soil matrix and macropores occurs during August in the Long Field model, when the emission rate temporarily decreases.

Unlike the Long 3D model, the Long Field model has gas emission rates from macropores under riparian-ET condition that appear greater than that under the corn-ET condition or under no-ET condition. The water saturation distribution for the macropore domain suggest that the Long Field model tends to have significant water storage variation during precipitation events, while the macropores within the Long 3D model tend to have more stable soil water contents in macropores. In addition, the Long Field model under riparian-ET condition has lower water saturation in macropores than that under corn-ET or no-ET condition. On the contrary, the variation of evapotranspiration conditions seems to have limited influence on the water saturation in the macropores in the Long 3D model.

Generally, the evapotranspiration process consumes soil water and enables the soil matrix and macropores to accept more water during precipitation within the heterogeneous field soils. Consequently, the soil GHG emission is enhanced. The water saturation in macropores of heterogeneous soil is more likely to be disturbed by the precipitation events and evapotranspiration conditions, which might result from the soil heterogeneity. Due to the high degree of variability in the soil water profile, including local regions of high saturation along soil interfaces, the hydraulic gradient between the soil matrix and the macropore might be influenced, which influences water transfer between the two domains. However, the difference between the sensitivity to the precipitation and evapotranspiration variation of the Long 3D model and the Long Field model may also result from the difference on the soil layer flatness, tile depth, and geological and hydraulic parameters. Finally, the similar transition of gas emission curves observed in both the Long 3D model and the Long Field model suggests that both the rain intensity and frequency can increase the gas emission from soil.

5.8.3 General Comparison

Figure 39 and Figure 40 show the summary of the long-term simulation results of the Long 3D and Long Field model respectively. The gas emission from the soil matrix overwhelms that from the macropores in the Long 3D model. In the Long Field model, the opposite condition occurs.

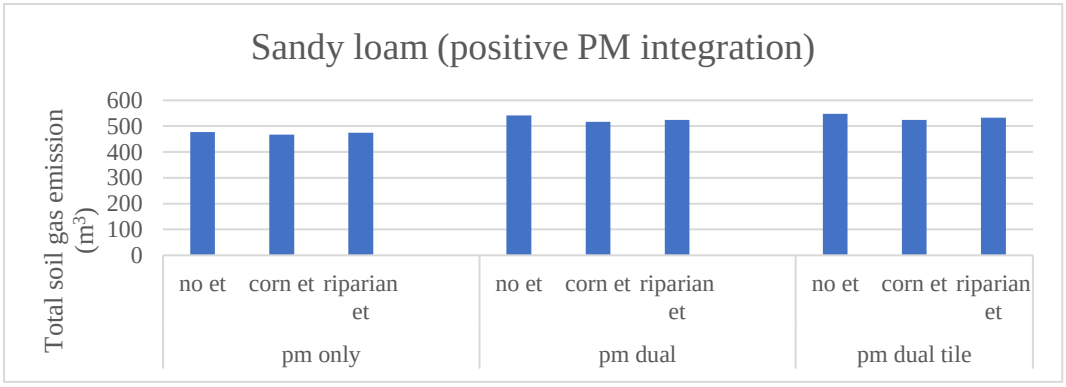

(a)

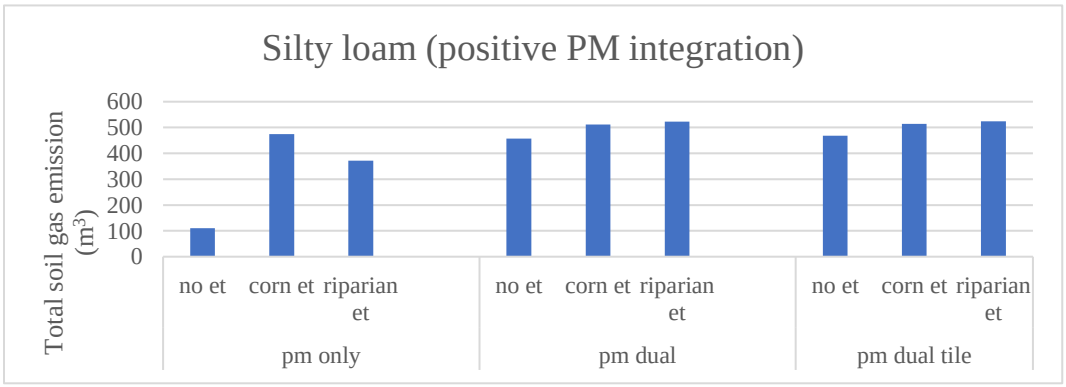

(b)

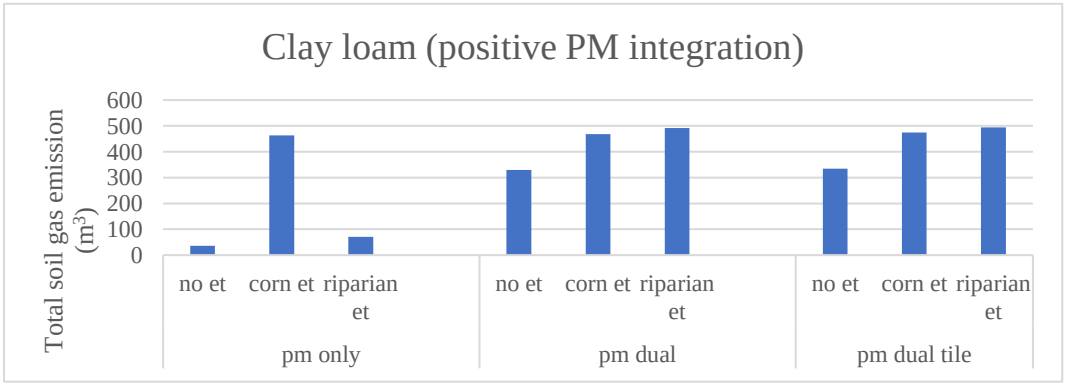

(c)

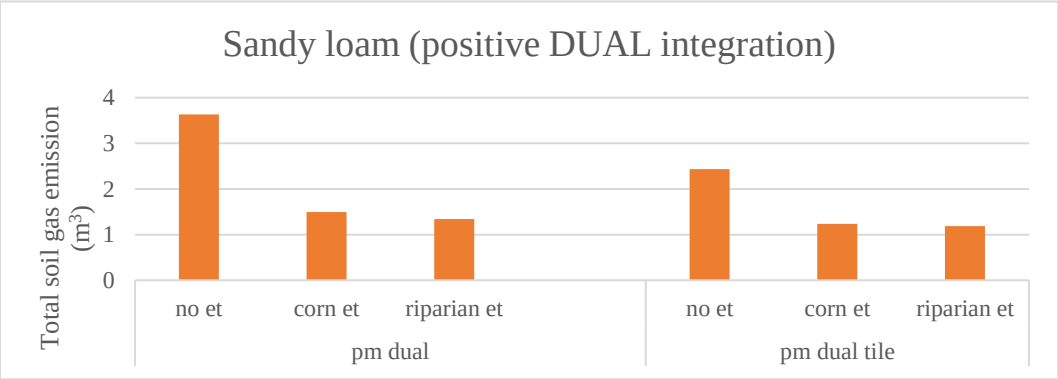
Sandy loam (positive DUAL integration)
Total soil gas emission (m3)
4
3
2
1
0
no et
corn et
riparian et
pm dual
no et
corn et
riparian et
pm dual tile

(d)

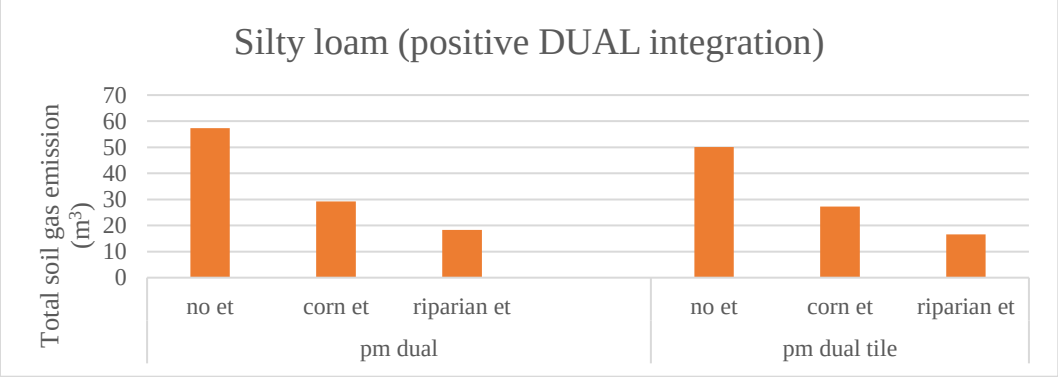
Silty loam (positive DUAL integration)
Total soil gas emission (m3)
70
60
50
40
30
20
10
0
no et
corn et
riparian et
pm dual
no et
corn et
riparian et
pm dual tile

(e)

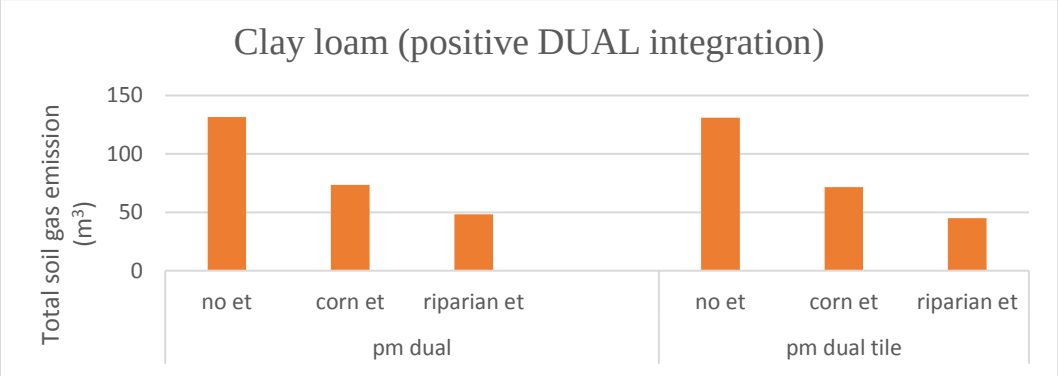
Clay loam (positive DUAL integration)
Total soil gas emission (m3)
150
100
50
0
no et
corn et
riparian et
pm dual
no et
corn et
riparian et
pm dual tile

(f)

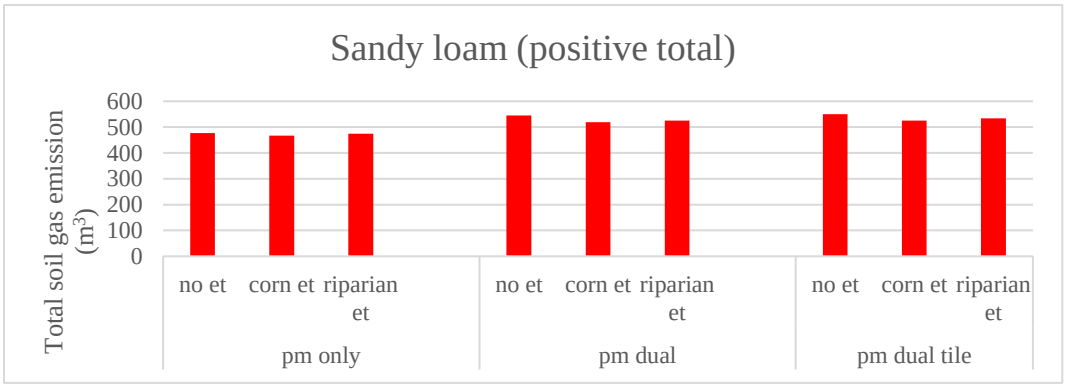

(g)

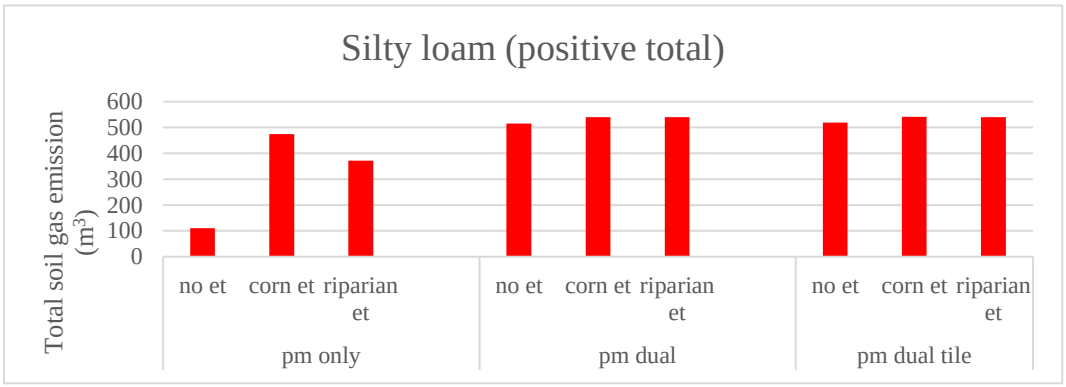

(h)

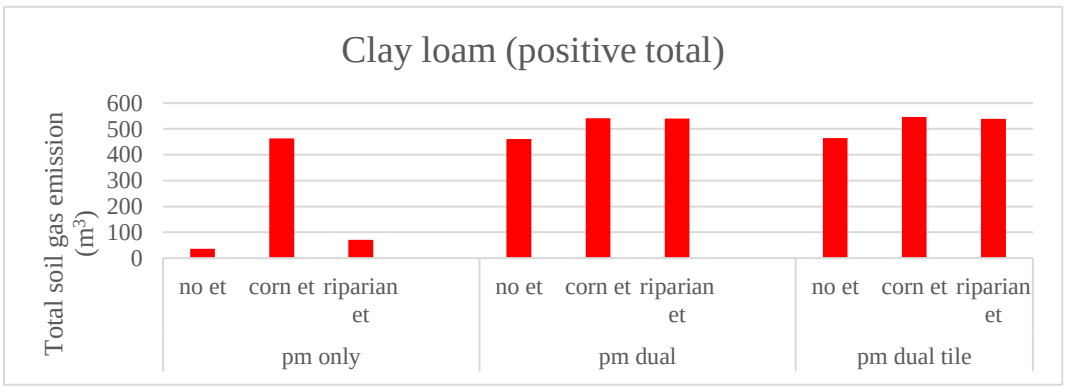

(i)

Figure 39. Long-term simulation results of the 3D flow test model with different soil types under varying evapotranspiration conditions. (a), (b), and (c) are the total gas emissions from the soil matrix. (d), (e), and (f) are the total gas emissions from the macropores. (g), (h), and (i) are the total gas emissions from the entire soil systems, which equal to

the sum of gas emissions from the soil matrix and macropores.

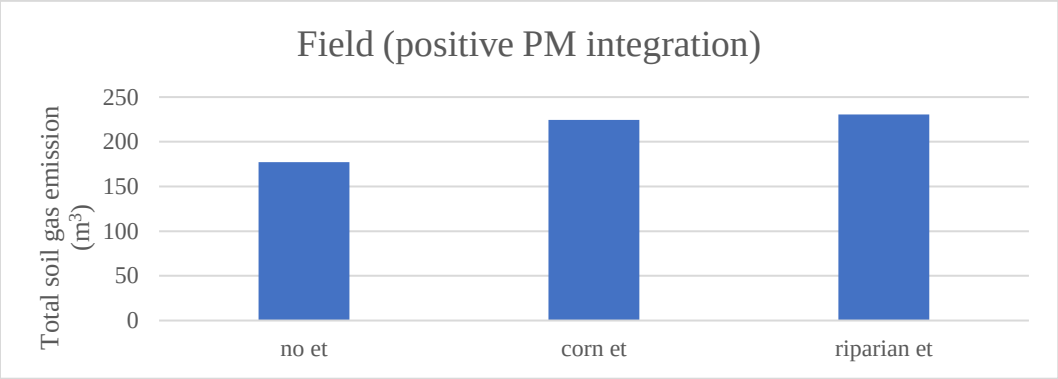

(a)

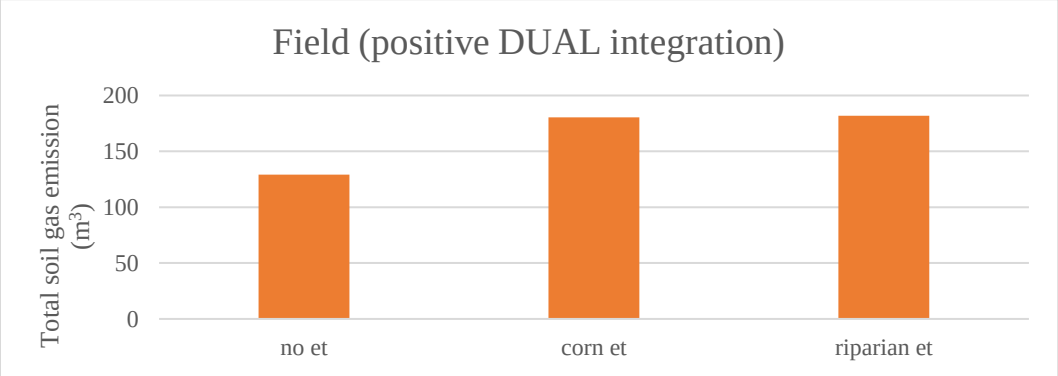

(b)

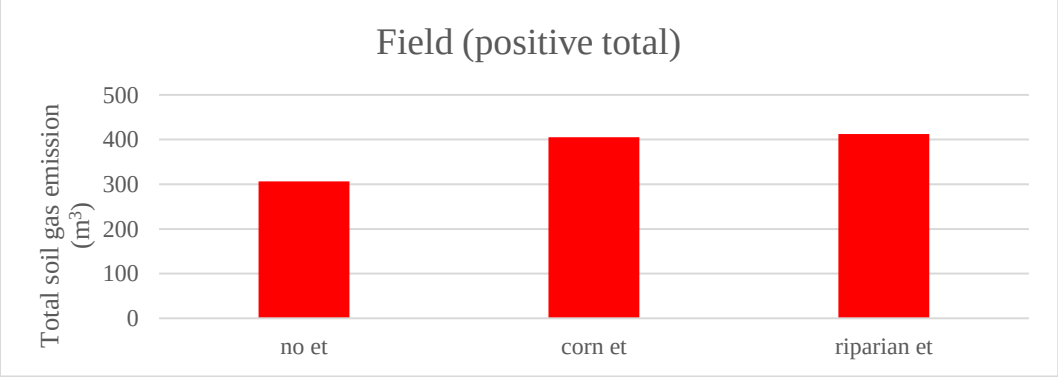

(c)

Figure 40. Long-term simulation results of the Field model under varying evapotranspiration conditions. (a) and (b) are the total gas emissions from the soil matrix and macropores

respectively. (c) is the total gas emission from the entire soil system, which equals to the sum of gas emissions from the soil matrix and macropores.

The results of the Long 3D model represent the response of homogeneous soils under long- term precipitation and evapotranspiration conditions. Generally, the gas emission from the soil matrix under the riparian-ET condition is larger than that under the corn-ET condition or the no-ET condition. However, an opposite consequence occurs on the gas emission from macropores. Such contradiction might be caused by the different role that evapotranspiration plays in the model. In the soil matrix of less permeable soils, evapotranspiration removes water from the soil pores and enables the soil to take in more water during precipitation events. Thus, more gas emission from the soil matrix will occur. However, the evapotranspiration may act as a water sink in the macropores and limits the fluctuation of the water table, which decreases the gas emission from macropores. The water and gas transportation in the macropore is complicated and further investigation is required.

There are two exceptions that do not follow the general trend of gas emission in the Long 3D model. The first is that the variation of PET conditions has negligible influence on the gas emission from the soil matrix of the sandy loam. The sandy loam relies mainly on the soil matrix to transport the infiltrated water and generally has low water tables and discharges rapidly. Hence, the evapotranspiration may act as a water sink, reducing the total amount of infiltrating water limiting the water storage increase during precipitation events. Thus, the gas emissions from the soil matrix under different ET conditions are similar in magnitude, with the emission under no-ET being the highest. The second exception occurs in the pm-only systems with the silty and clay loam. The gas emission from the soil matrix under the riparian-ET is much lower than that under the corn-ET. The low gas emission may relate with the water saturation conditions. The soil matrix remains fully saturated during the most of the time in the system under the riparian-ET, but has observable saturation variations in the system under the corn-ET. Such difference may be caused by the stability of

evapotranspiration conditions. The surge of corn-ET during summer may lead to the variation of water saturation and accelerate the soil gas emission. On the contrary, the riparian-ET tends to be more steady, which tends to have less influence on the water saturation. Hence, it is significant to consider the difference of vegetation types and PET variation when making soil GHG emission management plans.

The results of the Long Field model represent the response of heterogeneous soils under long-term precipitation and evapotranspiration conditions. Generally, the soil matrix of the Long Field model acts the same as that of the Long 3D model with low permeability soils. Unlike in the Long 3D model, the gas emission from the macropores in the Long Field model increases as the evapotranspiration is incorporated in the simulation. The water ponding within the subsurface along stratigraphic unit boundaries due to the soil heterogeneity may cause the higher sensitivity of the water saturation in macropores to the precipitation and evapotranspiration variations. Meanwhile, the evapotranspiration lowers the water saturation in macropores and enables them to accept more water during precipitation events. Consequently, greater soil gas emission is observed in Long Field model under corn-ET and riparian ET. However, the Long Field model and the Long 3D model are not only different with respect to soil heterogeneity, but also with the ground surface topography, tile location, and geological and hydraulic parameters, which can also lead to the difference in the results of the two models. Further investigation might be required.

Chapter 6

Conclusions and Expectations

The soil emission is considered as an important contributor of the atmospheric GHG. During precipitation events, the GHG-rich soil gas is pushed out from soils when the infiltrated water fills the soil pores. To diminish the soil GHG emission, it is significant to investigate the soil gas mobility.

It is difficult to monitor the movement of soil gas. In this research, the soil water saturation is simulated instead of the soil gas saturation. It is assumed that the soil pores are occupied either by water or by gas. It is also assumed no compression, dissolution, or reaction occurs on water or soil gas. Hence, the variation of water saturation can be converted to the variation of gas saturation. Therefore, the soil gas mobility can be investigated.

The conceptual 3D flow test model, conceptual 1D flow model, and 3D flow Field model are built using HGS program. The conceptual 3D flow test model represents a conceptual structureless soil, while the Field model represents the structured soil in the WEBS field site. The influence of the soil matrix, macropores and agricultural tiles on the water transportation in the partially saturated soils is investigated.

The results suggest that the macropores may enhance the water storage increase during storms and promote the soil GHG emission. The macropores can strengthen the drainage capacity and lead to a low soil water saturation before storms. Thus, soils with macropores may accept more infiltrated water and release more soil gas than soils without macropores during precipitation events. However, the volumetric fraction of the macropores seems to have limit influence on the water and gas transportation.

The role that the agricultural tile plays in soil water and gas transportation depends on the drainage capacity and the water saturation condition. In permeable soils with low water saturation, the tile may reduce the soil GHG emission because it controls the fluctuation of

water table and diminish the water storage increase during storms. However, the tile may enhance the soil GHG emission in less permeable soils or under soils with high water saturation, because it promotes the drainage capacity and lowers the initial water saturation to enable the soils to accept more water during precipitation events. Thus, more gas can be released form the soils. No direct relationship is shown between the soil heterogeneity and the role that the tile plays.

Meanwhile, the increase of tile depth may enhance the soil GHG emission. The deep tile may not function as efficiently as the shallow tile in draining the infiltrated water. Besides, the soil with a deep tile tend to have lower water saturation before storms compared with the soil with a shallow tile. Thus, the water storage increase and soil gas emission will be greater in the soil with deeper tile during storms. The soil heterogeneity and the elevation of local water table may influence the strength of tile depth effect. The soil depth effect is stronger in the structured and heterogeneous field soil than in the massive conceptual soils, because it is harder for the deep tile to drain the infiltrated water in the Field model when water ponding occurs in soil layers above. When then water table is lower than the tile throughout the precipitation events, the tile will function poorly in draining water and lead to greater water storage increase and soil degassing.

The increase of tile spacing may also enhance the soil GHG emission. When the spacing between tiles increases and less tiles are installed in the soil system, the drainage capacity of the system is weakened. Hence, more water storage increase will occur during storms and result in greater soil GHG emission.

Besides the soil system components, the soil types, weather, soil heterogeneity, ground surface topography, and precipitation and evapotranspiration conditions can also influence the soil GHG emission. However, the effect of those factors are highly influence by the drainage capacity and soil saturation condition.

Generally, permeable soils with high drainage capacity tend to have greater soil gas emission. Under the dry weather, soils tend to have low water saturation before precipitation

events and have more space to accept the infiltrated water. Hence, the soil degassing may become higher when the weather is dry. The soil gas emission from the macropores may occupy a larger fraction of the total soil gas emission in the structured and heterogeneous soils than in the massive soils, because macropores play more important roles in groundwater redistribution when water ponding occurs due to soil heterogeneity. Ground surface topography may promote the soil GHG emission by forming surface water ponding as water recharges.

Soil GHG emission may increase with the storm intensity and frequency, but decreases as the evapotranspiration elevates. However, when soils become fully saturated during the storm, the increase of storm intensity will have negligible promotion on soil GHG emission. For permeable soils, the GHG emission from soils with different vegetation types are similar. For impermeable soils, the GHG emission from the riparian zone is slightly higher than that from the corn field when the soils are unsaturated.

Overall, the mechanism of soil degassing is complex and relates with multiple factors. In order to diminish the soil GHG emission, several approaches can be adopted. First, the installation of agricultural tiles may help to diminish the soil GHG emission. The soil heterogeneity and local water saturation conditions need to be considered before the installation, the agricultural tiles should contact with the macropores and be lower than the water table during precipitation events. Narrowing the tile spacing may efficiently decrease the water storage variation and control soil GHG emission in permeable soils. Second, flattening the ground surface may reduce the surface water ponding and subsequently diminish soil GHG emission. Third, the soil GHG emission can be diminished by limiting the water input to the soil through smart irrigation. Fourth, the vegetation types with stronger PET may help to control the soil GHG emission.

Bibliography

American Society for Testing and Materials. (1985). Classification of Soils for Engineering Purposes: Annual Book of ASTM Standards. American Society for Testing and Materials.

Aquanty Inc. (Aquanty), 2015a. HGS Reference Manual. Manual for HydroGeoSphere code. Aquanty, Inc. Waterloo, ON. https://www.aquanty.com/. (Accessed 12.02.2018). 98

Aquanty Inc (Aquanty), 2015b. HGS User Manual. Manual for HydroGeoSphere code. Aquanty Inc. Waterloo, ON. https://www.aquanty.com/. (Accessed 12.02.2018).

Beven, K. & Germann, P. (1982). Macropores and water flow in soils. *Water Resources Research*, 18(5), 1311–1325. https://doi.org/10.1029/WR018i005p01311

California Department of Water Resources. (2021). IWFM: Integrated Water Flow Model. Retrieved on 9th February, 2021 from https://water.ca.gov/Library/Modeling-and-Analysis/Modeling-Platforms/Integrated-Water-Flow-Model

Costanza-Robinson, M., & Brusseau, M. (2002). Gas phase advection and dispersion in unsaturated porous media. *Water Resources Research*, 38(4), 7–1–7–9. https://doi.org/10.1029/2001WR000895

Environment and Climate Change Canada. (2018). National inventory report 1990–2016: greenhouse gas sources and sinks in Canada. Public Inquiries Centre, Gatineau, QC, Canada.

Fatumah, N., Munishi, L., & Ndakidemi, P. (2019). Variations in Greenhouse Gas Fluxes in Response to Short-Term Changes in Weather Variables at Three Elevation Ranges, Wakiso District, Uganda. *Atmosphere*, 10(11), 708–. https://doi.org/10.3390/atmos10110708

Freeze, R., Cherry, J., & Freeze, R. (1979). *Groundwater.* Englewood Cliffs, N.J: Prentice-Hall.

Frey, S. (2021). Personal communication from Senior Hydrogeologist, Aquanty Inc., Waterloo, Canada.

Frey, S., Hwang, H., Park, Y., Hussain, S., Gottschall, N., Edwards, M., & Lapen, D. (2016). Dual permeability modeling of tile drain management influences on hydrologic and nutrient transport characteristics in macroporous soil. *Journal of Hydrology (Amsterdam)*, 535, 392–406. https://doi.org/10.1016/j.jhydrol.2016.01.073

Frey, S., Rudolph, D., Lapen, D., & Ball Coelho, B. (2012). Viscosity dependent dual-permeability modeling of liquid manure movement in layered, macroporous, tile drained soil: VISCOSITY DEPENDENT, ANISOTROPIC DUAL PERM MODEL. *Water Resources Research*, 48(6). https://doi.org/10.1029/2011WR010809

Frey, S., Rudolph, D., & Parkin, G. (2012). Spatial and temporal influences on hydraulic properties in macroporous tile-drained soil. *Soil Science Soc. of America J*., vol. 76:350-360, doi:10.2136/sssaj2011.0194.

Gerke, H., van Genuchten, M., & Gerke, H. (1993). A dual-porosity model for simulating the preferential movement of water and solutes in structured porous media. *Water Resources Research*, 29(2), 305–319. https://doi.org/10.1029/92WR02339

Gerke, H.H., Köhne, J.M., 2002. Estimating hydraulic properties of soil aggregate skins from sorptivity and water retention. *Soil Sci. Soc. Am*. J. 66 (1), 26–36.

Ghanbarian-Alavijeh, B., Liaghat, A., Huang, G., & Van Genuchten, M. (2010). Estimation of the van Genuchten Soil Water Retention Properties from Soil Textural Data. *Pedosphere*, 20(4), 456–465. https://doi.org/10.1016/S1002-0160(10)60035-5

Ghane, E. (2018). Agricultural Drainage. Retrieved on 19th March, 2021 from https://www.canr.msu.edu/agriculture/uploads/files/agriculturaldrainage-2-2-18-web.pdf

Google. (2019). WEBS field site map. Retrieved in 2019 from https://www.google.ca/maps/place/Kanata,+Ottawa,+ON/@45.2510198,-75.8340602,11z/data=!4m5!3m4!1s0x4ccdff86df946877:0x286ff73092245b34!8m2!3d

45.3088185!4d-75.8986835

Hamamoto, S., Moldrup, P., Kawamoto, K., & Komatsu, T. (2009). Effect of particle size and soil compaction on gas transport parameters in variably saturated, sandy soils. *Vadose Zone Journal*, 8(4), 986-995.

Harter T. and H. Morel-Seytoux (2013). Peer Review of the IWFM, MODFLOW and HGS Model Codes: Potential for Water Management Applications in California's Central Valley and Other Irrigated Groundwater Basins. Final Report, California Water and Environmental Modeling Forum, August 2013, Sacramento. http://www.cwemf.org

Healy, R. W., Striegl, R. G., Russell, T. F., Hutchinson, G. L., & Livingston, G. P. (1996). Numerical Evaluation of Static-Chamber Measurements of Soil—Atmosphere Gas Exchange: Identification of Physical Processes. *Soil Science Society of America Journal,* 60(3), 740-747.

IPCC. (2013). Summary for Policymakers. In: Climate Change 2013: The Physical Science Basis. Contribution of Working Group I to the Fifth Assessment Report of the Intergovernmental Panel on Climate Change [Stocker, T.F., D. Qin, G.-K. Plattner, M. Tignor, S.K. Allen, J. Boschung, A. Nauels, Y. Xia, V. Bex and P.M. Midgley (eds.)]. Cambridge University Press, Cambridge, United Kingdom and New York, NY, USA.

Jarvis, N. (2007). A review of non-equilibrium water flow and solute transport in soil macropores: principles, controlling factors and consequences for water quality. *European Journal of Soil Science*, 58(3), 523–546. https://doi.org/10.1111/j.1365-2389.2007.00915.x

Kristensen, K., & Jensen, S. (1975). A model for estimating actual evapotranspiration from potential evapotranspiration. *Hydrology Research*, 6(3), 170-188.

Neira, J., Ortiz, M., Morales, L., & Acevedo, E. (2015). Oxygen diffusion in soils: Understanding the factors and processes needed for modeling. *Chilean Journal of Agricultural Research*, 75(s1), 35–44. https://doi.org/10.4067/S0718-58392015000300005

Oertel, C., Matschullat, J., Zurba, K., Zimmermann, F., & Erasmi, S. (2016). Greenhouse gas emissions from soils—A review. Chemie Der Erde - Geochemistry - Interdisciplinary *Journal for Chemical Problems of the Geosciences and Geoecology*, 76(3), 327–352. https://doi.org/10.1016/j.chemer.2016.04.002

Ontario Ministry of Agriculture, Food and Rural Affairs. (2020). *The Online Gardener's Handbook 2010 Chapter 3: A Word about Soil the Nature of Soil*. Retrieved on 3rd March, 2020 from http://www.omafra.gov.on.ca/english/crops/gardbk/gh-ch3-1soil.htm#structure

Panday, D., & Nkongolo, N. (2015). Effect of Soil Air and Water on Greenhouse Gases Emissions in a Corn-Soybean Rotation. *Procedia Environmental Sciences*, 29, 293–294. https://doi.org/10.1016/j.proenv.2015.07.222

PC-Progress. (2019). *Hydrus-1D - PC-PROGRESS.* Retrieved on 3rd March, 2020 from https://www.pc-progress.com/en/Default.aspx?hydrus-1d

Pourbakhtiar, A., Poulsen, T., Wilkinson, S., & Bridge, J. (2017). Effect of wind turbulence on gas transport in porous media: experimental method and preliminary results. *European Journal of Soil Science*, 68(1), 48–56. https://doi.org/10.1111/ejss.12403

Regan, R.S. and Niswonger, R.G., (2021). GSFLOW version 2.2.0: Coupled Groundwater and Surface-water FLOW model: U.S. Geological Survey Software Release, 18 February 2021.

Scanlon, B. Nicot, J. & Massmann, J. (2002). *Soil Gas Movement in Unsaturated Systems.* Retrieved on 3rd, March, 2020 from http://www.beg.utexas.edu/staffinfo/Scanlon_pdf/ScanlonSoilPhysComp02.pdf

Soil Science Society of America. (2020). *Glossary of Soil Science Terms.* Retrieved on 3rd March, 2020 from https://www.soils.org/publications/soils-glossary#

South nation conservation. (2018). *Water Levels and Precipitation.* Retrieved on 3rd March,

2020 from https://www.nation.on.ca/water/watershed-conditions/water-levels-and-precipitation

Sponseller, R. (2007). Precipitation pulses and soil CO2 flux in a Sonoran Desert ecosystem. *Global Change Biology*, 13(2), 426–436. https://doi.org/10.1111/j.1365-2486.2006.01307.x

U. S. Department of Agriculture. (1918). *Department Bulletins Nos. 701-725, with contents and index.* Retrieved on 3rd March, 2020 from

U.S. Department of Agriculture. (2019). *ROSETTA Class Average Hydraulic Parameters*. Retrieved on 3rd March, 2020 from https://www.ars.usda.gov/pacific-west-area/riverside-ca/agricultural-water-efficiency-and-salinity-research-unit/docs/model/rosetta-class-average-hydraulic-parameters/

United States Department of Agriculture. (2020). *Soil Texture Calculator.* Retrieved on 3rd March, 2020 from https://www.nrcs.usda.gov/wps/portal/nrcs/detail/soils/survey/?cid=nrcs142p2_054167

Vermoesen, A., Ramon, H., & Van Cleemput, O. (1991). Composition of the soil gas phase. Permanent gases and hydrocarbons. *Pedologie*, 41(2), 119–132.

Welling, S. (1997). *Comparative performance of 50 mm diameter drainage pipe VS standard 100 mm diameter drainage pipe.* Nova Scotia Agricultural College Truro, Nova Scotia, Canada.

Widurska, I. (2020). Effects of seasonal climate and landscape position on greenhouse gas pathways in partially saturated agricultural soils, Dept. of Earth and Environmental; Sciences, MSc thesis (in progress).

Widurska, I. (2021). Personal communication from MSc student, University of Waterloo, Waterloo, Canada.

Yan, G., Mu, C., Xing, Y., & Wang, Q. (2018). Responses and mechanisms of soil greenhouse gas fluxes to changes in precipitation intensity and duration: A meta-analysis for a global perspective. *Canadian Journal of Soil Science*, 98(4), 591–603.

https://doi.org/10.1139/cjss-2018-0002